Improving the Evaluation of Fracture Critical Bridges Using Measured Rainflow Response

by

Peter Kenneth Dean, B.C.E.

Thesis

Presented to the Faculty of the Graduate School of

The University of Texas at Austin

in Partial Fulfillment

of the Requirements

for the Degree of

Master of Science in Engineering

The University of Texas at Austin

May 2005

Improving the Evaluation of Fracture Critical Bridges Using

Measured Rainflow Response

Approved by
Supervising Committee:

Supervisor: Sharon L. Wood

Karl H. Frank

Dedication

This thesis is dedicated to all the friends I have made over the past two years. Our time together was too short, but I have no doubt our friendships will continue to grow for the rest of our lives.

Acknowledgements

I would like to thank the following people for all of the help that they have provided during the course of this research.

I would like to thank Dr. Sharon Wood for her insightful guidance throughout this project. Without her, I would not be writing this today. Most of all, I appreciate the hard work and long hours it took to get this thesis into form. Thank you.

I would also like to thank Alan Kowalik, P.E. for his constant help and cooperation. Without him, I would have had a boring car ride to our bridge locations.

I would like to thank Dr. Karl Frank for being a reader of this thesis. When I was crunched for time, he was able to help me get finished.

I would also like to thank my family: mom, dad, Bob, Jesse, and Lissy. You guys were always there to push me in the right direction when it mattered and to keep raising the bar. Mom and dad, the constant support (and cookies) over the past two years has made this experience so much easier.

The friends I have made over the past two years also deserve a warm thank you. Many of us met as a result of our program, but our interests go so much farther than that. I have made more close friends in the past two years then in any other point in my life. I am sad to be leaving you all, but excited to see what the future holds for us. 602!

May 5, 2005

Abstract

Improving the Evaluation of Fracture Critical Bridges Using

Measured Rainflow Response

Peter Kenneth Dean, M.S.E.

The University of Texas at Austin, 2005

Supervisor: Sharon L. Wood

A strain data acquisition system known as MicroSAFE was used in the field to evaluate two fracture critical bridges for the Texas Department of Transportation. This system was tested for its applicability for future use by TxDOT. The first bridge is located in downtown Austin, TX and is an exit ramp for Interstate-35. The MicroSAFE units were used to record rainflow strain data and that information was used to determine a fatigue life for the bridge. A second bridge south of San Antonio, TX was also evaluated and the rainflow data was corroborated with a weigh-in-motion sensor located near the bridge. The MicroSAFE units were found to be a viable option for TxDOT, with the data suggesting that the determination of a fatigue life should affect the inspection schedule for a bridge.

TABLE OF CONTENTS

LIST OF FIGURES

ix

LIST OF TABLES

CHAPTER 1

Introduction

1.1 OVERVIEW

A significant number of bridges within the state of Texas are considered to be fracture critical. The AASHTO Manual for Condition Evaluation defines fracture critical members as "tension members or tension components of members whose failure would be expected to result in collapse of a bridge" [1]. Many of the fracture critical bridges in Texas also have unique structural systems or structural geometries. TxDOT is interested in closely monitoring these bridges for several reasons. One, many of these bridges present unique issues in both the inspection of the bridge and the evaluation of the bridge's structural health. Two, the fracture critical nature of these bridges requires TxDOT to run in-service inspections on a short schedule, costing extra time and money [10].

TxDOT Project 0-4096 is being used to evaluate bridge monitoring systems that provide response information that will make inspection of these bridges easier and more thorough and provide data to support recommendations that some fracture critical bridges do not need to be inspected as frequently as currently required [12].

1.2 RECENT RESEARCH BY THE UNIVERSITY OF TEXAS AT AUSTIN

In the previous two years, funding for this project was directed towards the research and development of two types of monitoring systems. The first type of system was a GPS-based system from monitoring structural systems. The second system was a miniature data acquisition system developed by Invocon,

Inc. This system could provide rainflow counting data during inspection, or could function as a long term monitoring system to collect real-time data. These units, called MicroSAFE units, record strains during normal loading conditions. This information is essential in the study of fracture critical bridges [3].

1.3   SCOPE OF PROJECT

Based upon the results of the previous research and the wishes of TxDOT, the research team decided to continue the study of the miniature data acquisition systems. The MicroSAFE system was used successfully in laboratory studies prior to the start of this portion of the project. During this phase of the research, the MicroSAFE units have been used extensively in the field on two bridges that are designated as fracture critical by TxDOT. The rainflow data resulting from these field tests has been compared with the results of finite element models of the bridges being studied. A fatigue life analysis can be completed with the measured data and a suggestion can be made to TxDOT regarding the remaining life of the structure.

Chapter 2 contains an explanation of rainflow data, a summary of MicroSAFE operating information for the units, and how fatigue life is calculated. Chapter 3 presents general information about the first field test, the I-35 exit ramp for 12th Street in Austin. Chapter 4 compares the results of the first field test with the finite element model and discusses the fatigue life analyses. Chapter 5 includes general information on the second field test, the I-35 crossing of Medina River south of San Antonio. Chapter 6 compares the measured response of the Medina River Bridge with the finite element model and weigh-in-motion data recorded near the bridge. Chapter 7 presents conclusions and recommendations to TxDOT.

CHAPTER 2

Miniature Data Acquisition System
and Rainflow Data

2.1 OVERVIEW

Data acquisition systems have been used to monitor the response of bridges for many years in both short and long-term applications. The majority of these systems have been developed by university researchers and provide data that can be analyzed to evaluate the condition of the bridge. Unfortunately, most of these systems are inconvenient to use on a consistent basis due to lengthy setup times, complicated data retrieval and analysis, and bulky parts. These issues do not create a serious problem for researchers, but are a large concern for Departments of Transportation, who are responsible for inspecting bridges in this country [3].

The MicroSAFE data acquisition system, developed by Invocon, Inc., is specifically designed to eliminate many of these problems. The MicroSAFE devices are easy to install in the field, make it simple to retrieve data, and are small enough to be used almost anywhere. The unit is designed to record data from a 120-Ω strain gage, and if desired, convert this raw data to rainflow counts. Each unit can record up to forty-five days of rainflow data in the field with a single battery and the data are easily retrievable with a laptop and the MicroSAFE software [7]. The many applications of these devices have been identified during this research project. The ease of setup and data retrieval have made these units very popular in Ferguson Structural Engineering Laboratory, from recording a day or two of data to determining if a fatigue test was cycling in the same load

cycles to running month-long rainflow collection tests in the field. The MicroSAFE units have been very useful.

This Chapter is divided into three sections. The ASTM E 1049-85 rainflow counting algorithm is explained in Section 2.1. The features of the MicroSAFE data acquisition system are summarized in Section 2.2. Finally, the basis for fatigue life analyses is discussed in Section 2.3.

2.2   RAINFLOW COUNTING

Rainflow counting is a method for simplifying a complex strain history into a histogram of cycle amplitudes. The rainflow data are extremely useful because the number of cycles a structure experiences at specific strain levels is the only data required to predict the fatigue life.

A compilation of acceptable procedures for cycle-counting methods used with fatigue analysis is found in ASTM E 1049-85(1997). This includes a recommended rainflow counting algorithm. The algorithm is best described using the brief loading history in Figure 2-1. The units on the vertical axis can be assumed to be directly proportional to both stress and strain in the specimen. Conveniently, this algorithm is applicable to both the evaluation of previously recorded data and real time data.
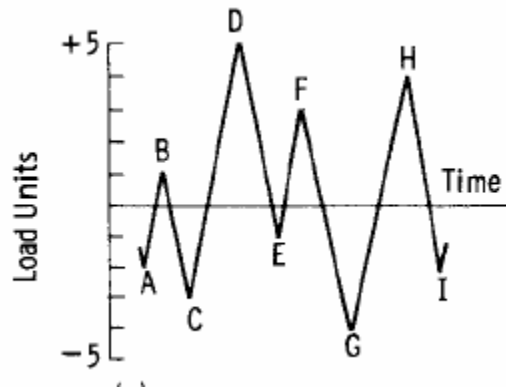
Figure 2-1: Sample Strain History [2]

The strain history in Figure 2-1 is examined in a point-by-point fashion beginning with data point A.   A series of Boolean checks are performed to compare the current strain with the adjacent maximum and minimum strains in the history. In this manner, the number of cycles within predetermined ranges are calculated. To learn more about this algorithm please refer to the ASTM standard and the paper by Bilich found in the References section.

Table 2-1: Cycle Counts Per Range

Range (unit)	Cycle Counts	Events
10	0	
9	0.5	D-G
8	1	C-D, G-H
7	0	
6	0.5	H-I
5	0	
4	1.5	B-C, E-F
3	0.5	A-B
2	0	
1	0	

The final cycle counts from the sample strain history are shown in the previous table. With real data, the cycles are not always integers and as a result, the each event is placed in a bin with a specific range. For example, assuming a bin size of 3 units, a cycle with amplitude of 3.3 would fall in a bin with a range from 3.0 to 6.0.

2.3   MICROSAFE DATA ACQUISITION SYSTEM

The MicroSAFE unit, short for Micro Stress Analysis and Forecasted Endurance unit, is a miniature smart sensor that measures and records data using the ASTM Rainflow Cycle Counting Algorithm.   The MicroSAFE device communicates with the user using a Graphical User Interface (GUI). This allows for convenient unit programming, viewing, and data retrieval. The GUI can be installed on any computer and wiring is completed using a standard serial or USB port.

2.3.1   System Description

Each individual MicroSAFE unit consists of three components: the MicroSAFE processor, a battery pack, and a communication cable.   The MicroSAFE processor records the strain history.   The electronics within the processor convert the analog signal from a strain gage to digital and then processes the data using the rainflow counting algorithm.   The processor is connected to the battery pack.

The battery pack has two significant functions. It provides power to the MicroSAFE processor and communication between the PC and the processor. The external four-pin cable provides two pins for communication and two pins for

power to the processor. The battery has an expected life of 45 days when recording rainflow data.

The communication cable is a three-pin connector which connects the battery pack to the serial port of a computer. A converter can also be used to convert the cable from a serial port to a USB. The three pins are used for one ground pin and two communication pins [7].

2.3.2 Graphical User Interface

The Graphical User Interface (GUI) is the software used to communicate with the MicroSAFE devices. To begin, the MicroSAFE system has four operational modes: Idle, Active Acquisition, Waiting, and Auto-Zeroing. The system is in Idle mode before it is programmed to collect data, after the data collection period has ended, or after the collection period has been cancelled. The Active-Acquisition mode refers to the time when the unit is acquiring strain data. After acquisition is complete, the unit returns to Idle mode. Between acquisition periods, the unit enters Waiting mode. There are two types of Waiting modes, Waiting For First Period and Waiting Between Periods. Waiting For First Period occurs when the unit has been programmed but the collection period has not begun. If data have been collected during one period, and the unit is waiting to begin collecting data during the next period, the mode will be Waiting Between Periods. The last possible mode is the Auto-Zero function which occurs eight seconds before the start of each acquisition period and centers the raw data around the starting strain value. As common sense would expect, this does not affect the Rainflow Analysis.

The Main Program Window of the GUI (Figure 2-2) has seven buttons which will perform different functions for the user. Two buttons, the Comm #

button and the About button are related to communication with the computer. Additional information on these buttons is provided in the MicroSAFE users manual. The other five buttons will be discussed in more detail below.
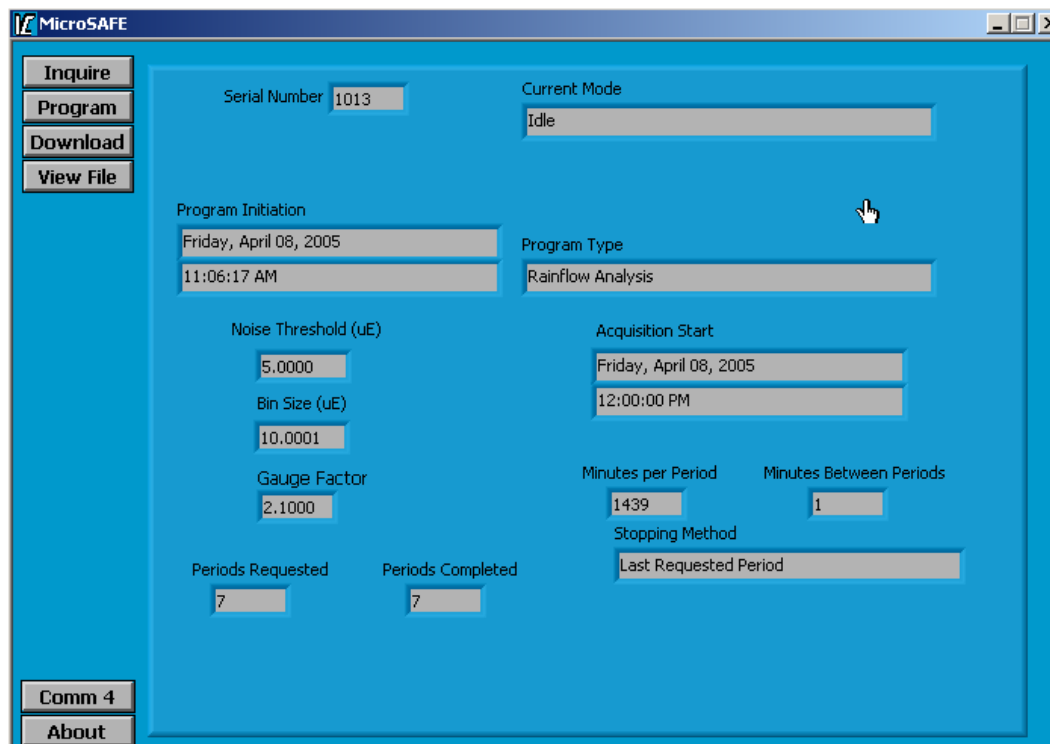
Figure 2-2: Main Program Window of GUI

The top left button, Inquire, serves the very simple but useful function of refreshing the display fields in this window. The Program button allows the user to set up the next data acquisition periods. The Download button copies the data from the MicroSAFE unit into a user specified location. This option is only available when the unit is in Idle mode or after the first period in a multiple-period acquisition is completed. The View File button allows the user to view a histogram of the Rainflow data files in the MicroSAFE window. The Cancel

Acquisition button is only available after the unit has been programmed for Rainflow Analysis Only or Record Raw Data Only, and can be used to terminate data acquisition during an acquisition period.

During Active Acquisition, the Main Program Window provides feedback about the status of the unit. These fields include a displaying of the unit's serial number, the current mode of the unit, and the number of minutes until completion of the period. Other fields display information about how the unit was programmed including when the unit was last programmed, the type of acquisition being performed (Rainflow Only, Rainflow and Raw, or Raw Only), and the noise threshold selected. The noise threshold is a user-selected value that separates noise from data. Any rainflow cycles below this threshold are not counted in the first bin [7].

2.3.3 Programming the MicroSAFE Units

The programming of the MicroSAFE devices depends on the information that is known about the structure to be instrumented. During programming, the user must specify the number and length of acquisition periods, the bin size, and the noise threshold. The next few paragraphs will discuss the program parameters that can be changed in program setup (Figure 2-3).

The top pull-down menu allows the selection of the Program Type. The possible options are Rainflow Analysis Only, Rainflow Analysis With Raw Data, and Record Raw Data Only.
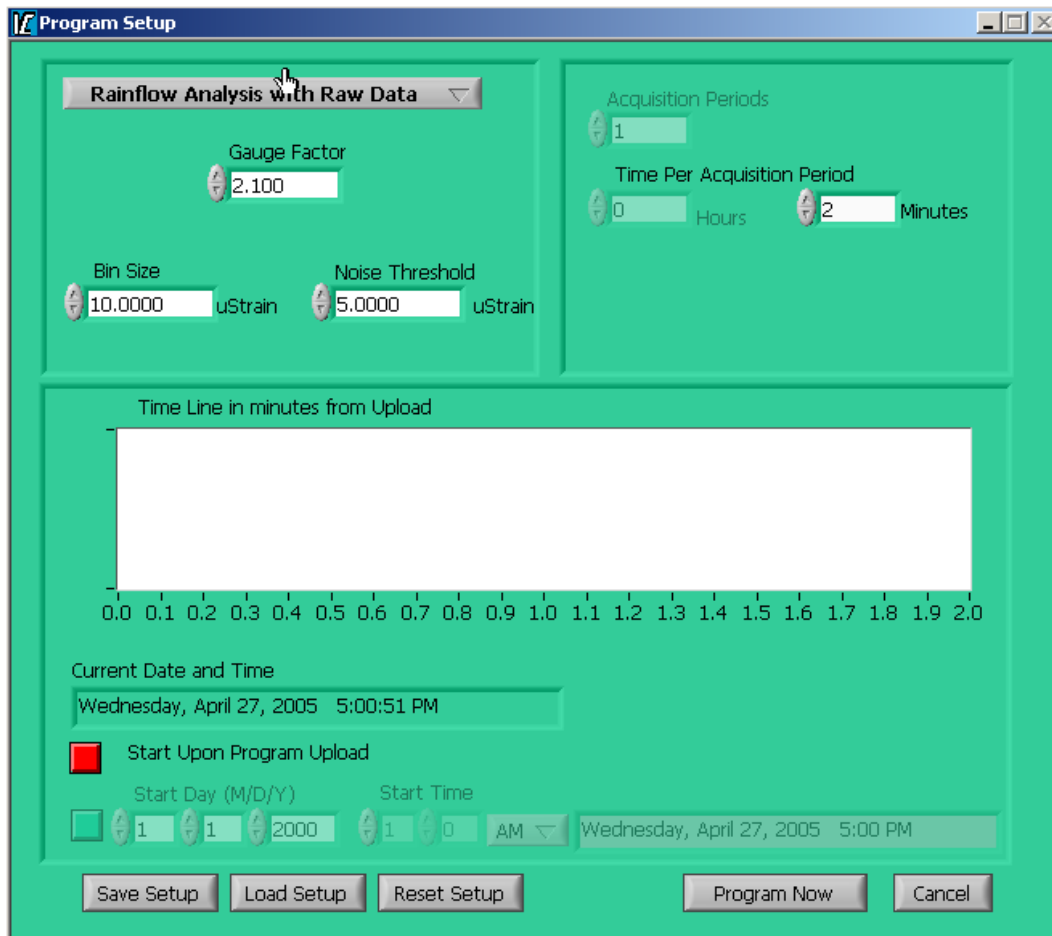
Figure 2-3: GUI Set to Record Rainflow Analysis with Raw Data

The Gauge Factor must be entered for the strain gage. Gauge factors are specified by manufacturers and can be found on documentation about the strain gauge. The user must also specify the bin size and the noise threshold [7]. Bin Size may be the most important selection made on this screen. It determines the microstrain range for each of the 32 bins in a Rainflow Analysis. In most cases, it is desired that all data fall somewhere within the 32 bins. As an example, if the largest strain expected was 300 microstrain, then an unconservative choice for Bin Size would be 10 microstrain. Thirty-two bins, each with a ten-microstrain range

would accurately record all data from zero to 320 microstrain. The recommended bin size would be 15 $\mu\varepsilon$ for this case, a safety factor of 1.5. In many cases, the maximum strain range is not known. If too small a bin size is selected, a large number of cycles will be recorded in the largest bin, and the rainflow data will not provide a complete representation of the response. If too large a bin size is selected, most of the cycles will be recorded in the small bins and the larger bins will be empty. In this case, the resolution of the rainflow data may not be sufficient. Guidelines for selecting the bin size are discussed in Chapters 3, 6, and 7.

The Noise Threshold, which was discussed earlier, is best determined with a combination of experience and, if possible, raw data. The shape of the strain history should give the user a general idea of the level of noise. Normal noise thresholds in this project ranged from 3 to 5 microstrain depending on the application. Also, the noise threshold must always be less than the Bin Size [7].

The number of desired data collection periods is entered in the Acquisition Periods box. Only one period can be defined for Raw or Rainflow and Raw analyses, but from 1 to 512 periods can be used with Rainflow Analysis Only. Time Per Acquisition Period establishes the time that data are collected during each acquisition period. Permissible values depend on the acquisition mode and the processor memory. For raw data collection, permissible times vary from 1 to 33 min. For combined rainflow and raw data collection, permissible times vary from 1 to 59 min. When only rainflow data are being collected, permissible times vary from 1 min to 23 hr 59 min. The Time Between Acquisition Periods box applies only to Rainflow Analysis Only, and it must be at least one minute. The data are stored in non volatile memory during this time. If a battery were to fail during an acquisition period, the data in non volatile memory are retained and only the data recorded during the current acquisition period are lost [7].

11
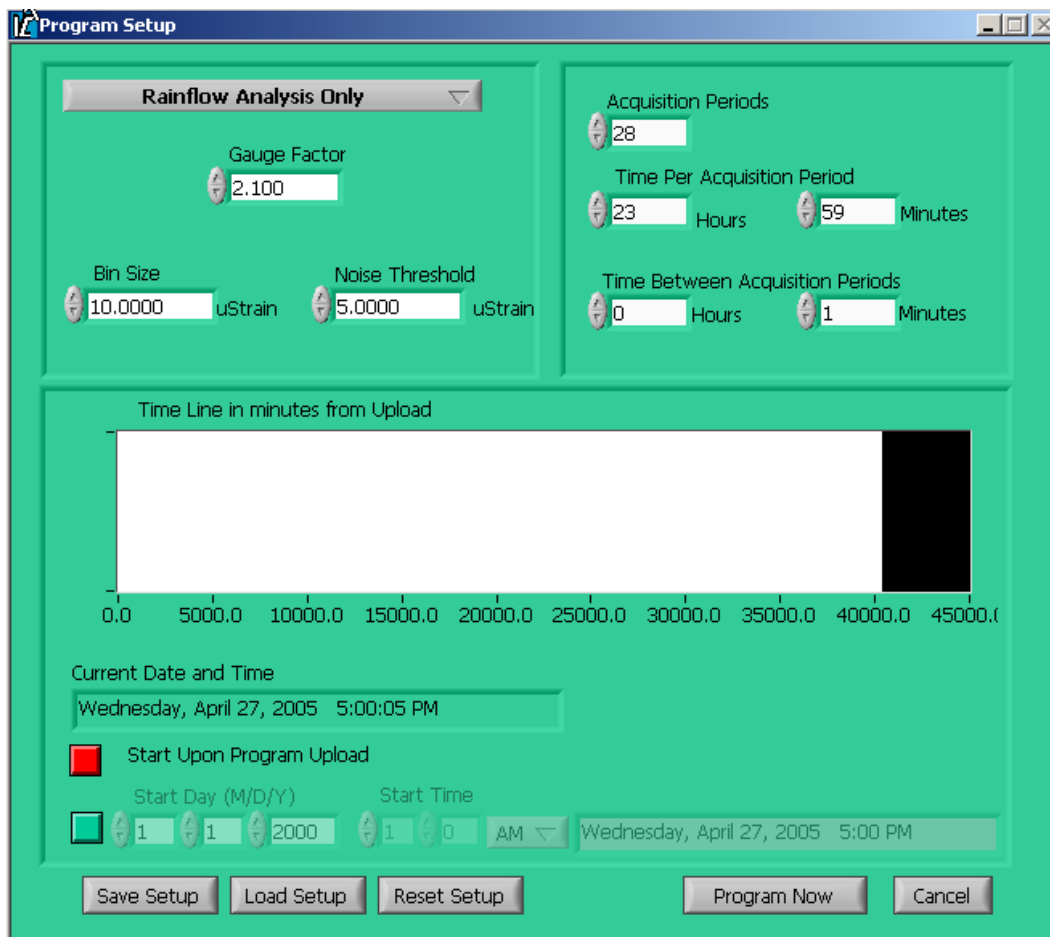
Figure 2-4: GUI Set to Record Rainflow Analysis Only

When the units were installed in the field, the most common settings for Rainflow Analysis Only were for an acquisition period of 23 hr and 59 min and a time between periods of 1 min. With this configuration, each acquisition period is 24 hr, and the data from each 24-hr period are stored in separate files.

The Start Preference option gives a choice between program startup times. The program can be started upon upload, or at a user-specified time. Although starting upon program upload is useful for testing the units and in applications with a single strain gage, multiple units were used simultaneously in this project

and it was convenient for each unit to have the same acquisition period. For this reason, choosing the same start time for all units is very convenient. In specific situations where other data are being received and compared to the strain data, it can be useful to set all acquisition period lengths and times to correspond to the lengths and times of the other data.

2.3.4   Downloading and Viewing MicroSAFE Data

Downloading and viewing of MicroSAFE data is essential in the process of using the MicroSAFE devices. Downloading can be done in either the Idle mode or in the Active Acquisition mode if at least one period has been completed. If the Download button is available, pressing it and selecting the desired location on the hard drive will remove the data from the MicroSAFE device and place the data in the location specified.

The data can be viewed using the GUI by now pressing the View File button. The raw data from a sample period is shown in Figure 2-5 and the rainflow data from that same period is shown in Figure 2-6. This is a quick way of checking the success of the data collection and there are many viewing options within this window, but for most continued analysis of the data, exporting the information to Microsoft Excel is more convenient.
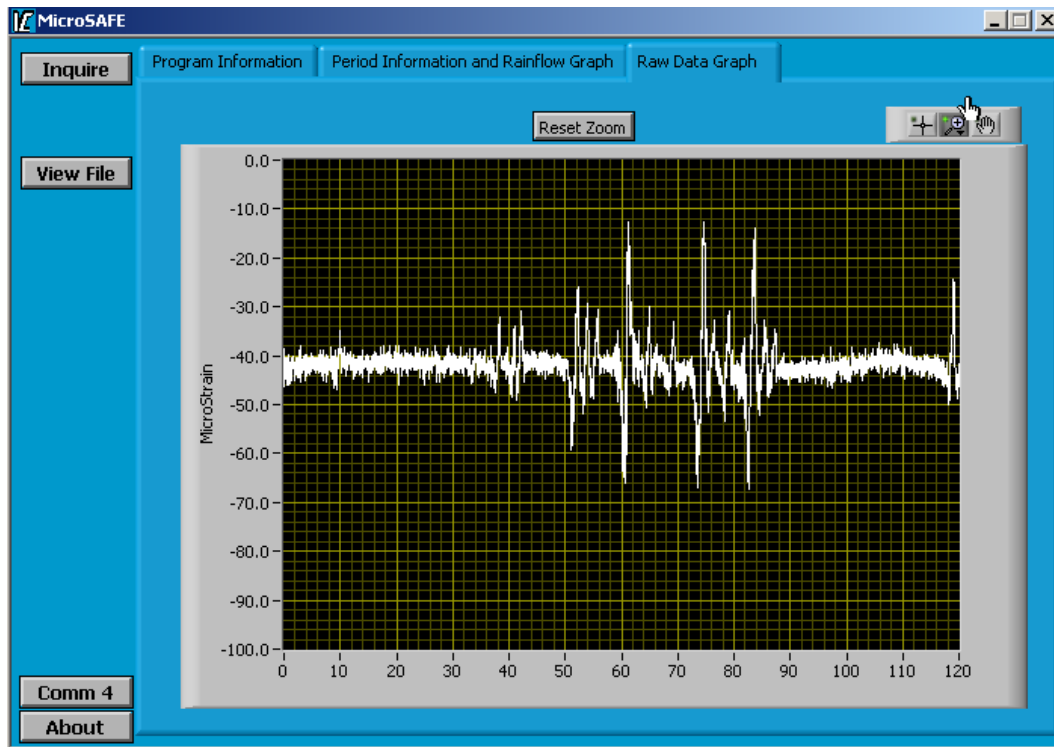
Figure 2-5: Viewing a Raw Data File with the MicroSAFE GUI
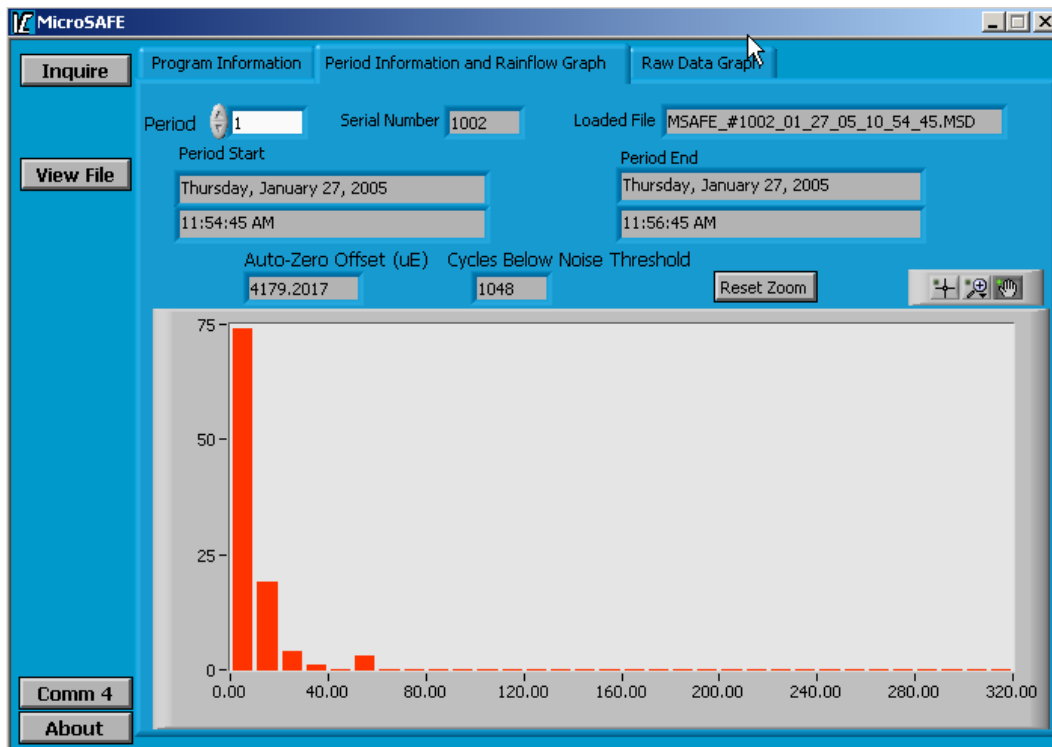
Figure 2-6: Viewing a Rainflow Data File with MicroSAFE

This was a brief introduction to the properties, capabilities, and usage of these MicroSAFE devices. A much more detailed look can be found in the Users Guide prepared by Invocon, Inc [7].

2.4   FATIGUE LIFE

The definition of fatigue life varies from source to source. It is often described by materials manufacturers as "the number of cycles of stress that can be sustained prior to failure for a stated test condition" [9].   More descriptive definitions can also be found. "Fatigue life is the number of cycles of fluctuating stress and strain of a specified nature that a material will sustain before failure

15

occurs. Fatigue life is a function of the magnitude of the fluctuating stress, geometry of the specimen and test conditions. An S-N diagram is a plot of the fatigue life at various levels of fluctuating stress" [8]. While none would disagree that these definitions are true, fatigue life often comes down to one major issue, which is made obvious in the Ohio DOT glossary which defines fatigue life simply as "the length of service of a member" [11].

2.4.1   Consideration of Fatigue in Design

The fatigue provisions in the current AASHTO Design Specifications are based upon a comprehensive study of steel beams. The experimental program was designed to determine the importance of various parameters that were assumed to influence the fatigue behavior. The results of the study demonstrate that the fatigue life, N, depends on the applied stress range, S_R:

$$N = A \times S_R^{-n} \qquad\qquad (2.1)$$

where A and n are empirical constants. The value of n was determined to be approximately 3 for welded and riveted details [4]. The value of A is a function of the geometry of the connection detail. Studies were done to determine appropriate values for A depending on the detail category (Table 2-2). AASHTO used these fatigue studies to develop design curves for fatigue life and stress range [6].

Table 2-2: Detail Category Constant, A from AASHTO [1]

Detail Category	Constant, A times 10^8 (ksi^3)
A	250.0
B	120.0
B'	61.0
C	44.0
C'	44.0
D	22.0
E	11.0
E'	3.9

The use of these curves required the determination of the design stress range for critical connection details. With this information, the appropriate S_R –N curve could be used to estimate fatigue life. One problem with this method is that the curves were developed using constant amplitude stress histories, traffic loading is highly variable. Thus, a relationship between variable amplitude and constant amplitude stress histories must be used to apply the AASHTO design curves to bridges [6].

2.4.2   Fatigue Life Analysis

The following discussion is summarized from Hoadley, Frank, and Yura. Using an assumption made by Minor that fatigue damage accumulates linearly, it is possible to relate variable amplitude to constant amplitude stress histories. The linear damage equation proposed by Minor is:

$$\sum \frac{n_i}{N_i} = 1.0 \qquad\qquad (2.2)$$

where n_i is the number of cycles at stress range, S_{Ri}, in a variable amplitude stress history and N_i is the fatigue life at S_{Ri}. The fatigue life may be written as:

$$N_i = AS_{Ri}^{-n} \tag{2.3}$$

Combining Equations (2.2) and (2.3), Equation (2.4) eliminates the N_i from consideration:

$$\sum \frac{n_i}{AS_{Ri}^{-n}} = 1.0 \tag{2.4}$$

The number of cycles at a stress range (n_i) can be written as a function of the total number of cycles to failure (N) at any stress range and the fraction of the total number of cycles at a certain stress range (γ_i):

$$n_i = \gamma_i \times N \tag{2.5}$$

Substituting and rearranging Equations (2.4) and (2.5) gives:

$$\frac{N}{A} \sum \gamma_i S_{Ri}^{n} = 1.0 \tag{2.6}$$

A new parameter can now be introduced called effective stress range (S_{RE}):

$$S_{RE}^{n} = \sum \gamma_i S_{Ri}^{n} \tag{2.7}$$

18

Combining and rearranging (2.6) and (2.7) results in:

$$N = A \times S_{RE}^{-n} \qquad (2.8)$$

where N is the total number of cycles to cause failure in a variable amplitude stress history [6].

Equation (2.8) is in a similar form to Equation (2.1). Equation (2.1) relates the fatigue life, N, to a constant amplitude stress range, S_R, while Equation (2.8) relates N to the effective stress range, S_{RE}. As a result, the effective stress range can be defined as the constant amplitude stress range which would produce the same fatigue life as the variable stress history from which it was derived.

Given rainflow data, the effective stress range is easily calculated. A series of strain ranges and the number of cycles at each strain range are reported by each MicroSAFE unit. Each stress range (S_{Ri}) can be calculated by multiplying the mean strain by Young's modulus:

$$S_{Ri} = \varepsilon_i E \qquad (2.9)$$

where ε_i is the average strain range in bin i, E is the modulus of elasticity, and i varies from one to thirty-two. The effective stress range can now be calculated from the stress ranges by summing the results from all thirty-two bins:

$$S_{RE} = \left[\sum_i \gamma_i S_{Ri}^{3} \right]^{\frac{1}{3}} \qquad (2.10)$$

Where γ_i is the number of cycles in bin i divided by the total number of cycles [6].

19

The number of cycles to failure can be found using Equation (2.8). Once this is known, fatigue life can be estimated. It is also possible for a structure to have an infinite fatigue life, which means the structure is not expected to fail due to fatigue. In order to have an infinite fatigue life, the structure must never see a stress range greater than the threshold stress range defined by its detail category. The appropriate thresholds are listed in Table 2-3.

Table 2-3: Threshold Stress Range from AASHTO [1]

Detail Category	Threshold (ksi)
A	24.0
B	16.0
B'	12.0
C	10.0
C'	12.0
D	7.0
E	4.5
E'	2.6

CHAPTER 3

General Information and Setup of I-35 12th Street Exit Ramp

3.1 OVERVIEW

Bridges that have been classified as fracture critical have recently become more expensive to inspect due to stricter federal regulations. In the past, TxDOT used a five-year inspection schedule for fracture critical bridges. However, the inspection frequency must be reduced to two years by 2006.

Fracture critical bridges lack redundancy, so the failure of one member could cause collapse of the bridge. The 12th Street Exit Ramp is considered fracture critical because there are only two longitudinal girders. Due to the proximity of this exit ramp to downtown Austin, very few trucks use this ramp. The more frequent inspections are not expected to provide sufficient information to justify the additional costs. Therefore, the rainflow data collected from this bridge will provide valuable information about the fatigue life of the bridge and will help TxDOT develop priorities for fracture critical inspections.

3.2 12TH STREET EXIT RAMP GEOMETRY

The 12th Street Exit Ramp from I-35 in downtown Austin has an unusual geometry. A plan view of the ramp is shown in Figure 3-1. The bridge rests on a skewed abutment on the north end and a square abutment on the south end. These abutments are approximately 254 ft apart under the west girder and 155 ft apart

under the east girder. A column is positioned near the middle of the west girder, creating a two-span continuous beam with spans of approximately 126 and 127 ft.

The width of the bridge is 27 ft - 8 in. This distance is spanned by a series of transverse floor beams (W18x64 sections) spaced 4 ft on center. A C9x15 channel runs longitudinally down the center of the floor beams, the entire length of the bridge.

Figure with plan view and thickness tables.

Flange Thickness	Web Thickness	
1-1/2"	1/2"	20'-2"
2"	1/2"	15'-0"
2-3/4"	7/16"	17'-6"
2-3/4"	3/8"	49'-0"
2-3/4"	7/16"	17'-6"
2"	1/2"	15'-0"
1-1/2"	1/2"	20'-2"

East Girder

West Girder

Floor Beams

Box Girders

N

	Web Thickness	Flange Thickness
21'-2"	1/2"	1"
9'-0"	7/16"	1-1/2"
47'-0"	3/8"	1-1/2"
30'-0"	7/16"	1"
40'-0"	1/2"	2"
30'-0"	7/16"	1"
47'-0"	3/8"	1-1/2"
9'-0"	7/16"	1-1/2"
21'-2"	1/2"	1"
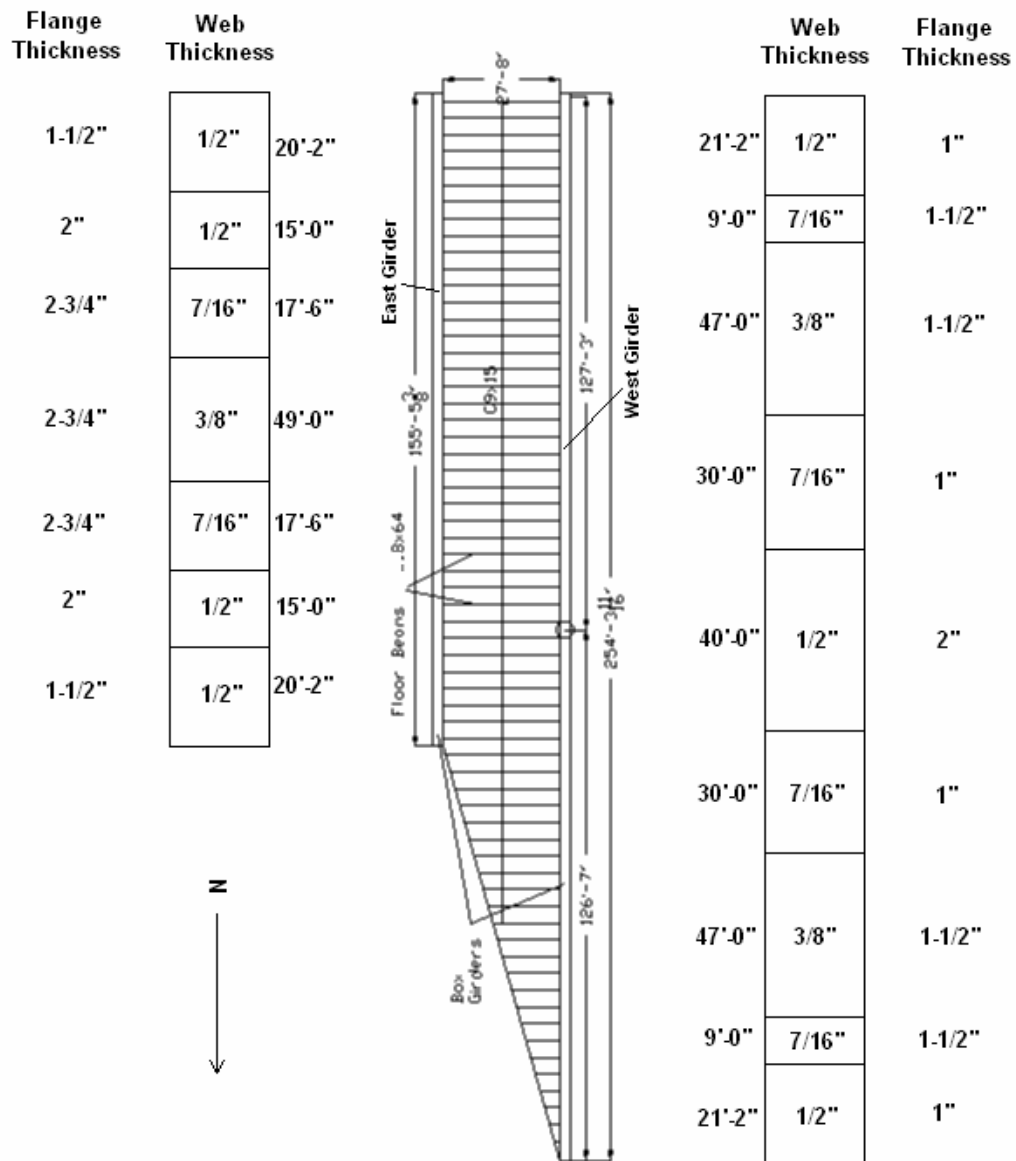
Figure 3-1: Plan View of 1-35 12th Street Exit Ramp

The bridge is considered to be fracture critical because there are only two longitudinal girders. The configuration of the box girder, deck, and floor beam system is shown in Figure 3-2. The box girders have outer dimensions of 4ft in height and 2 ft – 6 in. in width. The flange and web thicknesses vary along the length of the girders. At any location, the same thickness plates were always used to fabricate the top and bottom flanges of the box.

The floor beams are connected to the box girders near the bottom flange with two bolts through a 4-in. wide and ½-in. thick plate. A 7-in. concrete slab is supported by the floor beams, but is not connected to the box girders.

A photograph of the bridge is shown in Figure 3-3. It was taken from a location to the north-west of the bridge. From the picture one can see the diagonal abutment to the left and the midspan column to the right. The large box girders and the closely-spaced floor beams are also apparent.
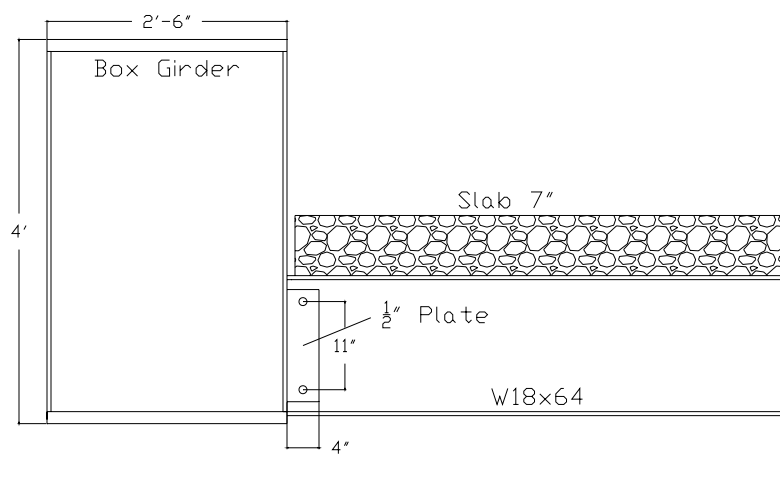
Figure 3-2: Box Girder and Slab Cross-Section

Figure 3-3: Southeast View of Exit Ramp

3.3   FINITE ELEMENT MODEL

A finite element model of the bridge was developed using SAP2000. The first step to creating a model of the 12th Street exit ramp was to input all section sizes. The properties of standard members, such as the C9x15 and the W18x64, are integrated into SAP and do not need to be input by the user. The properties of members that are unique to this structure, such as the box girders, need to be input by the user. As was discussed in Section 3.2, the exterior dimensions of the box girder remain the same, but flange and web thicknesses change regularly along

the length of the girder. Figure 3-4 displays the eight variations in flange and web thickness found in this structure.
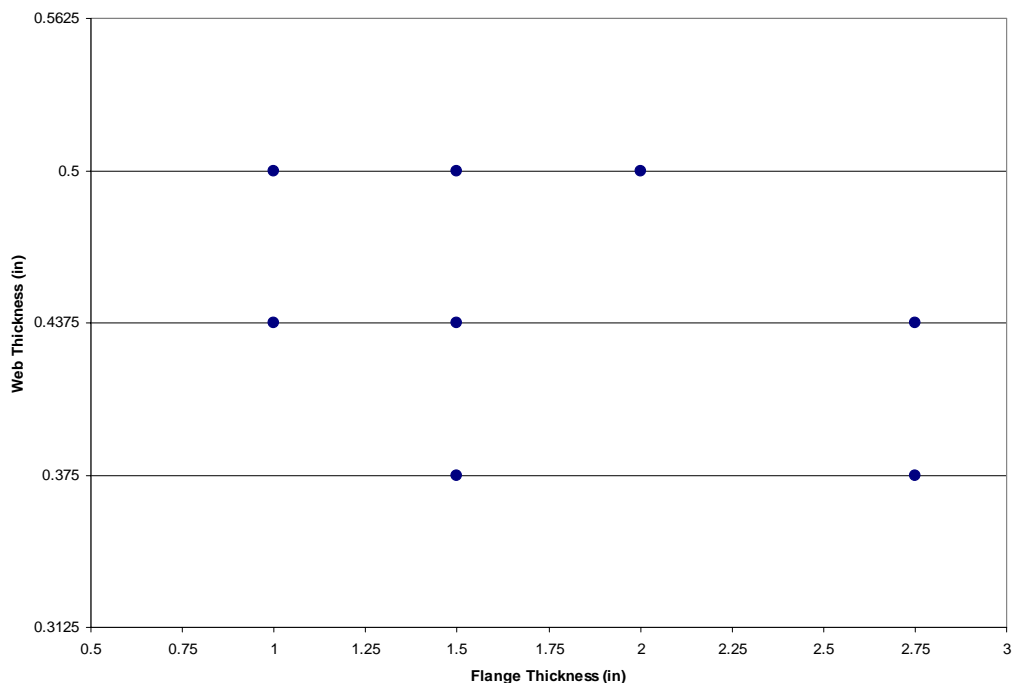
Figure 3-4: Box Girder Variations

Once all the possible box girder sizes were input into SAP2000, the model could be assembled. Figure 3-5 and Figure 3-6 show two different three-dimensional SAP2000 views of the computer model. One can see the small breaks in the continuous box girders which show the areas where the flange thickness changes. The floor beams are visible, as is the center channel running parallel to the girders. The small triangles found under the center of the west box girder and under the two ends represent pinned supports at the column and abutments, respectively.

26
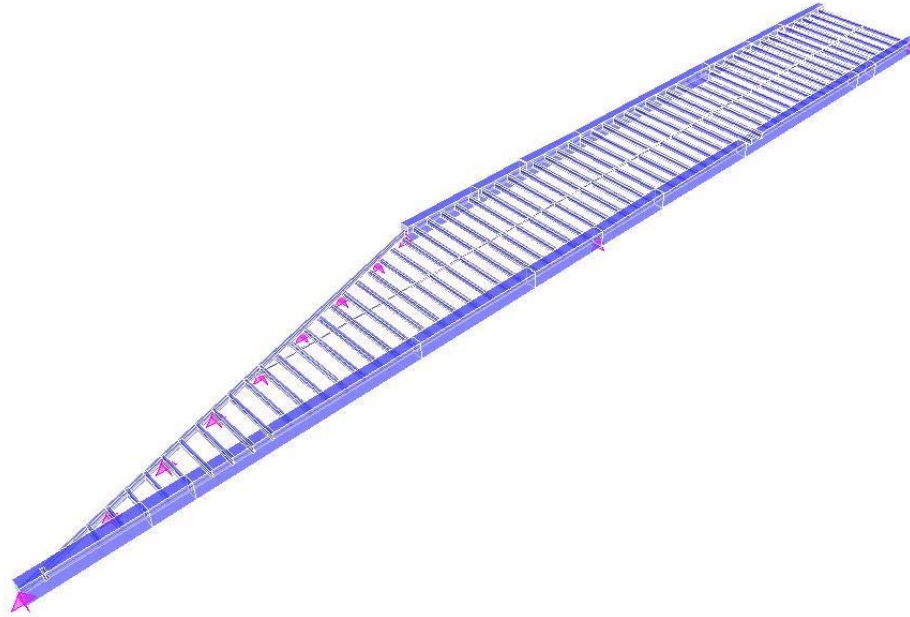
Figure 3-5: View of SAP Model from North West

The slab was not modeled in the finite element program due to its location in respect to the box girders. As seen in Figure 3-2, the slab is supported inside the box girders on the floor beams. Therefore, the slab has no effect on the strain that the box girders experience when subjected to a given moment. In the SAP model, the slab only affects the deformed shape and has no influence on the moments due to a moving load.

27
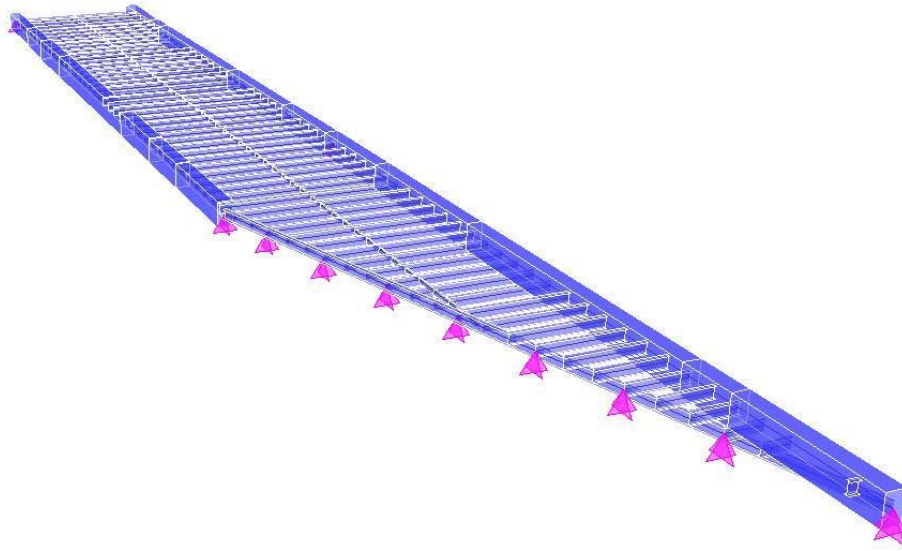
Figure 3-6: View of SAP Model from North East

The initial SAP analysis corresponds to design conditions. Because this bridge is wide enough to carry two lanes of traffic, the bridge was analyzed using two design HS-20 vehicles and lane loads over two lanes of traffic.

The calculated deformed shape of the structure is shown in Figure 3-7. Although the scaling is obviously extreme, the deformed shape can give the user a feeling for where the bridge may see large deformations, and thus, high stresses and strains. The deformed shape indicates the largest deformations near midspan for the east girder and near midspan of the south span for the west girder.

28
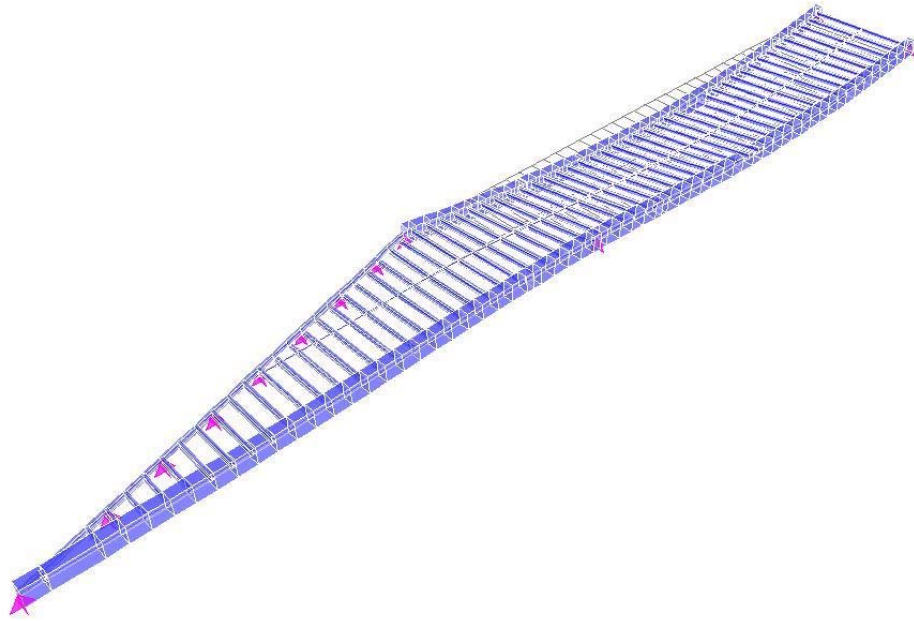
Figure 3-7: SAP Deformed Shape for Exit Ramp

The calculated moment envelopes for the west and east girders are given in Figure 3-8 and Figure 3-9, respectively.
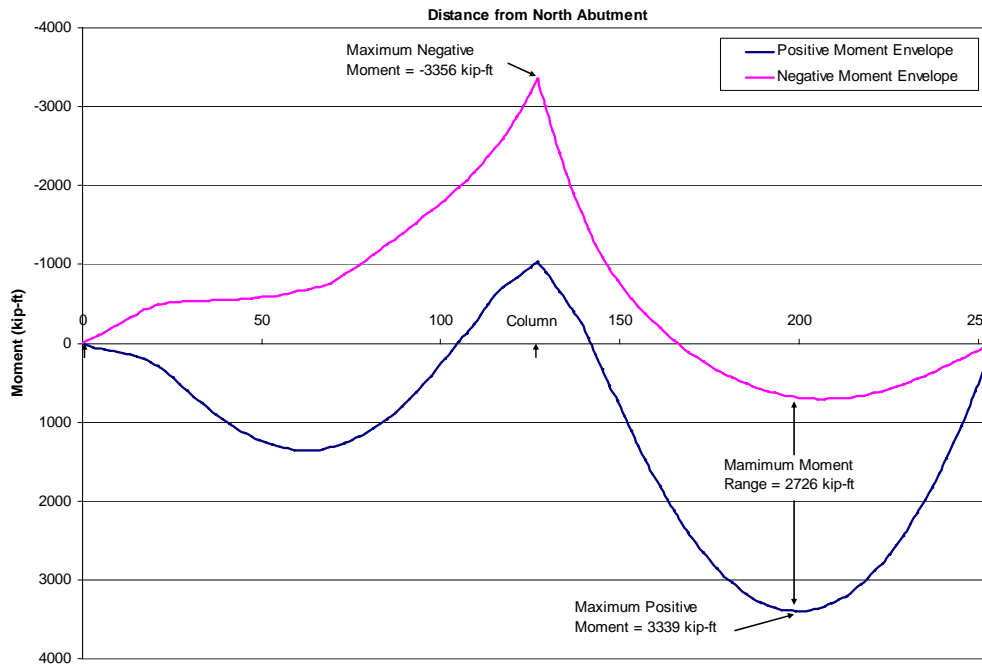
Figure 3-8: Moment Envelope for West Girder

Distance from North Abutment
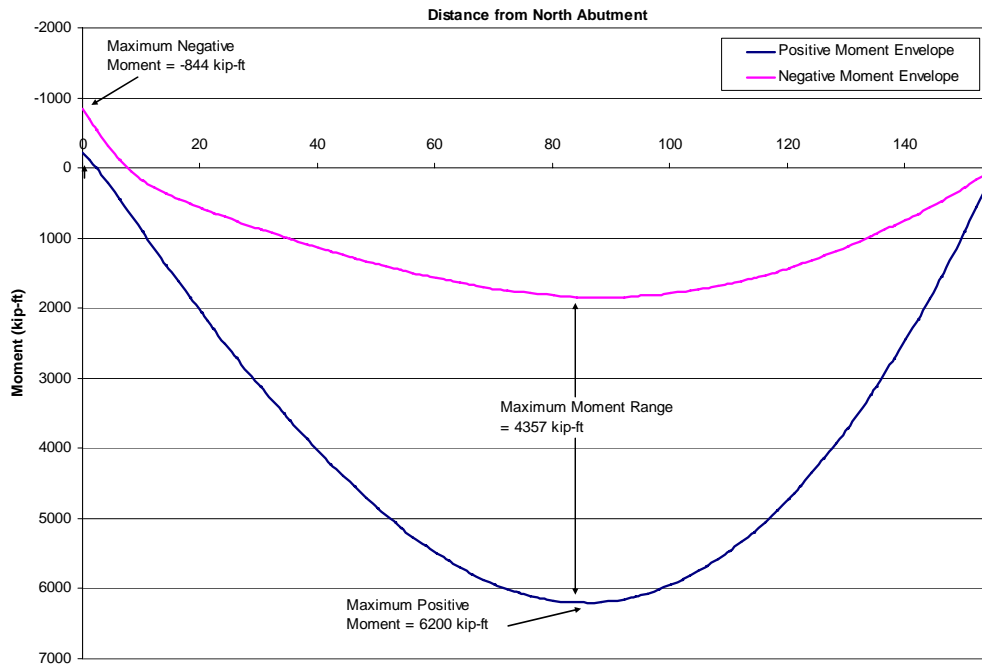
Figure 3-9: Moment Envelope for East Girder

The negative moment occurring at the north end of the east girder is a result of a fixed connection to the beam sitting on top of the abutment. Although all supports in this structure are modeled as pins, which cannot transfer moment, the fixed connection to the beam on the angled abutment can transfer moment. This results in a small negative moment at the north end of the east girder.

The stress in the longitudinal girders can be calculated from the moment envelopes using elementary beam theory:

$$\sigma = \frac{Mc}{I} \tag{3.1}$$

31

where σ is the flexural stress, M is the longitudinal moment, c is the distance from the centroid of the cross section to the neutral axis, and I is the moment of inertia. Because the slab was not attached to the longitudinal girders (Figure 3-2), the values of c and I correspond to the steel box section only. The flexural stresses can be converted into strain by dividing by Young's modulus.

Although the bridge deck is wide enough to accommodate two lanes of traffic, the bridge is marked with one lane and two shoulders. In addition, due to the location of the exit ramp in downtown Austin, very few trucks cross the bridge. Therefore, the recorded strain ranges are expected to be significantly less than those corresponding to the initial SAP analysis.

3.4   MicroSAFE Unit Application

The MicroSAFE units were installed on the 12th Street Exit Ramp on April 21, 2004. At this time, TxDOT was conducting the required fracture critical inspection for the bridge, and a lift truck was available for use by the research team. A two-person team from the University of Texas completed the installation in a couple of hours.

Before the units were installed, the critical areas of the bridge were identified from the SAP2000 output (Figure 3-10). These areas were determined to be midspan of the east box girder (location F) and the midspan of the south span of the east box girder (location D). These locations experience the largest moments, but they also have the largest flange thicknesses. As a result, units were also placed at the change in flange thickness closest to midspan. The flange change on the west box girder was instrumented with location E and the flange change on the east box girder with location G.

32

Instruments were also placed on the north span of the west girder. The maximum moments for this span do not occur near midspan, so the strain gage was applied at the flange change closest to the area of maximum moment (location A). Two other units were installed on the floor beams on either side of the column. Location B is on the floor beam to the north of the column and location C is on the floor beam south of the column. The location of all units is summarized in Table 3-1.

Table 3-1: Unit Locations and Descriptions

Location	Description	Girder	Unit	Notes
A	Flange thickness change	West Girder	1006	Proper data collection
B	Floor beam just north of column	Transverse Floor Beam	1005	Proper data collection
C	Floor beam just south of column	Transverse Floor Beam	1013	Proper data collection
D	Near midspan of south span	West Girder	1002	Proper data collection
E	Flange thickness change	West Girder	1003	Proper data collection
F	Midspan	East Girder	1001	Proper data collection
G	Flange thickness change	East Girder	1004	Strain gage placement error
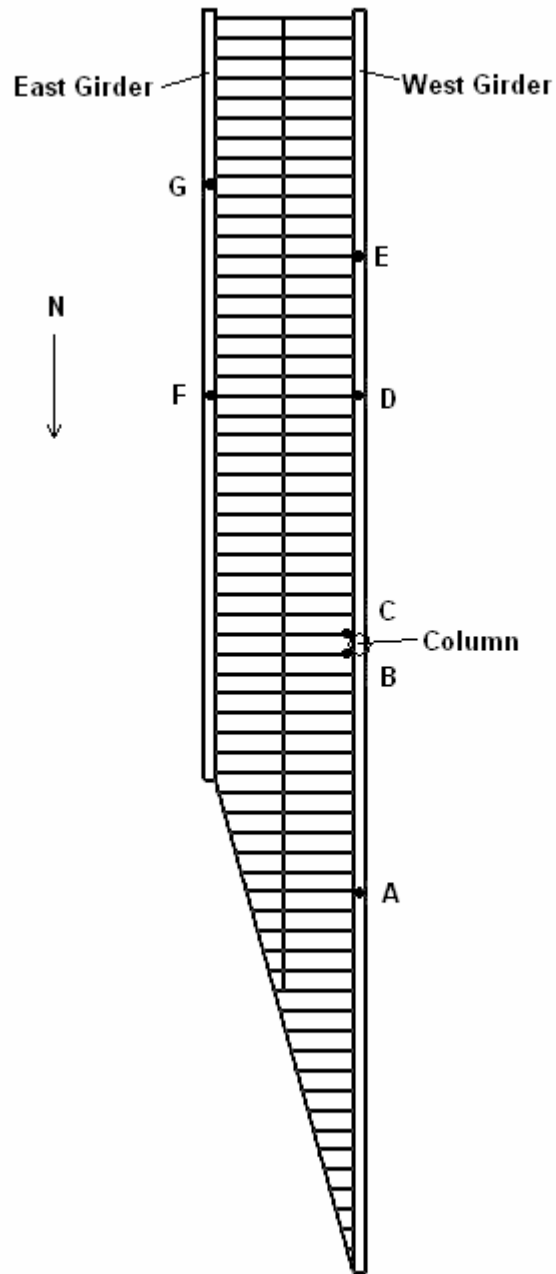
Figure 3-10: MicroSAFE Unit Locations

The first step in the process for installation of the MicroSAFE units
applying the strain gages. Figure 3-11 shows a strain gage being applied at
location G. It is being placed on the thinner flange immediately south of the
change in thickness. One can also see from this figure a closer view of the weld
detail on the box girder and the floor beam framing into the girder.

Figure 3-11: Strain Gage Application

After installing a strain gage, the MicroSAFE device can be set up. As
discussed in Chapter 2, the two components that are left in the field are the battery
and the processor. These are connected to the strain gage via a terminal block.

The units were attached to the bottom flange of the floor beams using velcro. The unit can be seen sitting on the floor beam and being attached to the strain gage in Figure 3-12.

Figure 3-12: MicroSAFE Unit Installation

With the strain gage attached to the MicroSAFE device, data can be collected. Using the communication cable which runs from the battery to the laptop (Figure 3-13), the MicroSAFE sensor was programmed. In this situation, the unit was programmed to collect five minutes of rainflow and raw data. From the resulting histogram and raw data plot, bin sizes could be estimated so all the

data would be captured in a long-term test. The MicroSAFE sensor was then reprogrammed to collect rainflow data for 28 days with the appropriate bin sizes. To collect as much data as possible, the units were set to their maximum length of 23 hours and 59 minutes of data collection per 24-hour period. Figure 3-13 shows the unit being programmed, as well as a good view of the strain gage and MicroSAFE device.

The process of recording five minutes of data and then setting the bin sizes was repeated for all seven units. As it turned out, the bin sizes were set too small, a result of light traffic during the raw data collection period, and the units were placed back into the field for a one-week collection period on July 6, 2004. For this period the bin sizes were increased significantly, most by a factor of 2.5, and all data except for one or two cycles fell within the revised limits.

Figure 3-13: Recording Raw Data

CHAPTER 4

Comparison of Results and Fatigue Life Analysis

4.1 OVERVIEW

The measured response of the 12th Street Exit Ramp from Southbound I-35 in downtown Austin is presented in this chapter. The rainflow data are discussed in Section 4.1 and the results of the SAP analyses are summarized in Section 4.2. The measured response is compared with the calculated results in Section 4.3. Fatigue analyses of the bridge are discussed in Section 4.4.

4.2 MEASURED RAINFLOW DATA

The rainflow data collected for the 12th Street exit ramp were gathered during two separate periods. The first was a 28-day period beginning on April 21, 2004. The second period lasted 7 days and began on July 6, 2004. Throughout this chapter, the 28-day period will be called Phase 1 and the 7-day period will be called Phase 2.

4.2.1 Temperature Effects

The first major concern when dealing with rainflow data is the effect of temperature fluctuations on the results. An indication of the influence of thermal cycles was obtained during the second period that the Medina River Bridge was instrumented (Chapter 6). Because the results from that investigation influence all the rainflow data, the data are presented in this section. The thermal response of an aluminum bar with a single, two-wire strain gage was recorded. Because the bar was not attached to the bridge, no load-inducing strain cycles were

39

anticipated. At the end of the 28-day recording period, one strain cycle was measured each day. The amplitude of the daily strain cycle is plotted as a function of the maximum temperature variation during the same 24-hr period in Figure 4-1.
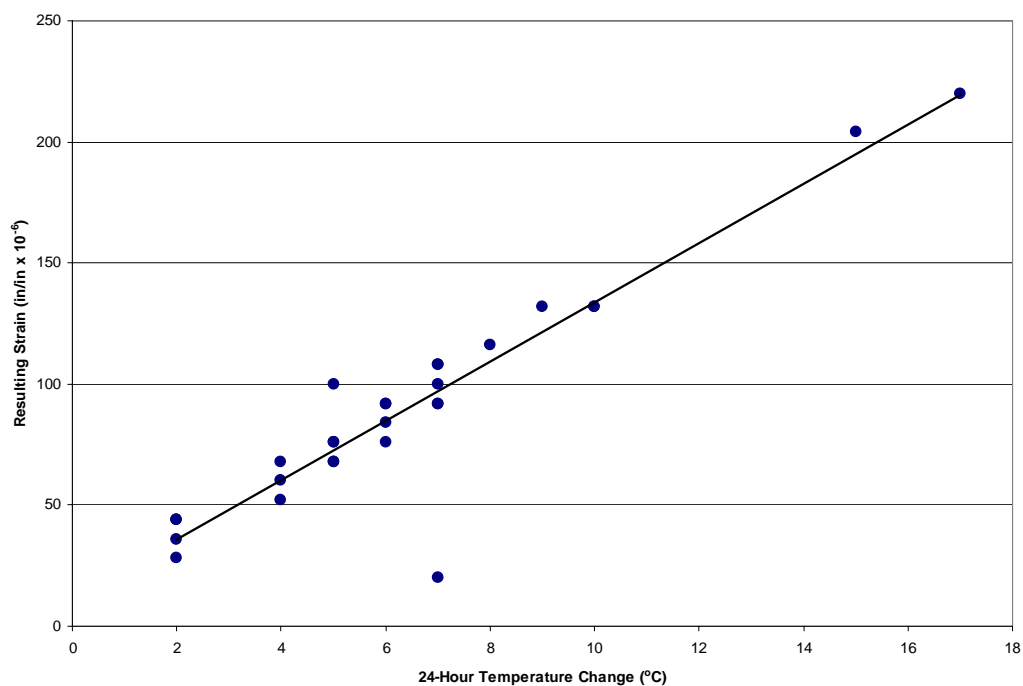
Figure 4-1: Temperature Affected Strains on Aluminum Bar

As expected, the results indicate a linear increase in strain variation with temperature differential. This implies that the rainflow data during each reporting period include one cycle due to temperature variations and numerous cycles due to load variations. The results of this simple test are not directly applicable to bridge monitoring for two reasons: (1) the thermal coefficient of expansion is

larger for aluminum than steel and (2) three-wire strain gages were used in the field and the third wire provides temperature compensation.

A second test was conducted at Ferguson Laboratory. A steel bar was instrumented with two, three-wire strain gages and one, two-wire strain gage. The specimen was monitored for 7 days, and the results are plotted in Figure 4-2. All three strain gages experienced strain cycles due to the thermal fluctuations; however, the magnitude of the strain cycles were less than shown in Figure 4-1 due to the lower coefficient of expansion for steel.
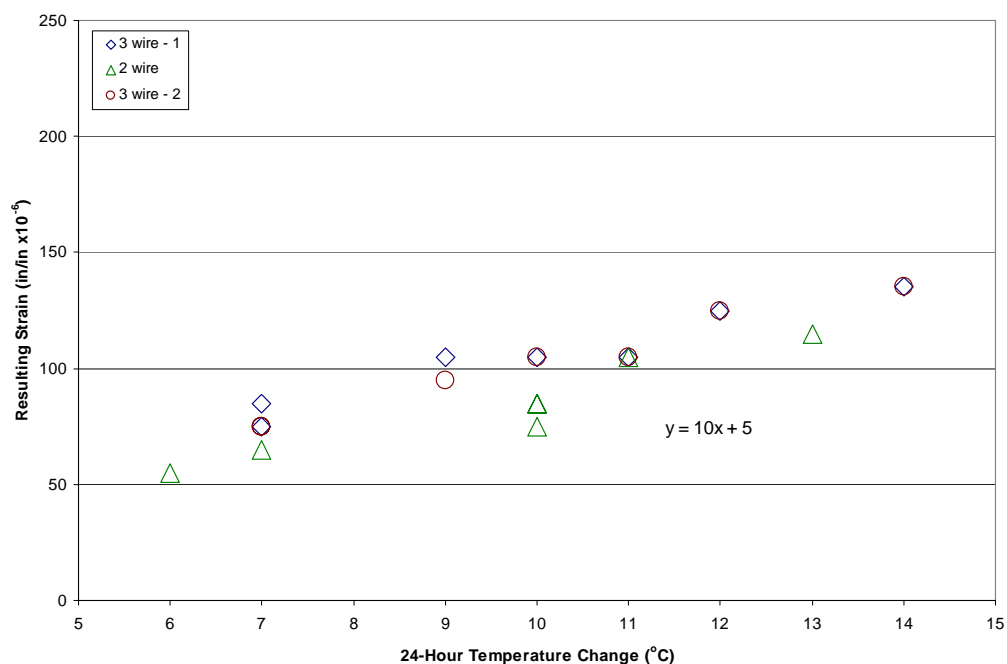
Figure 4-2: Temperature Affected Strains on Steel Bar with 2-Wire and 3-Wire Gages

Although the strain variations due to temperature are easily identified when the strain gage does not experience any loading cycles, the long-period thermal cycles are superimposed with the short-period cycles due to loading fluctuations when the response of the bridge is monitored. Therefore, the strain variation due to the thermal cycles is added to the largest strain variation recorded in the rainflow counts.

The MicroSAFE units record the temperature once an hour when collecting rainflow data, so the data can be corrected to eliminate the influence of temperature. For example, if the lowest temperature of the day, say 9 $^{\circ}$C, was recorded at 6 am and the highest temperature of the day, say 19 $^{\circ}$C, was recorded at 3 pm, then the temperature related-strain would be approximately 105 microstrain (Figure 4-2). As will be discussed in section 4.2.2, the bin sizes selected during Phase 2 were sufficiently large that essentially no cycles were recorded in the largest bin. However, a single cycle was typically recorded in a bin that was significantly larger than all other cycles. The raw rainflow data recorded during Phase 2 at location D are summarized in Table 4-1. The rainflow counts from the smallest twelve bins are not included in this table. During each of the seven days, a single cycle was recorded with a strain range at least 70 $\mu\varepsilon$ larger than the next largest cycle was recorded. The maximum temperature change for each day is the corresponding thermal strain range estimated from Figure 4-2 are also reported.

Table 4-1: Partial Rainflow Data Unadjusted for Temperature Effects

Location D							
Period Number:	1	2	3	4	5	6	7
Bin Median ($\mu\varepsilon$):							
105	0	1	3	1	0	2	0
115	1	1	1	0	0	0	2
125	1	1	1	1	0	0	0
135	0	0	0	0	0	0	1
145	1	0	2	1	1	0	3
155	2	0	0	0	0	0	0
165	0	0	0	0	0	0	0
175	0	0	0	0	0	1	1
185	0	0	0	0	0	0	0
195	0	0	0	0	0	0	0
205	0	0	0	0	0	0	0
215	0	0	0	0	0	0	0
225	0	0	0	0	0	0	0
235	0	0	0	0	0	0	0
245	0	0	0	0	1	0	0
255	1	0	0	0	0	0	0
265	0	0	0	0	0	0	0
275	0	1	1	0	0	0	0
285	0	0	0	1	0	0	0
295	0	0	0	0	0	0	1
Estimated Thermal Strain Range ($\mu\varepsilon$)	105	105	105	125	85	95	115

The estimated thermal strain range was then subtracted from the median strain in the largest bin with a recorded cycle. A cycle was added to the corresponding bin. The results are reported in Table 4-2, where all cycles exceeding 190 $\mu\varepsilon$ have been eliminated.

The correction is important because the largest recorded strain range is used to determine if the structure has a finite or infinite fatigue life.

All rainflow data reported in this chapter and in Chapter 6 were corrected for temperature effects using this procedure.

Table 4-2: Rainflow Adjusted for Temperature Effects

Location D							
Period Number:	**1**	**2**	**3**	**4**	**5**	**6**	**7**
Bin Median ($\mu\varepsilon$):							
105	0	1	3	1	0	2	0
115	1	1	1	0	0	0	2
125	1	1	1	1	0	0	0
135	0	0	0	0	0	0	1
145	1	0	2	1	1	0	3
155	3	0	0	0	1	0	0
165	0	0	0	1	0	0	0
175	0	1	1	0	0	0	1
185	0	0	0	0	0	0	1
195	0	0	0	0	0	0	0
205	0	0	0	0	0	0	0
215	0	0	0	0	0	0	0
225	0	0	0	0	0	0	0
235	0	0	0	0	0	0	0
245	0	0	0	0	0	0	0
255	0	0	0	0	0	0	0
265	0	0	0	0	0	0	0
275	0	0	0	0	0	0	0
285	0	0	0	0	0	0	0
295	0	0	0	0	0	0	0

4.2.2 Measured Rainflow Response

Sample histograms from each phase of monitoring are shown in Figures 4-3 and 4-4. These histograms include all the data recorded during the monitoring period (noise is included). These bars represent the number of times that a cycle of a given strain range occurred during the 28-day and 7-day periods. Note that the maximum strains were 128 microstrain for Phase 1 and 320 microstrain for Phase 2. As explained earlier, the maximum strains are a direct result of the selected bin size. There are thirty-two bins which collect the rainflow data. A bin size of 4 $\mu\varepsilon$ was used in Phase 1 and it was increased to 10 $\mu\varepsilon$ in Phase 2.
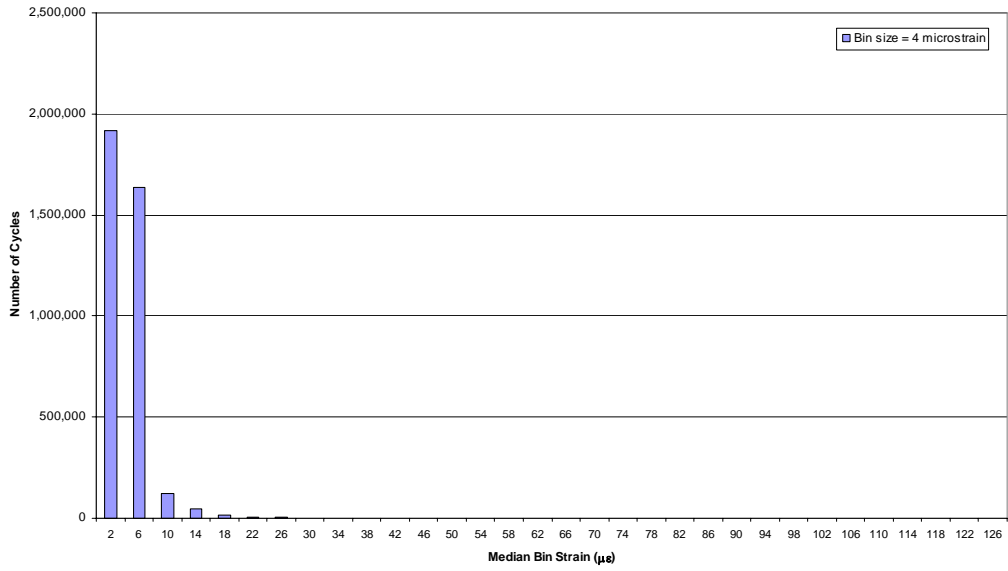
Figure 4-3: Rainflow Data Recorded by Location D during Phase 1
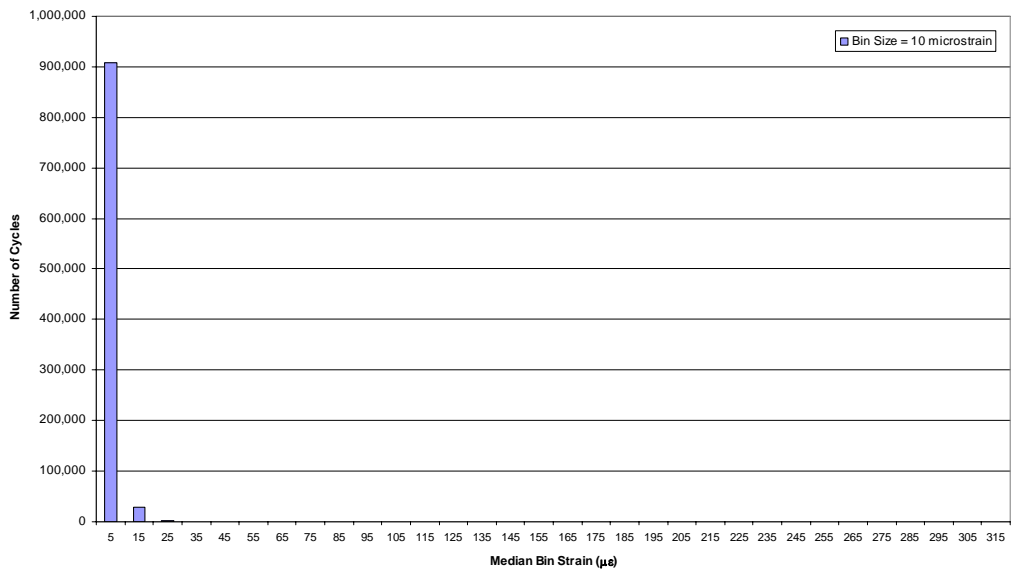
Figure 4-4: Location D during Phase 2

45

While these two plots display the data from only one unit (Location D), these histograms are representative of the other units. The most noticeable characteristic of both of these plots is the very large number of cycles in the lowest bins. This observation highlights the usefulness of two different phases of testing. In Phase 1, the smaller maximum strain (and thus, smaller bin size) allows for more than 90% of the data to fall in the first two bins, but does not have a sufficient number of bins to record the maximum measured strain. The last bin included 120 counts, meaning there were 120 cycles with a strain range larger than 124 $\mu\varepsilon$. While this may be useful information, it is probably more important to determine the maximum strain experienced by the bridge.

Phase 2 was designed to obtain this information. Figure 4-4 demonstrates that more than 95% of the data fall within the first bin during Phase 2. But in this case, no cycles were recorded in the last bin (mean strain of 315 $\mu\varepsilon$). The largest cycle corresponded to a median strain of 194 $\mu\varepsilon$ (Figure 4-12). The knowledge that the largest strain cycle recorded was between 187.5 and 200 $\mu\varepsilon$ in Phase 2 is much more useful than the knowledge that there were 120 cycles larger than 124 $\mu\varepsilon$ during Phase 1.

Figure 4-3 and Figure 4-4 are successful tools in demonstrating the large number of counts which fall in the first few bins, but do not provide much information about the number of cycles at the higher strain levels. This information is more easily viewed in a semi-log plot.
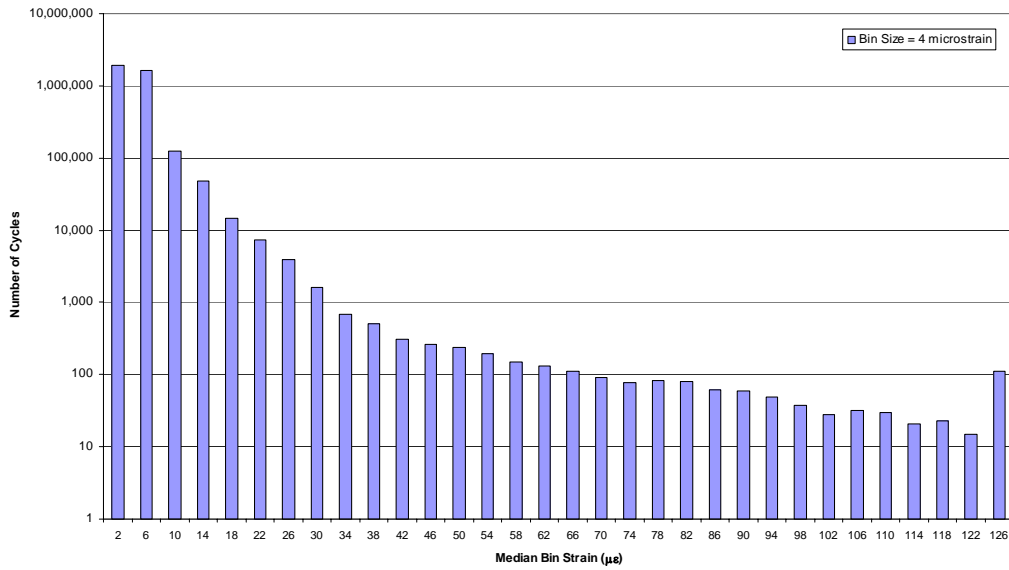
Figure 4-5: Semi-logarithmic Plot of Location D during Phase 1
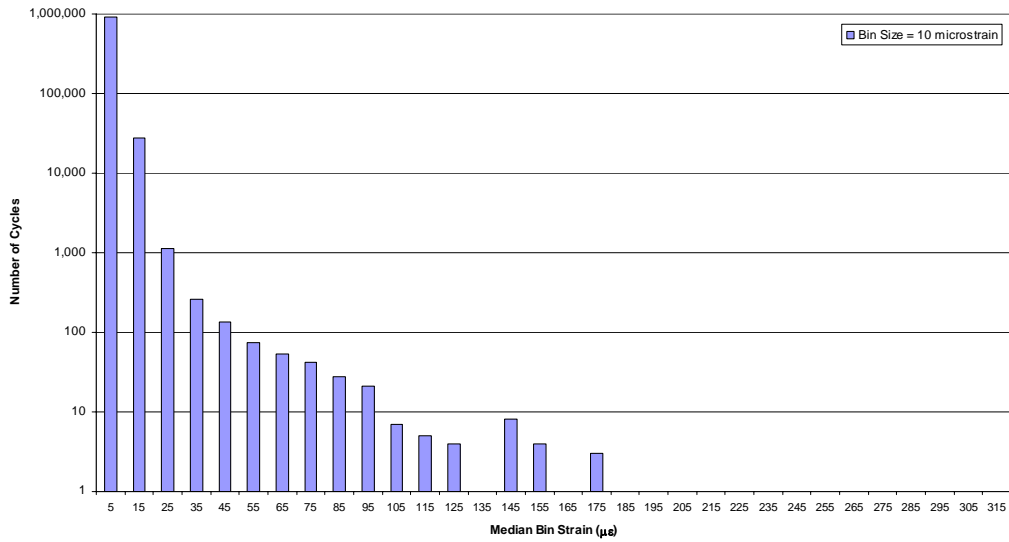
Figure 4-6: Semi-logarithmic Plot of Location D during Phase 2

Figure 4-5 clearly demonstrates why the data collected during Phase 1 were insufficient. The first thirty-one bins display the expected trend of decreasing numbers of cycles with increasing median strain, but a spike occurs in the last bin. By increasing the bin size, the maximum strain range is captured (Figure 4-6).

4.2.3   Response at Locations of Maximum Positive Moment

Two units were placed at locations where maximum positive moments were expected from the finite element model. Referring to Figure 3-10, these two locations were near midspan of the east girder (Location F) and near midspan of the south span of the west girder (Location D). The histograms for Location F are shown in Figures 4-7 and 4-8, for Phases 1 and 2, respectively. The response of Location D is shown in Figures 4-5 and 4-6.
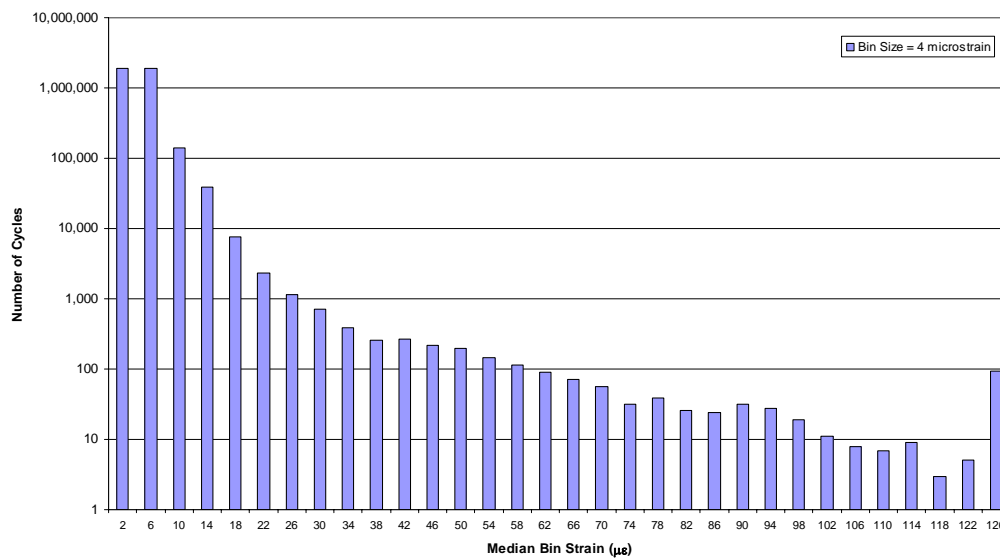
Figure 4-7: Semi-logarithmic Plot of Location F during Phase 1

Figure 4-8: Semi-logarithmic Plot of Location F during Phase 2

In order to compare the maximum positive moment response with the response at other locations along the bridge, a few points should be selected for easy comparison. The highest median bin strains that experienced more than 10,000, 1000, and 100 rainflow counts are summarized in Table 4.1. For Location F, the respective bin medians are 14, 26, and 58 $\mu\varepsilon$. For Location D, the bin medians are 18, 30 and 66 $\mu\varepsilon$. From these select data points, it can be determined that Location D experiences more cycles at larger strain ranges. While this is not a quantitative analysis, it is a quick way to compare the results from different locations because the same number of vehicles passed each location.

4.2.4   Response at Locations of Changing Flange Thickness

Three units were placed on the 12th Street exit ramp at locations where the flange thickness changed. These locations were determined by finding the

49

position of the maximum positive moment and moving the unit toward the support to the location where the flange thickness decreased. While these locations see less moment, the reduction in cross-sectional area increases the resulting strain. As a result, the locations were compared with the locations of maximum positive moment.

One unit was placed along each of the three spans. Location E was along the south span of the west beam, location G was along the east span, and location A was along the north span of the west beam. Data from Location G will not be presented because the unit malfunctioned within hours of the start of the collection period. The unit was tested in between periods and determined to be working correctly. However, when placed back in the field, the unit began to once again receive erroneous data. It has since been determined that the errors were likely caused by the strain gage rather than the MicroSAFE unit.

Data from location E are shown in Figures 4-9 and 4-10, and data from location A are shown in Figures 4-11 and 4-12.
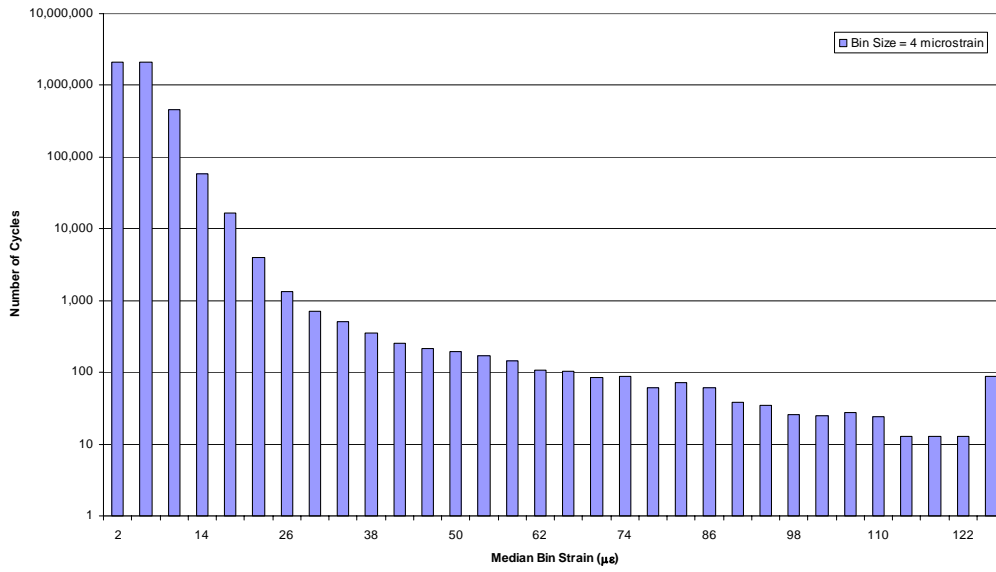
Figure 4-9: Semi-logarithmic Plot of Location E during Phase 1
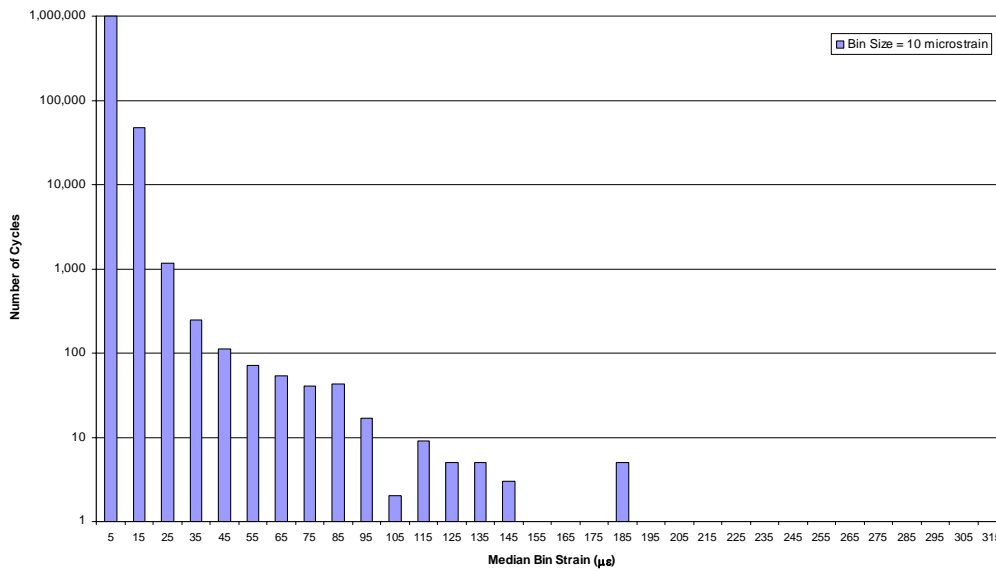
Figure 4-10: Semi-logarithmic Plot of Location E during Phase 2

51

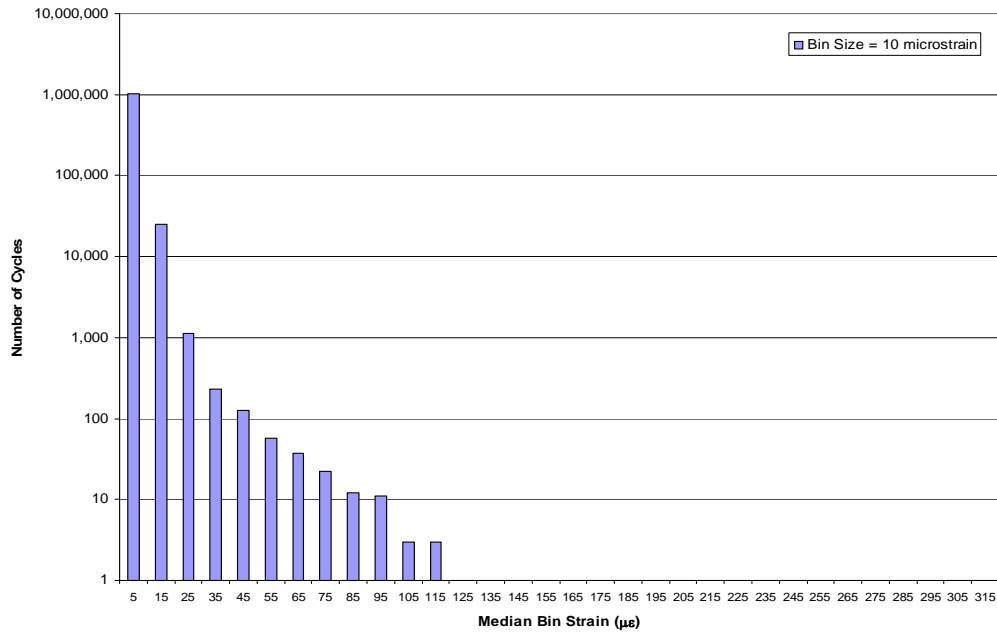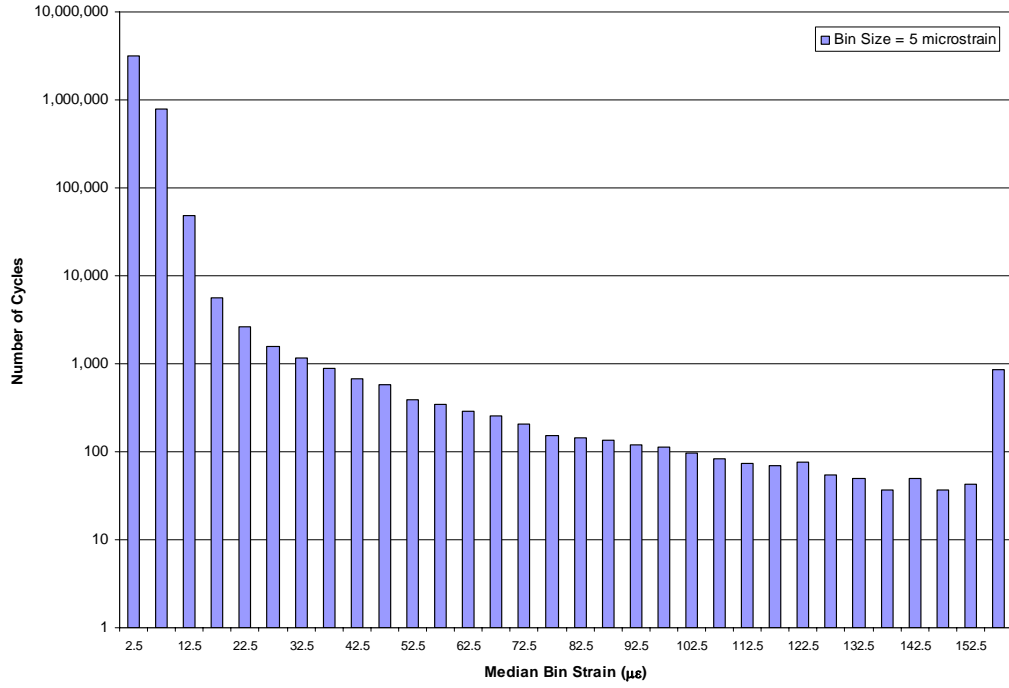*Figure 4-11: Semi-logarithmic Plot of Location A during Phase 1*
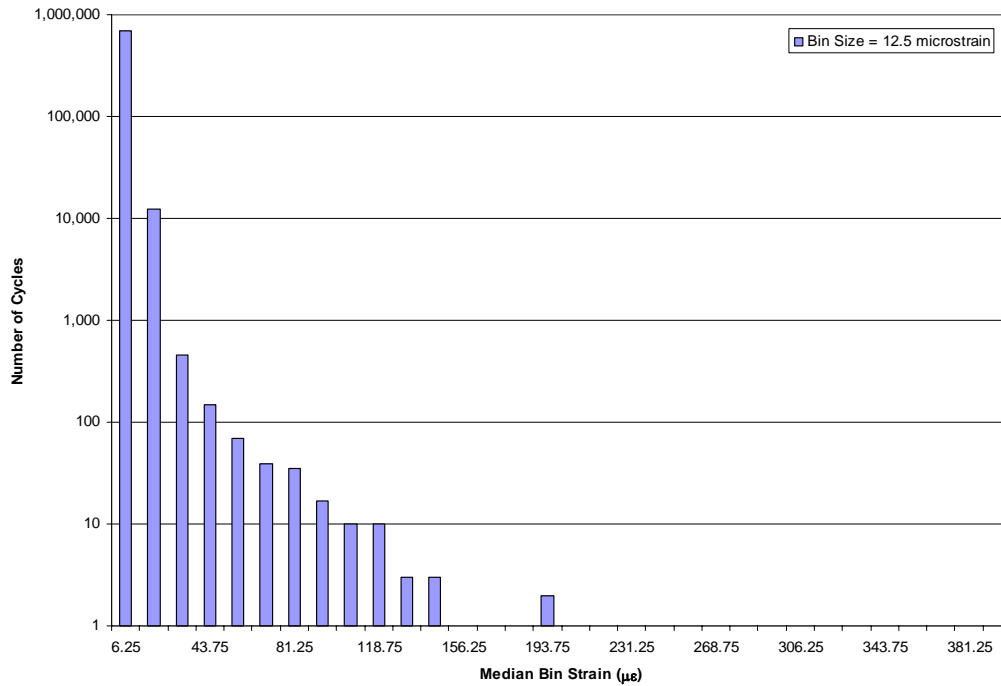
Figure 4-12: Semi-logarithmic Plot of Location A during Phase 2

As discussed in Section 4.2.3, the highest median bin strains that recorded rainflow counts of 10,000, 1000, and 100 provide a simple means of comparing the response at different locations.

These results are summarized in Table 4-3 and indicate the importance of monitoring strains at locations where the moment may not be highest, but where there is a decrease in cross-sectional area. Location E experienced strain ranges very similar to those at location D and location A experienced the largest number of high strain cycles. The importance of these observations will be discussed in Section 4.5 where the fatigue life analyses are presented.

Table 4-3: Simplified Comparison of Rainflow Data for Longitudinal Girders

Rainflow Counts	Median Bin Strains ($\mu\varepsilon$)			
	Location			
	F	D	E	A
10,000	14	18	18	12.5
1,000	26	30	26	32.5
100	58	66	66	97.5
1	225	185	195	206
Maximum Stress Range (ksi)	6.5	5.4	5.7	6.0

4.2.5   Response at Locations of Floor Beams

Two units were also placed on the floor beams with the largest negative moment.   Locations B and C were placed, respectively, on the floor beams immediately north and south of the column along the west beam.   The resulting histograms are shown in Figures 4-13 to 4-16.
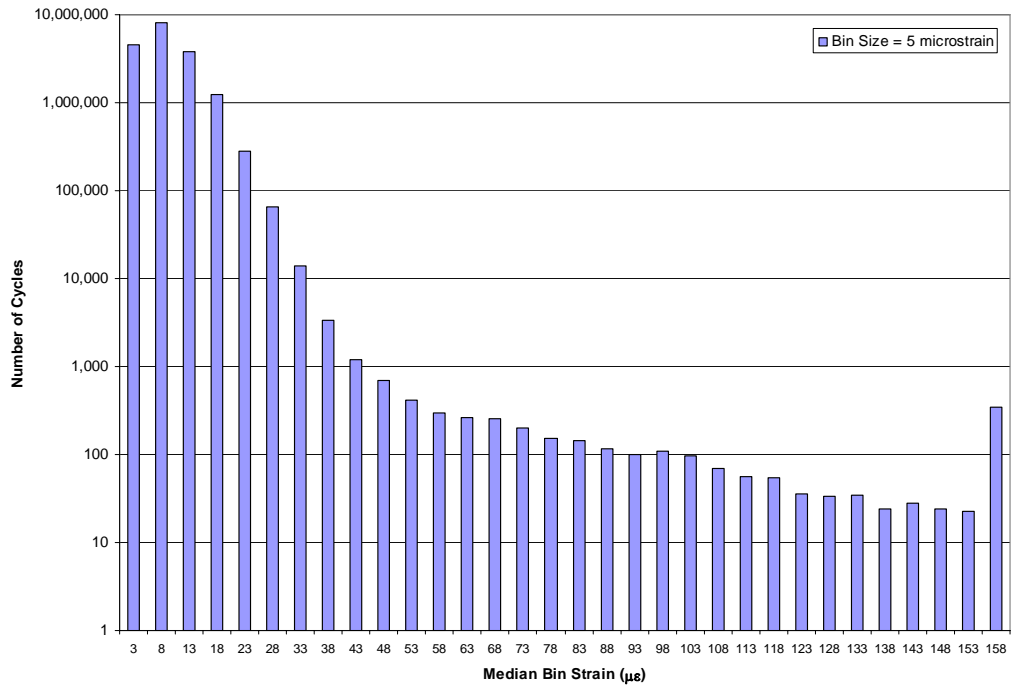
Figure 4-13: Semi-logarithmic Plot of Location B during Phase 1
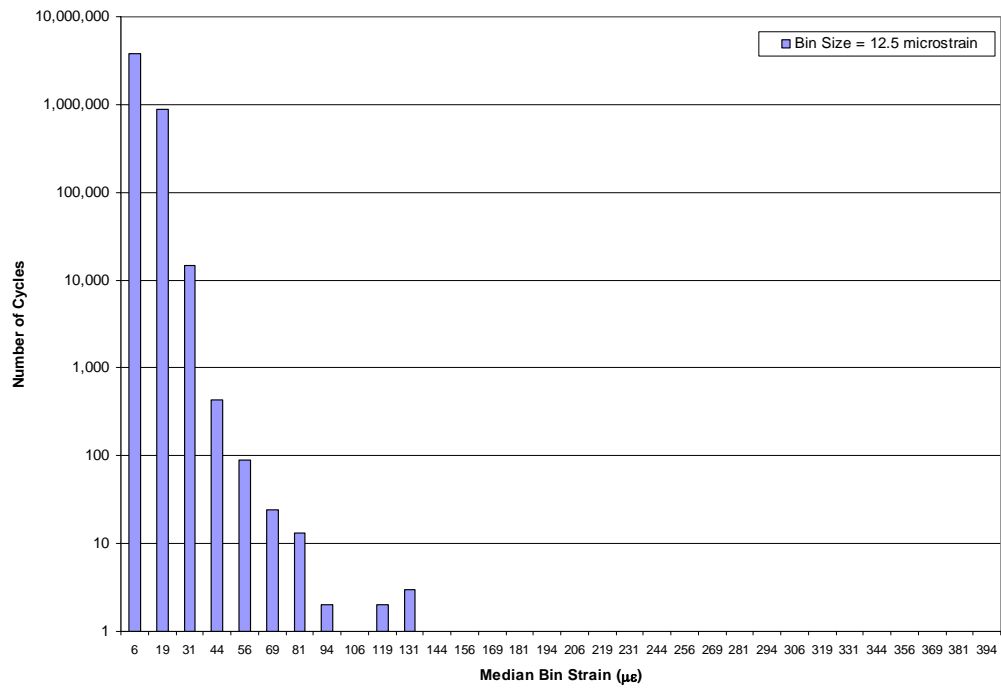
Figure 4-14: Semi-logarithmic Plot of Location B during Phase 2
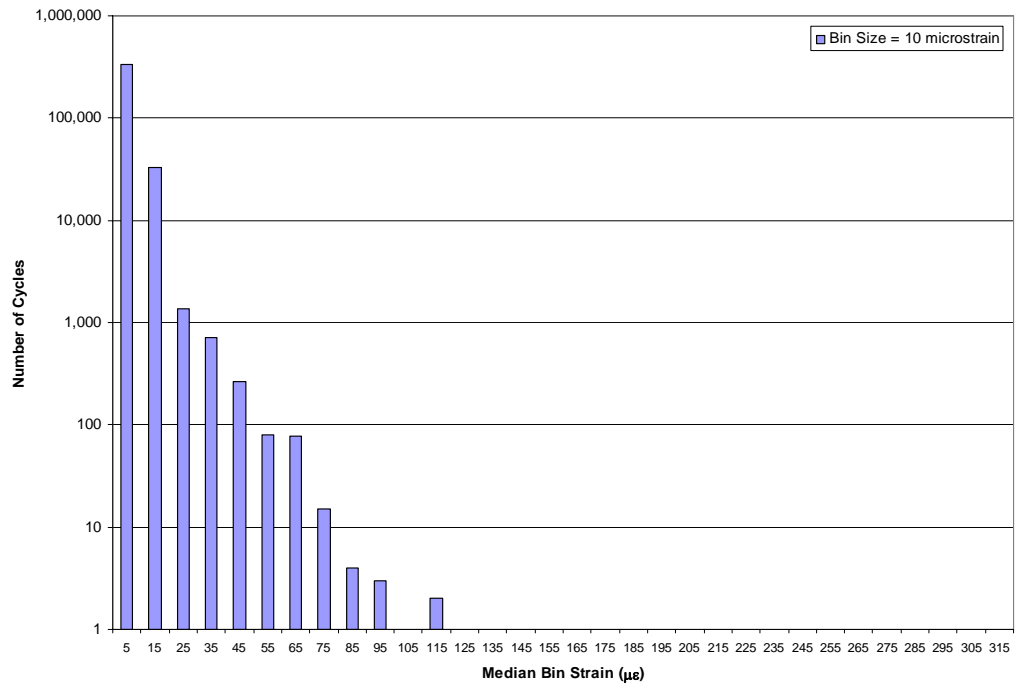
Figure 4-15: Semi-logarithmic Plot of Location C during Phase 1
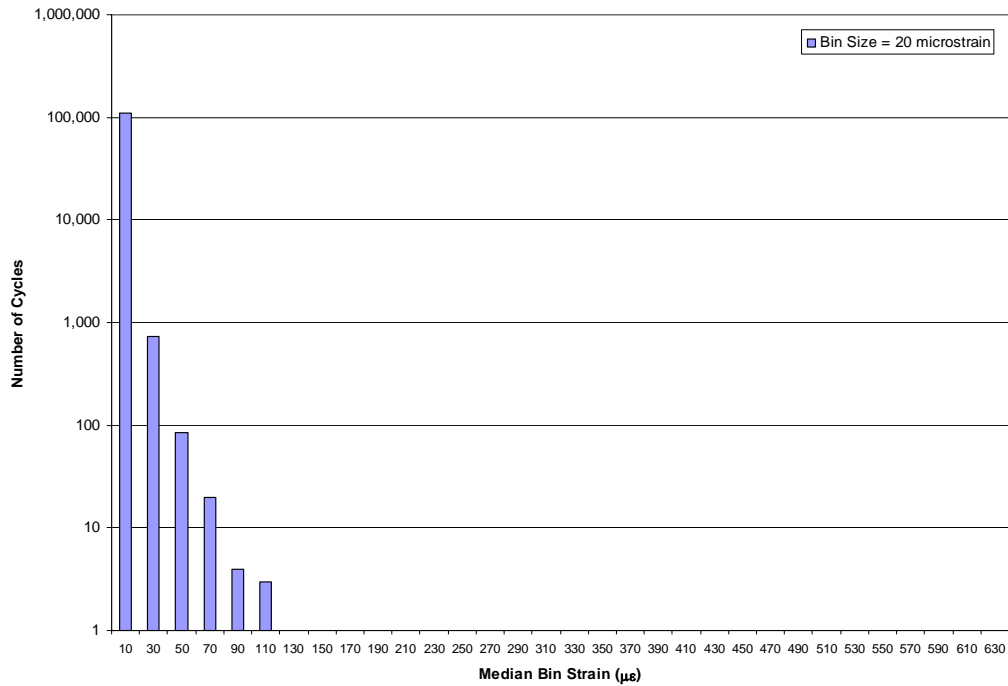
Figure 4-16: Semi-logarithmic Plot of Location C during Phase 2

During the first phase of monitoring, location B was unique because more cycles were recording in the second bin than in the first bin. This peculiarity was not observed at location C, although the MicroSAFE units were positioned on adjacent floor beams. The fact that significantly higher strain ranges were recorded at location B than location C during the first recording period is also unexpected. The maximum recorded strain ranges were similar during the second recording period.

4.3   SAP AND RAINFLOW COMPARISON

As discussed in Section 3.3, the 12th Street Exit Ramp was originally analyzed using two, HS-20 design vehicles. The resulting moment envelopes for

the west and east girders are shown in Figures 3-8 and 3-9, respectively. To compare these results with the measured rainflow data, the moments must be converted to strains.

The relationship between moment and flexural stress is given below. For this bridge, the moment of inertia was calculated using only the cross-sectional properties of the steel girders. The corresponding strains may be calculated by dividing the flexural stress by Young's modulus.

Because the rainflow bins were saturated during Phase 1, it was not possible to determine the maximum measured strain ranges. However, the analysis was conducted using the maximum effective strain range, which exceeds 99.99% of the total number of measured cycles. An example conversion from strain range to moment is given below:

Location F – Midspan of East Girder

Maximum effective strain range = 66 $\mu\varepsilon$

Modulus of elasticity = E = 30,000 ksi

Distance from centroid to extreme fiber = c = 25.75 in

Moment of Inertia = I = 113,258 in^4

Flexural Stress:

$$\sigma = (66 \times 10^{-6} \frac{in}{in})(30,000 ksi)$$

$$\sigma = 1.98 ksi$$

Moment:

$$M = \frac{I\sigma}{c}$$

$$M = \frac{(113{,}258in^4)(1.98ksi)}{25.75in}$$

$$M = 8{,}700kipin$$

An effective maximum moment range of 8,700 kip-in was calculated from the rainflow data at location F. The corresponding moment output from SAP created by two HS20 trucks was 51,400 kip-in. The same procedure was repeated using the data recorded during Phase 1. The results are summarized in Table 4-4 and Figure 4-17. As expected, the moment ranges inferred from the measured rainflow data are considerably less than the design values.
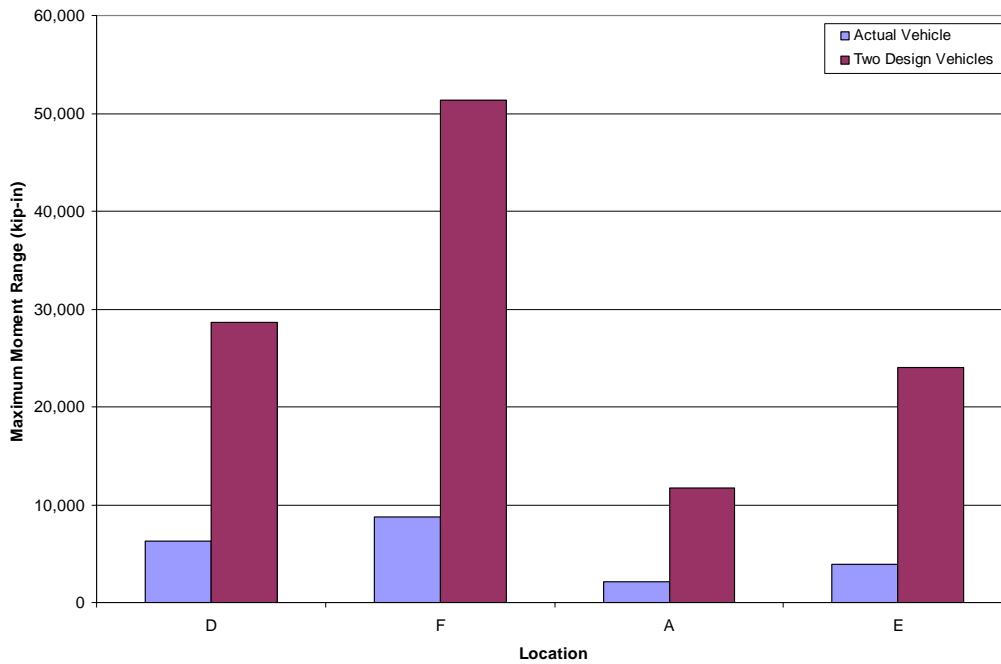
Figure 4-17: Comparison of Calculated and Measured Maximum Moment Ranges during Phase 1

Table 4-4: Moments Inferred from Rainflow Data during Phase 1

	Location					
	D	F	A	E	B	C
Maximum Effective Strain Range (µε)	90	66	42.5	78	67.5	65
E (ksi)	30,000	30,000	30,000	30,000	30,000	30,000
c (in)	24.50	25.75	24.00	24.00	9.20	9.20
I (in^4)	56,866	113,258	40,237	40,237	1,070	1,070
Moment from rainflow data (kip in)	6,270	8,710	2,140	3,920	236	227
Moment from two HS20 trucks (kip in)	28,600	51,400	11,750	24,030	872	922
Percentage of SAP Moment	21.9%	16.9%	18.2%	16.3%	27.0%	24.6%

The above information proves that the bridge does not experience any loads as extreme as two HS-20 vehicles. However, if an average 2-axle truck is used to determine moments, a consistent portion of the rainflow data falls above the 2-axle truck. This means that while the bridge never experiences the design loads, it does experience a few trucks heavier than the average 2-axle truck.

4.4   FATIGUE LIFE ANALYSIS

The first step in the fatigue life analysis is determining the detail category. The AASHTO Design Specifications assign a category of B' for built-up members with continuous, full-penetration groove welds with backing bars in place. However, the TxDOT inspection report identifies multiple locations within this box girder where tack welds are cracked. These flaws reduce the detail category to E for the longitudinal box girders.

The threshold stress range for detail category E is 4.5 ksi. The largest measured stress ranges vary between 3.5 and 5.8 ksi (Table 4-3), and the

61

maximum measured stress range exceeds the threshold stress at locations A, D, and E. Therefore, the longitudinal girders must be considered to have a finite fatigue life.

It is important to note that without the inspection report for the interior of the box girders, a detail category of B' would have been assigned to the longitudinal girders. This category has a fatigue threshold of 12 ksi, which exceeds the maximum stress ranges. If the detail category of B' had been used, the longitudinal girders would be considered to have an infinite fatigue life.

In order to determine the fatigue life, the effective stress range must be calculated. As discussed in Chapter 2, the effective stress range may be calculated directly from the measured rainflow counts.

In order to illustrate the fatigue life calculations, an example set of calculations is described in Section 4.4.1. The calculated fatigue life at each location along the longitudinal girders is prescribed in Section 4.4.2.

4.4.1   Example Fatigue Life Calculation

A portion of the measured rainflow results recorded at location E during Phase 2 are presented in Table 4-5. These data will be used to illustrate the calculations needed to determine the fatigue life. The format of Table 4-5 is similar to the output files from the MicroSAFE units. The first two lines identify the 24-hr collection period. The data in the remaining rows represent the number of cycles recorded above the noise threshold, which was 3 microstrain in this case. The left column contains the median strain for each bin. Ignoring noise for now, the first bin records any cycles between 0 and 10 microstrain, the second bin records any cycles between 10 and 20 microstrain, and so on. Because the noise threshold was 3 $\mu\varepsilon$, the first bin contains the number of cycles with ranges from 3 to 10 $\mu\varepsilon$ and the median strain is 6.5 $\mu\varepsilon$.

The rightmost column in Table 4-5 contains the total number of cycles during the four-day period. In most cases, more than four days of data would be used (usually 28 days), but four days will be used for this example.

Table 4-5: Four Day Rainflow Totals

Period Number:	1	2	3	4	
Date:	7/9/2004	7/10/2004	7/11/2004	7/12/2004	**Four-Day Total**
Bin Median ($\mu\varepsilon$):	Number of Cycles above Noise Threshold				
6.5	144,042	153,155	139,887	137,576	**574,660**
15	6,669	6,689	5,580	6,639	**25,577**
25	141	113	136	194	**584**
35	28	20	33	47	**128**
45	11	6	15	15	**47**
55	8	2	9	13	**32**
65	7	1	11	6	**25**
75	6	2	2	6	**16**
85	3	1	3	5	**12**
95	3	0	0	3	**6**
105	0	0	1	0	**1**
115	0	0	1	3	**4**
125	0	0	0	1	**1**
135	1	1	0	1	**3**
145	1	0	0	0	**1**
155	0	0	0	1	**1**
165	0	1	0	0	**1**
175	0	0	0	0	**0**
185	1	0	0	0	**1**
195	0	0	0	1	**1**
Total Number of Cycles					**601,101**

To continue the fatigue analysis, only the first and last columns are needed. These data are presented in the first two columns in Table 4-6. Column 2 in Table 4-6 is the S_{Ri}, the stress range for that bin. This is calculated by multiplying the median strain by the modulus of elasticity. One point to

63

remember: the bin median in the first column is reported in microstrain, which means that the value must be multiplied by 10^{-6} and then by the modulus to get a stress range in ksi.

Table 4-6: Fatigue Life Information

Median Strain ($\mu\varepsilon$):	Median Stress Range, S_{Ri} (ksi)	Number of Cycles	γ_i	$\gamma_i \times S_{Ri}^3$
6.5	0.195	574,660	0.956	0.0071
15	0.45	25,577	0.043	0.0039
25	0.75	584	0.001	0.0004
35	1.05	128	0.000	0.0002
45	1.35	47	0.000	0.0002
55	1.65	32	0.000	0.0002
65	1.95	25	0.000	0.0003
75	2.25	16	0.000	0.0003
85	2.55	12	0.000	0.0003
95	2.85	6	0.000	0.0002
105	3.15	1	0.000	0.0001
115	3.45	4	0.000	0.0003
125	3.75	1	0.000	0.0001
135	4.05	3	0.000	0.0003
145	4.35	1	0.000	0.0001
155	4.65	1	0.000	0.0002
165	4.95	1	0.000	0.0002
175	5.25	0	0.000	0.0000
185	5.55	1	0.000	0.0003
195	5.85	1	0.000	0.0003
			Total	0.0151
	Effective Stress Range, S_{Re} (ksi)			0.25

The weighting factors, γ_i, are calculated by dividing the total number of cycles in a bin by the total number of cycles in all bins. For this example, the cycles in the noise bin have not been included in the total number of cycles. The values of γ_i are reported in the fourth column of Table 4-6. The last column

represents the product of γ_i and S_{Ri}. The sum of the values in this column is reported, and the equivalent stress range corresponds to the cube root of the sum.

The effective stress at location E for the rainflow data recorded during the four day recording period is 0.25 ksi. The total number of cycles to failure can then be calculated from the effective stress range and the detail category constant defined by AASHTO. The value of A is 11.0×10^8 ksi^3 for a detail category E. The fatigue life, N, can be calculated where n is 3 for welded and riveted connections.

$$N = AS_{Re}^{-3}$$

$$N = (11.0 \times 10^8 \, ksi^3)(0.25 ksi)^{-3}$$

$$N = 70.4 \times 10^9 \, cycles$$

According to Table 4-5, the bridge experienced 601,101 cycles during the four-day period being considered. Assuming this represents an average number of cycles for any four-day period, a fatigue life (FL), in years, can be calculated as:

$$FL = \left(70.4 \times 10^9 \, cycles\right) * \left(\frac{4 days}{601,101 cycles}\right) * \left(\frac{1 year}{365 days}\right)$$

$$FL > 1200 \, years$$

The calculated fatigue life for this location, using only four days of data, is more than 1200 years.

4.4.2 Calculated Fatigue Life for Each Location

In the previous example all the data above the noise threshold were used to describe the fatigue life. The problem is that the noise threshold is selected by the user at the time the MicroSAFE unit is programmed and usually depends on the quality of the raw data collected prior to establishing the rainflow bins. Secondly, the noise threshold must be lower than the bin size, so if small strains are expected and each bin is set to 4 $\mu\epsilon$, for example then the noise threshold can be no greater than 3 $\mu\epsilon$. The lack of standardization in establishing a noise threshold level can be a problem when conducting a fatigue life calculation because the strain level at which loading cycles begin to reduce the fatigue life is not known.

The fatigue life data for the four instrument locations along the longitudinal girders are reported in Tables 4-7 to 4-10. Each table contains the calculated fatigue life for various stress range thresholds. Only the rainflow cycles above the stress range threshold are used to calculate the fatigue life.

Table 4-7: Fatigue Life of East Girder at Location F – Phase 1

Location F				
Description	Lower Limit Stress Range (ksi)	Number of Cycles	S_{RE} (ksi)	Fatigue Life (years)
All cycles (including noise)	0.000	24,526,365	0.118	2,095
All cycles above noise threshold	0.090	4,023,108	0.212	2,197
All cycles above 4 $\mu\epsilon$	0.120	2,095,050	0.259	2,333
All cycles above 8 $\mu\epsilon$	0.240	191,005	0.508	3,366
All cycles above 12 $\mu\epsilon$	0.360	52,364	0.741	3,956
All cycles above 16 $\mu\epsilon$	0.420	14,038	1.096	4,564

Table 4-8: Fatigue Life of West Girder at Location D – Phase 1

Location D				
Description	Lower Limit Stress Range (ksi)	Number of Cycles	S_{RE} (ksi)	Fatigue Life (years)
All cycles (including noise)	0.000	24,538,997	0.131	1,541
All cycles above noise threshold	0.090	3,760,049	0.241	1,596
All cycles above 4 $\mu\varepsilon$	0.120	1,841,156	0.302	1,666
All cycles above 8 $\mu\varepsilon$	0.240	202,716	0.588	2,053
All cycles above 12 $\mu\varepsilon$	0.360	79,472	0.780	2,234
All cycles above 16 $\mu\varepsilon$	0.420	30,926	1.034	2,469

Table 4-9: Fatigue Life of West Girder at Location E – Phase 1

Location E				
Description	Lower Limit Stress Range (ksi)	Number of Cycles	S_{RE} (ksi)	Fatigue Life (years)
All cycles (including noise)	0.000	24,384,231	0.135	1,413
All cycles above noise threshold	0.090	4,748,389	0.230	1,456
All cycles above 4 $\mu\varepsilon$	0.120	2,635,838	0.276	1,521
All cycles above 8 $\mu\varepsilon$	0.240	542,848	0.430	1,949
All cycles above 12 $\mu\varepsilon$	0.360	83,569	0.718	2,732
All cycles above 16 $\mu\varepsilon$	0.420	25,365	1.016	3,175

Table 4-10: Fatigue Life of West Girder at Location A – Phase 1

Location A				
Description	Lower Limit Stress Range (ksi)	Number of Cycles	S_{RE} (ksi)	Fatigue Life (years)
All cycles (including noise)	0.000	24,769,910	0.191	487
All cycles above noise threshold	0.090	3,986,118	0.350	492
All cycles above 5 $\mu\varepsilon$	0.150	840,807	0.584	503
All cycles above 10 $\mu\varepsilon$	0.300	64,582	1.350	531
All cycles above 15 $\mu\varepsilon$	0.450	16,810	2.104	539
All cycles above 20 $\mu\varepsilon$	0.600	11,209	2.404	542

As can be seen from Tables 4-7 to 4-10, the smallest calculated fatigue life is always calculated when all strain cycles are considered. Whether or not the shortest fatigue life is the most accurate is unknown, but it is always the most

conservative. Therefore, all cycles will be used to calculate the fatigue life in this thesis.

As discussed previously, the data included above from Phase 1 are more accurate at lower stress ranges, but the higher stress ranges are truncated. As a result, the calculated fatigue lives are different for the two reporting periods. The larger stress ranges included in Phase 2 increase the effective stress range slightly. This decreases the calculated fatigue life (Table 4-11).

Table 4-11: Calculated Fatigue Life from Phase 2

All Cycles (Including Noise)			
Location	Number of Cycles	S_{RE} (ksi)	Fatigue Life (years)
F	6,136,401	0.129	1,603
D	6,143,064	0.135	1,392
E	3,136,444	0.142	1,195
A	439,853	0.153	956

When compared to Tables 4-7 to 4-10, the effective stress ranges at locations F, D, E, and A increase between 3 and 14% using Phase 2 data. Surprisingly, the effective stress at location A is higher during Phase 1. However, the fatigue life of the 12th Street Exit Ramp is estimated to be more than 500 years. Currently, fatigue is not expected to limit the service life of this structure.

CHAPTER 5

General Information and Setup of the I-35 Medina River Bridge

5.1 OVERVIEW

The second fracture critical bridge examined in this study is the northbound Interstate-35 crossing of the Medina River. This bridge is located approximately 10 miles south of San Antonio, Texas. This bridge provides a unique opportunity as the subject of this study for two main reasons: (1) its unique design utilizes a drop-in center span supported on two cantilevers by large hinges and (2) a state-of-the-art weigh-in-motion sensor is positioned seven miles south of the bridge and records all truck traffic traveling on the roadway. This chapter includes a discussion of the basic geometry of the bridge and the finite element model developed to study its behavior.

5.2 MEDINA RIVER BRIDGE GEOMETRY

The northbound lanes of the I-35 Medina River Bridge were originally designed in 1935 to carry two lanes of traffic. The bridge comprises eleven spans and has an overall length of 273'-4". The structure was widened in the 1960s and the original concrete slab was replaced. During the renovation of the bridge, each of the twelve supports was widened by 18 ft to accommodate an extra lane and shoulder. The width of the original bridge was 30 ft.

The four spans at each end of the bridge are supported by steel girders with a concrete slab. The spans at the north end are 50'-2" long and the spans at

69

the south end are 48'-0" long. Six longitudinal girders supported the original bridge (on left in Figure 5-1). The two external girders were 36-in deep I sections (150 lb/ft) and the interior girders were 33-in deep I sections (125 lb/ft). Three additional girders of the same dimensions as the original exterior girders were added when the bridge was widened (on right in Figure 5-1). The girders in each of the eight spans are simply-supported and the 8-in concrete slab is continuous over all nine girders in the transverse direction. The joints between spans are open above each pier.

Figure 5-1: Underside of the 48-ft Spans on the Medina River Bridge

The center three spans of the bridge are longer than the eight simple spans. The two spans adjacent to the center span are 74'-2" and the center span is 125'-0". Two longitudinal girders support the center three spans in the original bridge.

70

The girders are built-up of plates and angles and vary in depth from 60" to 96". All connections within the built-up members are riveted. The three center spans are considered to be fracture critical. A plan and elevation of the fracture critical spans are shown in Figure 5-2.
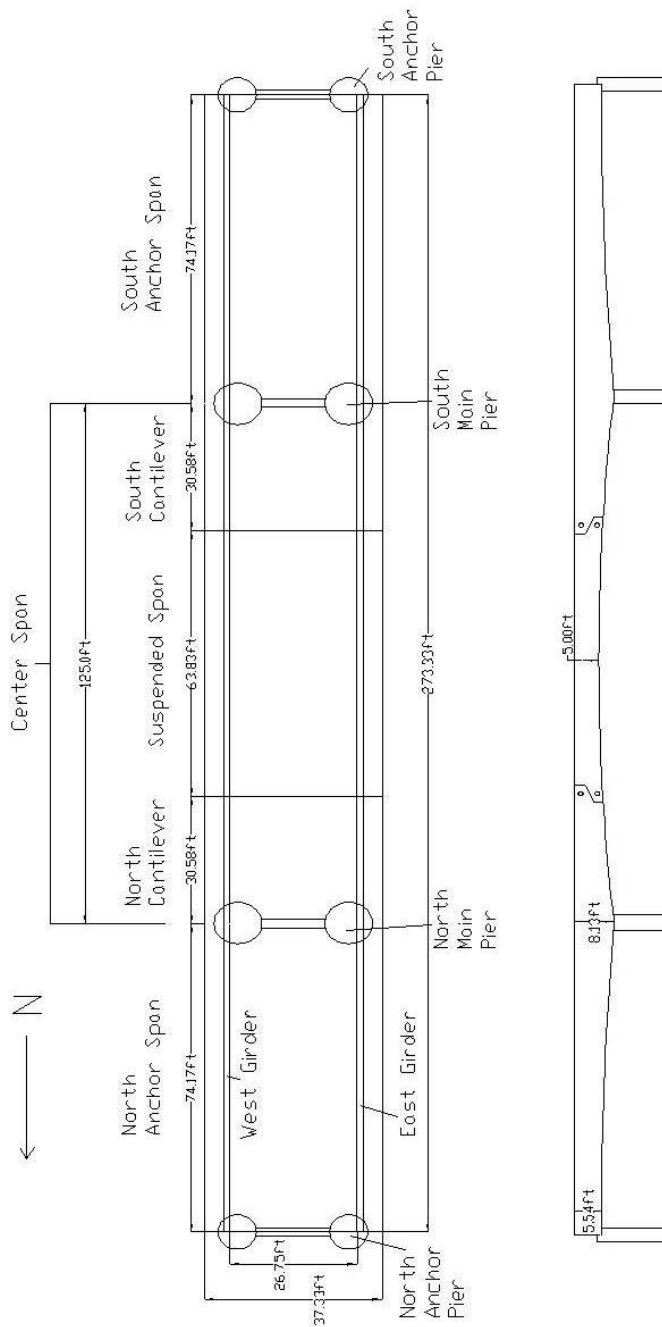
Figure 5-2: Plan and Profile View of Fracture Critical Spans

72

The center span (Figure 5-3) of the original structure is divided into three sections. A 63'-10" suspended span is supported by two 30'-7" cantilever spans. Pins are used to connect the ends of the cantilevers to the ends of the suspended span (Figure 5-4). The longitudinal girders are continuous over the main piers (Figure 5-2). The spans on either side of the cantilevers are called anchor spans, because they provide negative moment restraint for the cantilevers. The longitudinal girders in the anchor spans are simply-supported at the anchor piers (Figure 5-5).

Figure 5-3: Center Span of Medina River Bridge

Figure 5-4: Close-Up of the Cantilevered Span and Hinge

Figure 5-5: Transition from Simple Span to Anchor Span

The structural system used within the new bridge varies considerably from that in the original structure. Three, continuous longitudinal girders support the new portion of the bridge in the three center spans. Because the new and original structure behave very differently under load, the two structures are isolated within the center three spans. A 1-in longitudinal gap separates the concrete decks of the two portions of the bridge.

Only the three, fracture critical spans of the original portion of the Medina River Bridge (Figure 5-2) were instrumented in this investigation. The eight simple spans and the new portion of the center span were not considered to be fracture critical. A cross-sectional view of the center three spans of the original structure is shown in Figure 5-6.
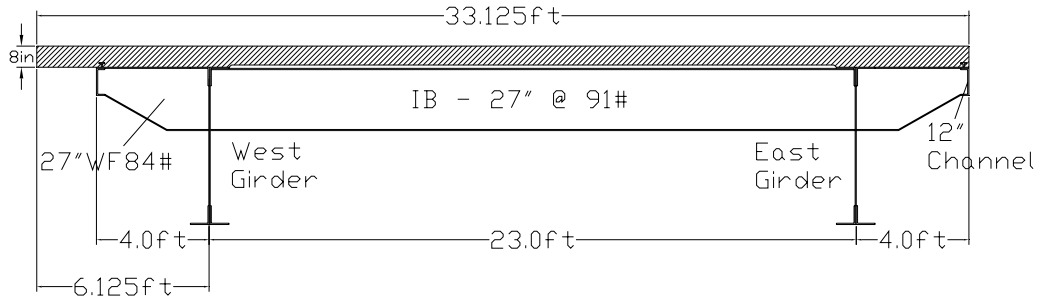
Figure 5-6: Cross-Section of Fracture-Critical Spans

The depth of the longitudinal girders in the anchor span varies from 5'-6½" above the anchor piers to 8'-0" above the main pier. The depth is reduced to 5'-0" at the center of the suspended span. The floor beams are spaced at 7'-6" along the length of the bridge. The transverse, wide flange cantilevers were added in the 1960s when the new portion was constructed. A single shear stud is located at the end of each transverse cantilever (Figure 5-6).

5.3   FINITE ELEMENT MODEL

A finite element model of all eleven spans of the Medina River Bridge was created in SAP2000. Both the original and the new members were included in the model. While it was expected that the new section would have minimal influence on the loading of the original members, the entire bridge was modeled to check this assumption. The results confirmed that the 1-in longitudinal gap was sufficient to isolate load applied to the center three spans of the new structure

76

from influencing the original structure. Only the development of the model of the fracture critical members will be described in this section.

5.3.1 SAP Input

The first step to creating this model was to input all section sizes. The properties of standard members, such as the W27x91 floor beams and the 33x125 I-beams in the end spans, are integrated into SAP2000 and do not need to be input by the user. The properties of members that are unique to this structure, such as the built-up, riveted, longitudinal girders, must be input by the user. As discussed in Section 5.2, the depth of the girders increases with distance from the piers toward the center span. In the actual structure, the variation in depth follows a parabolic curve, but in the SAP model, the variation was modeled as a series of linear changes. This creates a very similar effect. Figure 5-7 shows an elevation of the SAP model. The profile views in Figures 5-2 and 5-7 illustrate the differences between the as-built drawings and the finite element model. In Figure 5-6 the deck sits above the girders which maintain a constant top elevation and the change in depth only influences the elevation of the bottom flange. In SAP, it is easiest to model all members with a constant centerline. In this case, depth variations affect the top and bottom flanges and the slab has the same centroid as the girders. Although the shape of the girders looks different, the model is believed to give accurate results. The choice of effective slab width is discussed in more detail in Section 6.5. All calculations discussed in this section correspond to an effective width of 96 in.
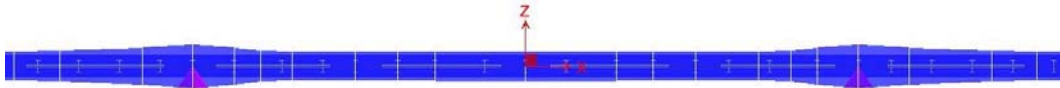
Figure 5-7: SAP Model of Girder Depth Variation

The support conditions at the piers were modeled as pins in SAP. The hinges supporting the suspended span were modeled as end releases of frame elements. The members at the end of each cantilever and the ends of the suspended span were assigned to release M3. The release of M3 means that shear can be carried across the joint but longitudinal moments cannot. The frame end releases are displayed as small dots at the end of each member in Figure 5-8.
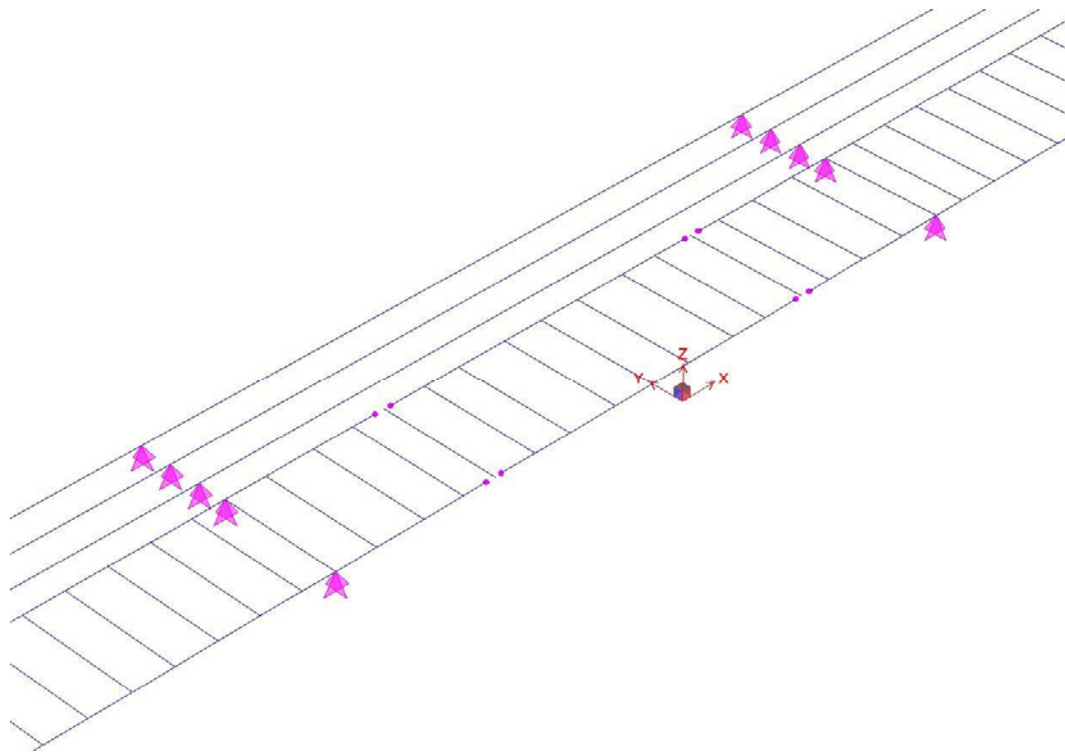
Figure 5-8: Member End Releases to Form Hinges

Figure 5-9 and Figure 5-10 show two different three-dimensional views of the bridge. The varying depth of the fracture-critical members may be seen in the middle three spans. The I-beams in the eight shorter spans at the ends of the bridge are also visible. Rectangles are used to represent the bridge deck and triangles represent the supports.
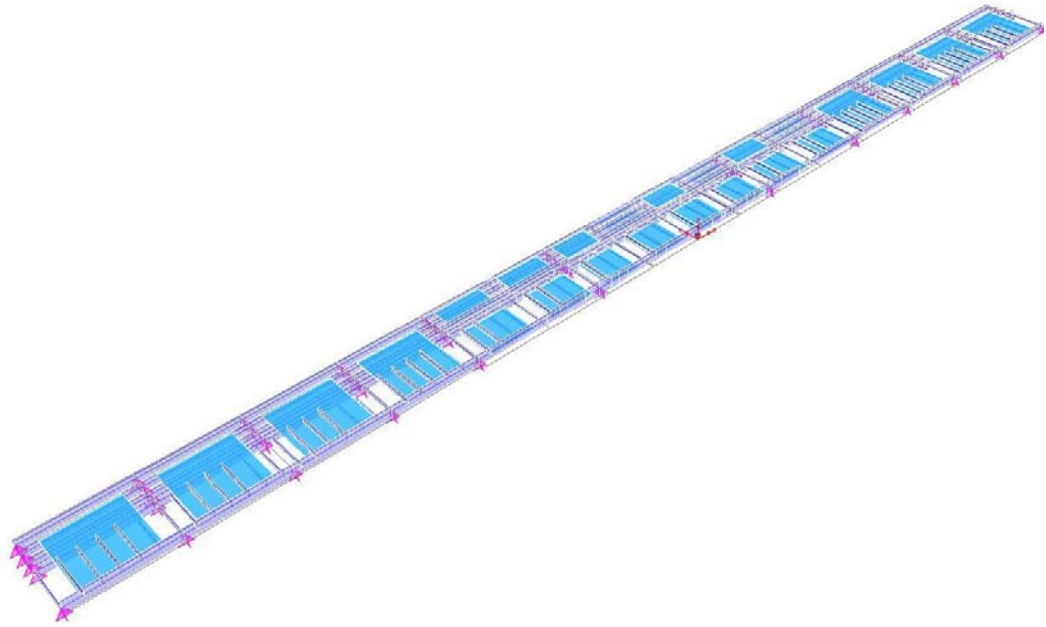
Figure 5-9: Three-Dimensional View of SAP Model
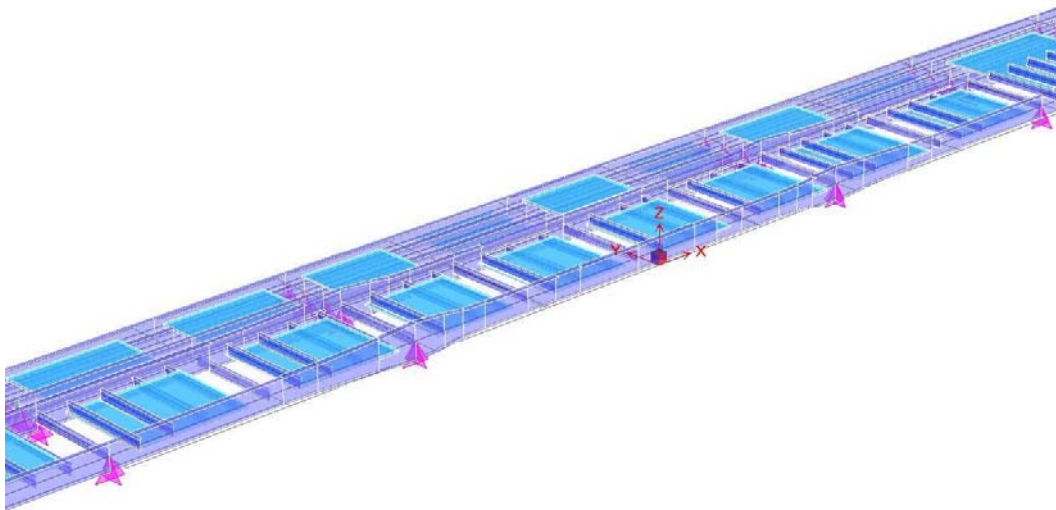
Figure 5-10: Detail of Center Spans in SAP Model

Because the northbound bridge is wide enough to carry three 12-ft lanes of traffic, the bridge was analyzed considering the self-weight, three lane loads, and three HS-20 design vehicles. Per the ASHTO LRFD specifications, the lane load was taken as 0.64 kip/ft. The location of the three lanes corresponds to the lanes marked on the bridge and is shown in Figure 5-11. The HS-20 vehicles were considered as moving loads and the SAP output includes the deflected shape and moment envelopes.
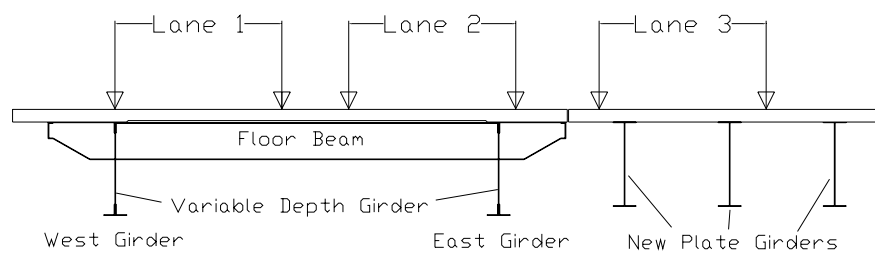
Figure 5-11: Location of Lanes Looking North

5.3.2 Calculated Response of Bridge

The deflected shape is shown in Figure 5-12 to an exaggerated scale. The largest deformations are observed in the anchor spans. Therefore, the largest strains are expected within these spans.
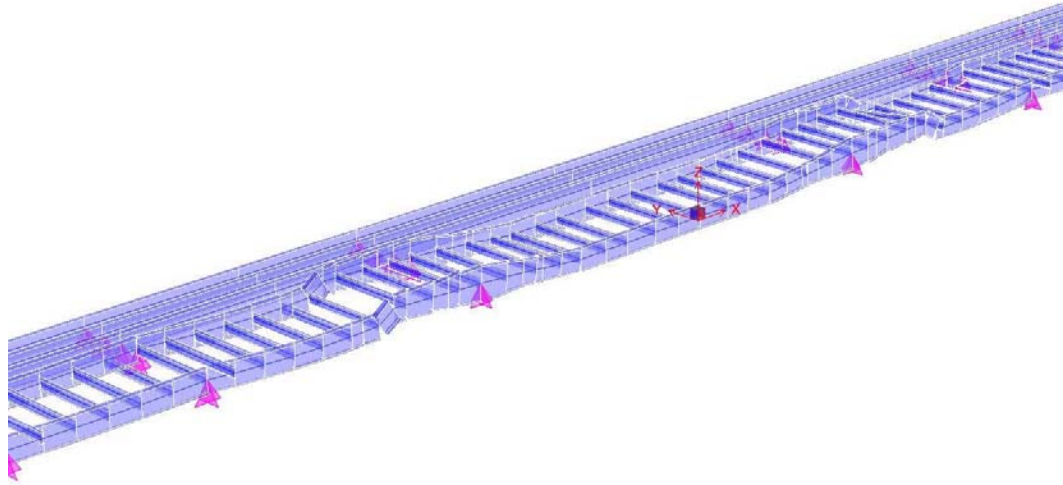
Figure 5-12: Calculated Deflected Shape

The moment envelope for the west girder in the original structure in the north anchor and center spans is shown in Figure 5-13. There is only a slight difference in the moment envelope for the east girder which can be explained by the minor differences in the location of the traffic lanes relative to the girders and the larger deck overhang on the west girder.
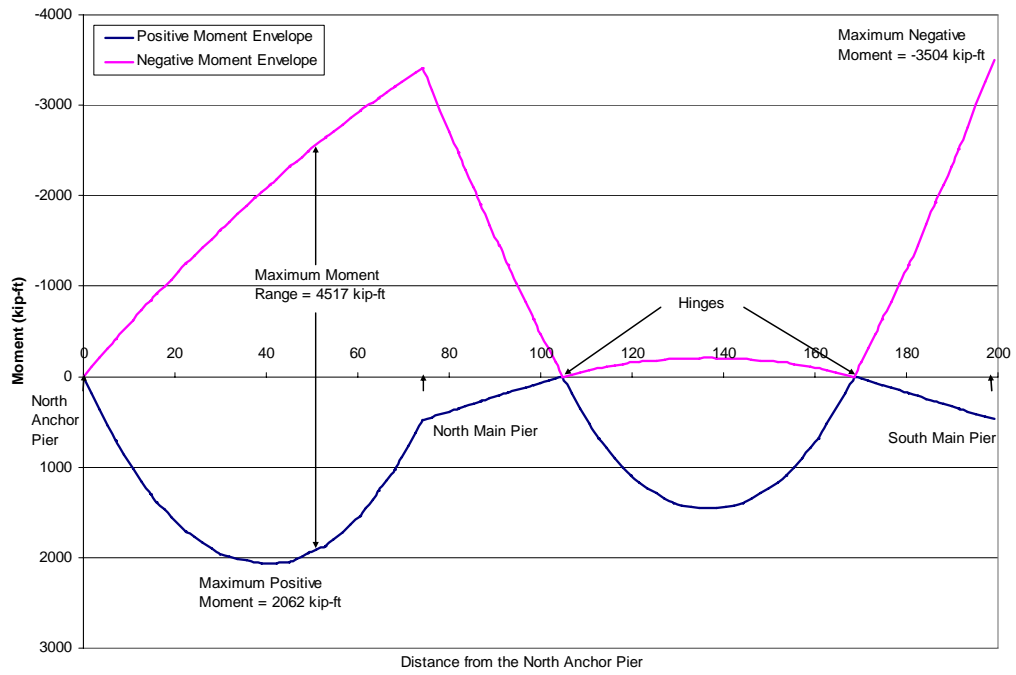
Figure 5-13: Moment Envelope for West Girder Due To HS-20 Truck Load in Three Lanes

CHAPTER 6

Measured Response and Fatigue Life Analysis of Medina River Bridge

6.1 OVERVIEW

The results for the Medina River Bridge are divided into six sections for discussion. Section 6.2 summarizes the weigh-in-motion (WIM) data. Section 6.3 discusses the placement of the MicroSAFE units. Section 6.4 presents the rainflow data collected in the field. Section 6.5 addresses the results of the SAP analysis. The rainflow data, the SAP analysis, and the WIM data are compared in Section 6.6. The results of the fatigue life calculations are presented in Section 6.7.

6.2 WEIGH-IN-MOTION DATA

A high-speed weigh-in-motion (WIM) sensor is located in the I-35 pavement seven miles south of the Medina River Bridge (Figure 6-1). The sensor records all truck traffic that travels along the interstate each day at this location. Because the Medina River Bridge is north of the WIM sensor, only northbound trucks were considered. In addition, the volume of truck traffic is expected to be higher at the WIM sensor than that crossing the bridge because the outer loop around San Antonio (Loop 1604) intersects I-35 between the WIM sensor and the Medina River Bridge. On average, more than 3,800 trucks pass the WIM sensor each day. A total of 21 different types of trucks were detected during the two recording periods (Table 6-1). The WIM sensor was shut down for repairs during

84

the second collection period and only recorded 18 days of data. The most common truck is identified as T01 and corresponds to a tractor trailer with five axles. This type of truck represents nearly 50% of the northbound traffic on I-35. A two-axle truck, T02, is the second most common and represents more than 30% of the truck traffic. None of the other 19 types of trucks represents more than 5% of the total truck traffic.

The important data from the WIM sensor include the number of axles, weight of each axle, and axle spacings from each truck. The measured data suggest that the sensor was triggered when a front axle of at least 3.5 kip crossed the sensor. Once triggered, the sensor recorded all subsequent axle weights and the axle spacings. The trigger threshold of 3.5 kip should be sufficient to eliminate passenger vehicles from the WIM data.

The distribution of recorded axle weights is shown in Figure 6-2. The majority of the axle weights were between 4 and 12 kip. Very few axles exceeded 20 kip.

Table 6-1: Summary of WIM Information

Truck Designation	WIM Label	Average Number of Trucks Per Day	Percentage of Total Trucks	Number of Axles	Mean Axle Weight (kip)	Overall Length (ft)	Total Weight (kip)
T01	332000	1,892	48.9%	5	10.6	59.2	53.2
T02	220000	1,288	33.3%	2	4.2	12.6	8.5
T03	337000	171	4.4%	5	11.5	62.9	57.6
T04	230000	140	3.6%	3	9.5	22.8	28.4
T05	322000	110	2.8%	5	3.7	38.4	18.4
T06	521200	57	1.5%	5	10.6	65.7	53.2
T07	190300	55	1.4%	3	12.5	30.2	37.5
T08	200900	33	0.8%	3	4.9	31.4	21.0
T09	431000	32	0.8%	4	9.7	51.9	39.0
T10	421000	20	0.5%	3	5.1	30.5	15.4
T11	331000	14	0.4%	4	7.5	38.7	29.9
T12	90000	13	0.3%	2	2.9	9.0	5.7
T13	190200	12	0.3%	2	10.5	24.3	21.0
T14	531200	11	0.3%	6	9.4	68.0	56.1
T15	333000	9	0.2%	6	8.5	62.9	50.9
T16	323000	6	0.1%	5	4.2	47.6	21.0
T17	632100	3	0.1%	6	10.1	73.5	60.6
T18	321000	2	0.1%	3	8.5	37.7	25.5
T19	422000	2	0.0%	4	4.3	35.8	17.1
T20	721240	0	0.0%	9	6.2	164.1	55.7
T21	723310	0	0.0%	9	3.5	76.1	31.5

Total	3,870
Minimum	1,748
Maximum	4,941

Table 6-2: WIM Axle Data for Truck T01

Truck	Axle Weight (kip)					Total Weight	Axle Spacing (ft)			
T01	1	2	3	4	5	(kip)	1 to 2	2 to 3	3 to 4	4 to 5
Minimum	7.5	3.6	3.6	3.5	3.1	21.3	17.8	3.8	34.7	3.8
Average	10.6	11.1	10.7	10.5	10.5	53.2	17.1	4.3	33.6	4.1
Maximum	11.5	17.0	16.8	17.4	17.4	80.1	17.4	4.0	35.3	4.0
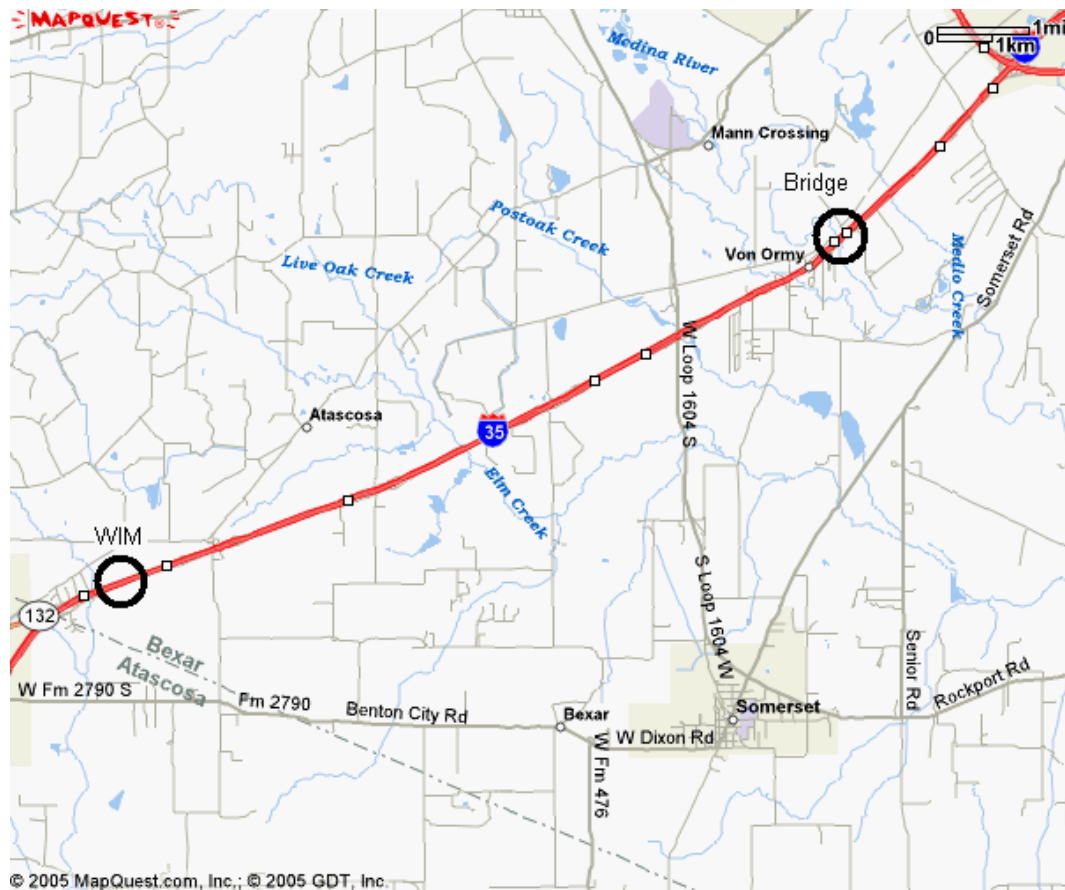
Figure 6-1: Map of I-35 South of San Antonio
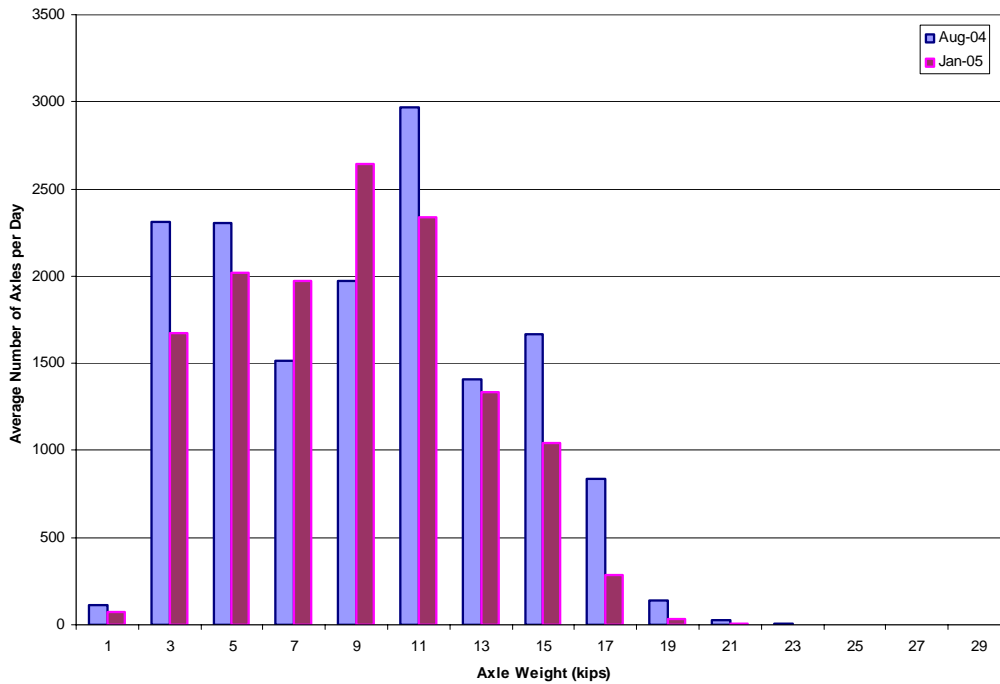
Figure 6-2: Axle Weight Distribution

6.3 MICROSAFE UNIT APPLICATION

The MicroSAFE units were used to monitor the response of the Medina River Bridge during two, 28-day periods. The units were installed on August 25, 2004 for the first collection period. At this time, TxDOT was conducting a required inspection of the bridge, and a snooper truck was available for the installation. One person from the University of Texas installed four units and the associated strain gages in a couple of hours. The second collection period began on January 25, 2005. The installation was completed in a few hours using a TxDOT bucket truck.

6.3.1 Center Span Installation

During the first collection period only one of the center cantilever spans was instrumented. The two areas of interest were identified from the SAP2000 output: (1) near the center of the cantilever span and (2) near the ends of the cantilever span. The cantilever was expected to experience large negative moments, which increase in the proximity of the support. Because the cross-sectional properties of the longitudinal girders vary within the cantilever span, the largest flexural strains did not necessarily occur at the location of maximum moment. The locations with the smallest flange thickness near the supports were selected for study. Theoretically, the end of the cantilever should experience no moment, but the units were positioned at this location to check that the hinge was working properly.

The north anchor and cantilever spans are shown in Figure 6-3. The four units positioned within the cantilever span are identified as locations D, E, H, and I (Table 6-3). All four strain gages were attached to the bottom of the bottom flange.

The procedure used to attach the strain gages to the bridge girders and the MicroSAFE units is discussed in Chapter 3. As opposed to collecting raw data during installation, which was used to set the bin sizes for the 12th Street exit ramp, a different technique was used for the Medina River Bridge. The calculated moments from SAP were converted to strain ranges and the bin sizes were preset in the MicroSAFE units prior to installation. This technique is not recommended, as it does not allow the installer to test the strain gage adequately or identify any differences between the measured and calculated response that can be observed by collecting raw data.

The data obtained from the center span were not expected to have an impact on the calculated fatigue life of the bridge. Rather, the purpose was to

check that the hinges were working properly. The most useful information recorded during this collection period was the weigh-in-motion data. This information provided a basis for the installation of units on the anchor span.
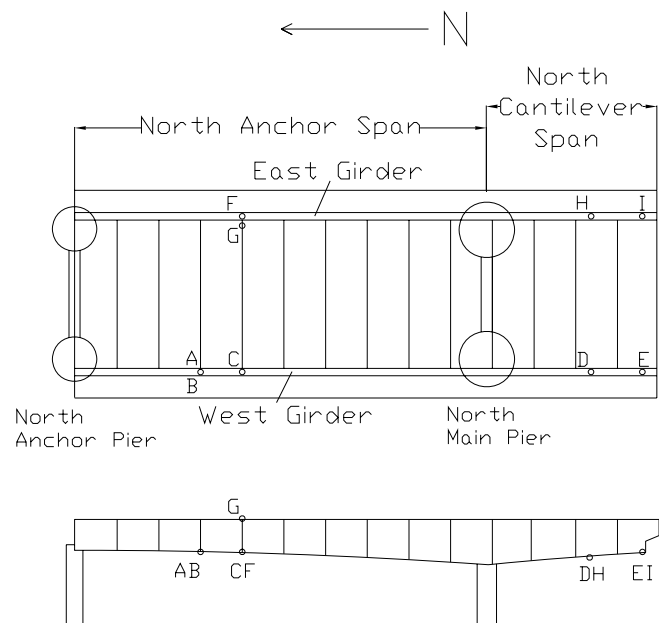
Figure 6-3: Locations of Nine MicroSAFE Units

Table 6-3: Location and Description of All MicroSAFE Units

Location	Description	Span/Girder	Unit	Acquisition Period	Notes
A	21-ft south of the North Anchor Pier	Anchor Span West Girder	1002	Jan-05	Battery falied after 21 days
B	21-ft south of the North Anchor Pier	Anchor Span West Girder	1005	Jan-05	Proper data collection
C	29-ft south of the North Anchor Pier	Anchor Span West Girder	1004	Jan-05	Proper data collection
D	18-ft south of the North Main Pier	Cantilever Span West Girder	1007	Aug-04	Proper data collection
E	1-ft north of hinge	Cantilever Span West Girder	1014	Aug-04	Proper data collection
F	29-ft south of the North Anchor Pier	Anchor Span East Girder	1001	Jan-05	Battery failed prior to data collection
G	29-ft south of the North Anchor Pier	Anchor Span Transverse Floor Beam	1007	Jan-05	Battery failed prior to data collection
H	18-ft south of the North Main Pier	Cantilever Span East Girder	1006	Aug-04	Proper data collection
I	1-ft north of hinge	Cantilever Span East Girder	1013	Aug-04	Battery failed prior to data collection
J	Temperature collection: not attached to bridge	West Girder	1006	Jan-05	Proper data collection

6.3.2   Anchor Span Installation

The second collection period began on January 25, 2005. Instruments were positioned on the anchor span during this 28-day collection period. The moment envelopes calculated from the HS-20 truck and the WIM data were used to select the locations of the instruments.

From the WIM data, the average T01 truck was used in SAP to determine positive and negative moment envelopes. The moment envelopes correspond to the maximum positive and negative moments due to the moving vehicle load.

Moments due to stationary loads are not included in the moment envelopes. The difference between the positive and negative moment envelopes corresponds to the maximum variation in moment at each location along the span.

Because all vehicles have more than one axle, the bridge experiences more than a single loading cycle as the vehicle crosses. Figure 6-4 shows the raw strain data recorded at location C as a truck crosses the bridge. As will be shown, the maximum variation in strain corresponds to the difference between the moment envelopes, while the smaller cycles correspond to multiple axles.

The shape of the raw strain data was reproduced by analyzing moving loads in SAP. A single, 10-kip point load was moved in 5-ft increments northward across the bridge. The corresponding moments at location A are shown in Figure 6-5. For the Medina River Bridge, the eight exterior simple spans transfer no moment to the anchor and center spans, so the moving load can be applied to only the three center spans.
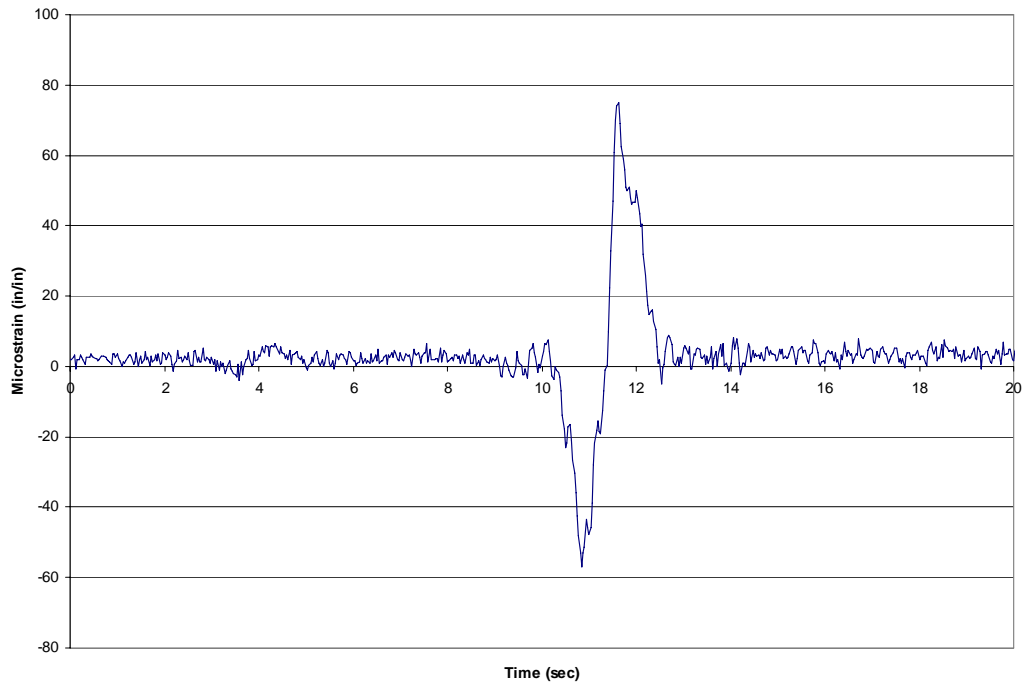
Figure 6-4: 20-seconds of Raw Data from Location C
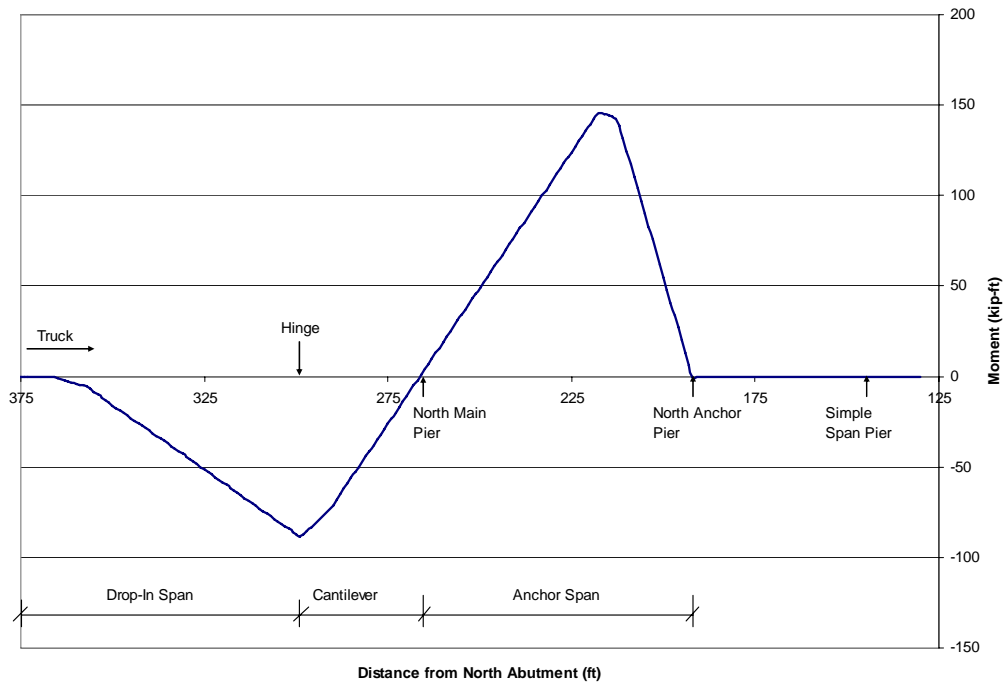
Figure 6-5: Location A Moving Load Analysis – 10 kip Load

The results of the moving load can be used to create a maximum moment range diagram for a truck with any number of 10-kip axles. In order to keep the analysis realistic, standard truck T01 average axle spacings were used with five 10-kip loads. As the T01 truck moves across the bridge, each axle generates moment at location A. These moments can be summed to obtain the total moment at location A (Figure 6-6).

94
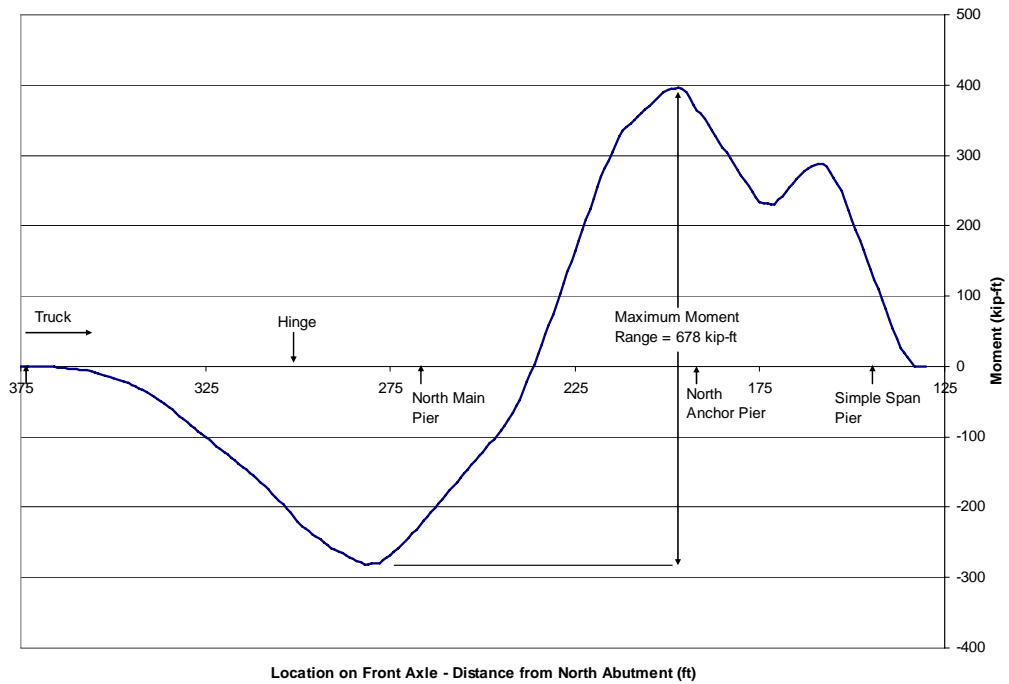
Figure 6-6: Location A Moving Load Analysis for Five 10-kip Axles

From Figure 6-6, the maximum variation in moment at location A is 678 kip-ft. A smaller cycle of 58 kip-ft is also observed. The maximum moment variation corresponds to the difference between the moment envelopes at location A, while the smaller cycle is lost in the moment envelope calculation. Therefore, the moment envelopes provide a means of determining the large-amplitude strain cycles experienced by the bridge. However, it is not possible to reproduce the complete rainflow response from the moment envelopes.

A single type T01 truck was used to select the instrument locations in the north anchor span. The average axle weights and axle spacings were used in this analysis (Table 6-2), and the vehicle was positioned in the left lane. The moment

95

envelope for the north anchor span is shown in Figure 6-7. Due to the similarity in values, only the envelope for the west girder will be shown.

Distance from North Anchor Pier (ft)
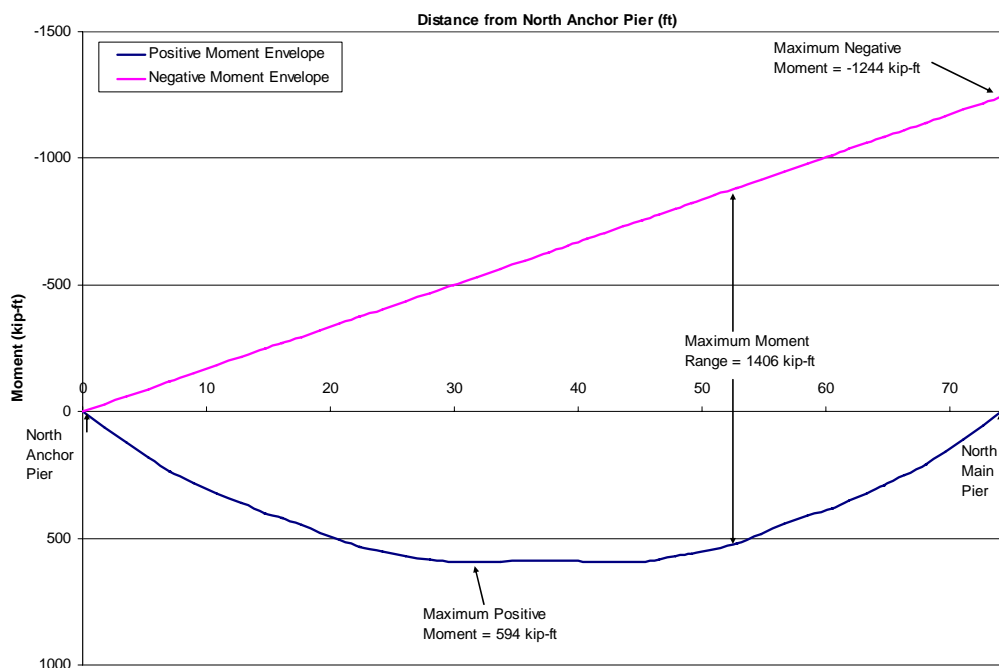
Figure 6-7: Moment Envelope for West Girder in North Anchor Span for Average T01 Vehicle

The largest positive moment occurs about 32-ft south of the north anchor pier, the largest negative moment occurs above the north main pier, and the largest moment range occurs approximately 53-ft south of the north anchor pier. The information provided by the moment envelope is useful in determining locations of maximum moment, but not necessarily maximum strains. Because

the depth and flange thickness of the girder increase in the vicinity of the main piers, the moment of inertia and distance to the centroid vary along the span. The strain range at a location depends on the moment range, the moment of inertia, and the distance from the centroid to the bottom flange. Figure 6-9 and Figure 6-10 show the increase in the centroid and moment of inertia of the girder along the north anchor span. These calculations are based on the following assumptions: the effective width of the concrete deck is 96 inches (based upon AASHTO recommendations) and the compressive strength of the concrete is 3000 psi. Both the noncomposite and composite sections are plotted. These sections provide the maximum and minimum limits for the sectional properties. As will be discussed in Section 6.5, some of these assumptions may not be appropriate, but they were used in the preliminary analysis to select the locations for the strain gages. The cross sectional dimensions and corresponding properties at location A are shown in Figure 6-8.

	I (in^4)	c (in)
Composite	94,610	57.6
Noncomposite	44,120	34.7
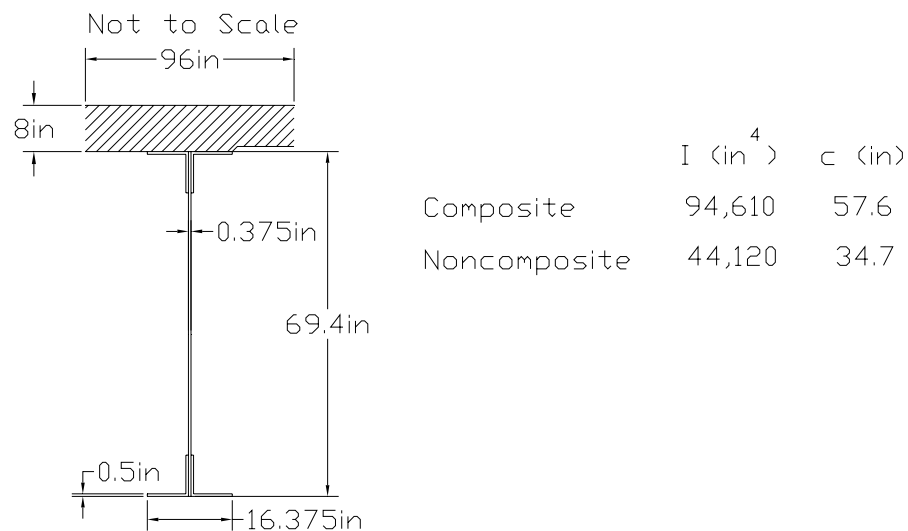
Figure 6-8: Typical Cross Section with Sectional Properties

97
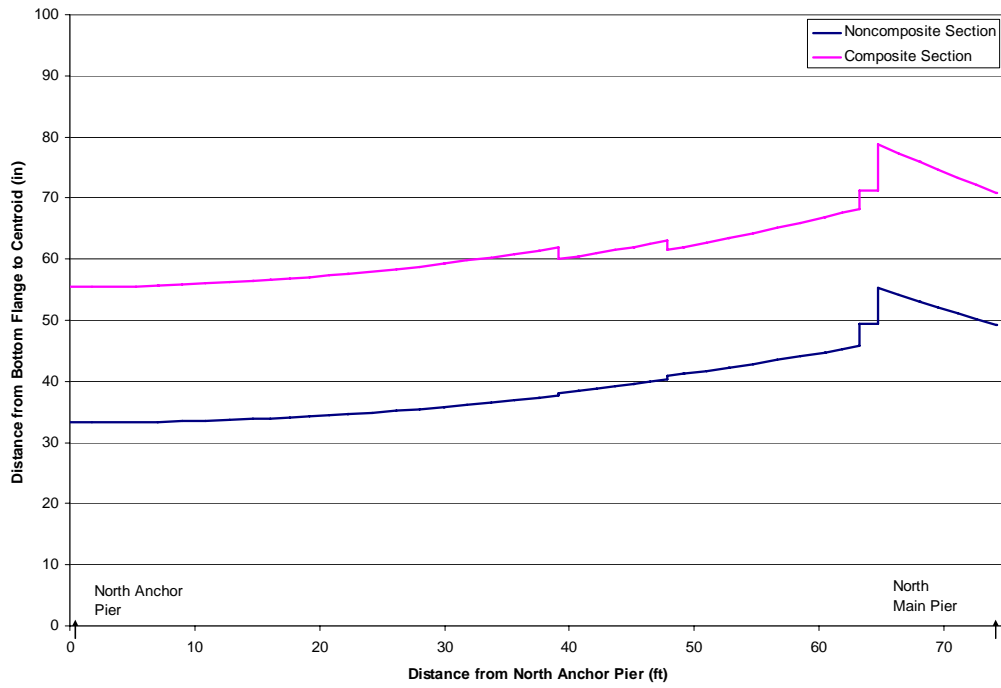
Figure 6-9: Distance from Bottom Flange to Centroid of Cross Section for North Anchor Span Girders

98
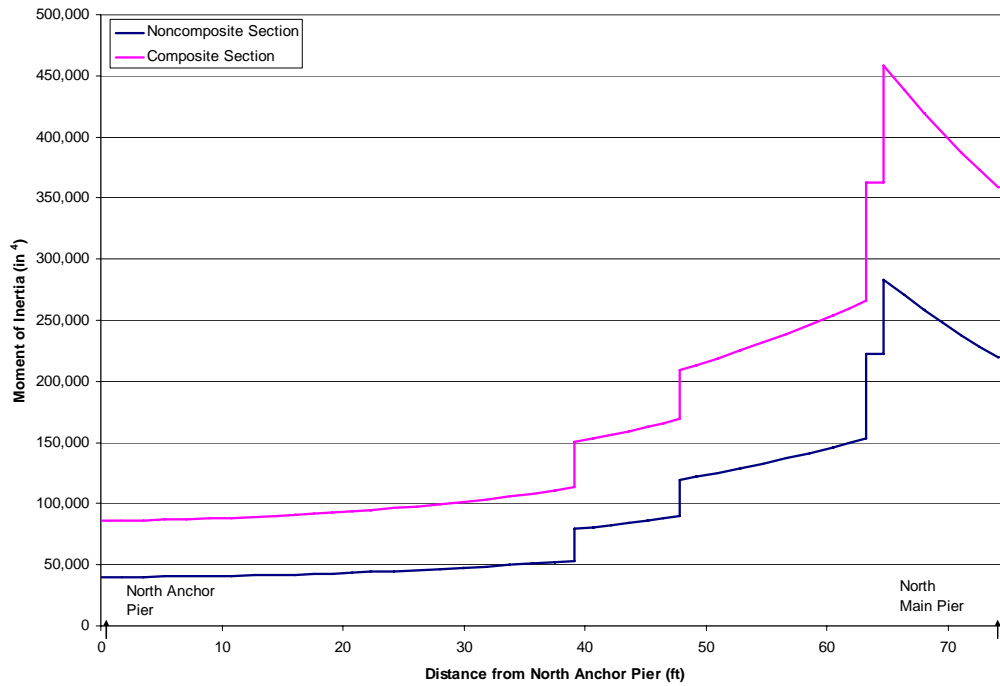
Figure 6-10: Moment of Inertia for North Anchor Span Girders

The combination of the moment envelope, the centroidal axis, and the moment of inertia provides enough data to determine maximum strain ranges (Figure 6-11).

99
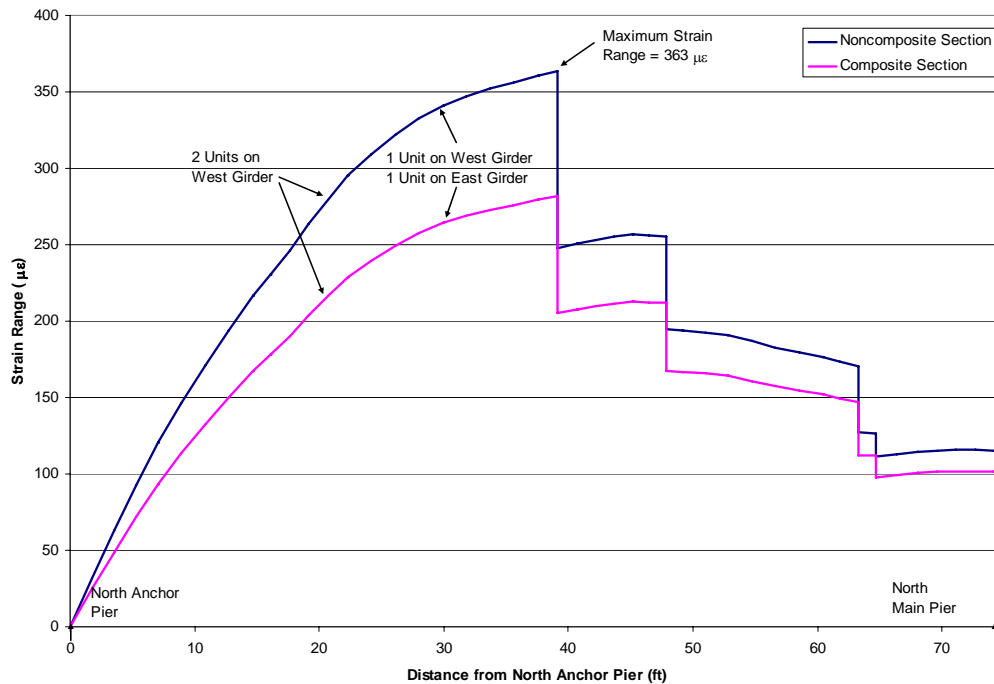
***Figure 6-11: Calculated Strain Ranges for West Girder, North Anchor Span
due to Average T01 Vehicle***

When determining unit placement, the maximum strain range was considered. Two units were placed on the west girder 10-ft north of the location of maximum moment range, at approximately 21-ft from the north anchor pier. This area experiences a high strain range even though it experiences a modest variation in moment because of its shorter girder web and small flange thickness. One unit was placed on the west girder approximately 30-ft south of the north anchor span to experience the maximum strain range. Another unit was placed in the same location on the east girder, with a fifth unit placed on the floor beam above it, measuring strains transverse to the roadway. A final and sixth unit was

100

placed in the field during this period to measure only temperature strains. The results of this were already discussed in Chapter 4.

The locations of the strain gages in the north anchor span are shown in Figure 6-3, and the additional details are provided in Table 6-3. All strain gages except G and J were attached to the bottom of the bottom flange of the longitudinal girders.

6.4   MEASURED RAINFLOW DATA

The rainflow data collected for the Medina River Bridge were gathered during two separate periods. The first was a 28-day period begun on August 25, 2004. The second period also lasted 28 days and was begun on January 25, 2005. The nomenclature used to describe the location of each unit was discussed in the previous section, and the procedure used to remove strain cycles attributable to temperature fluctuations is described in Section 4.2. All data presented in this chapter have been corrected to remove temperature effects.

6.4.1   Rainflow Data Measured in Cantilever Span

Two units were placed near the midspan of the cantilever. Location H is on the east girder and location D is on the west girder. The rainflow histograms for both units are shown in Figure 6-12 and Figure 6-13, respectively.
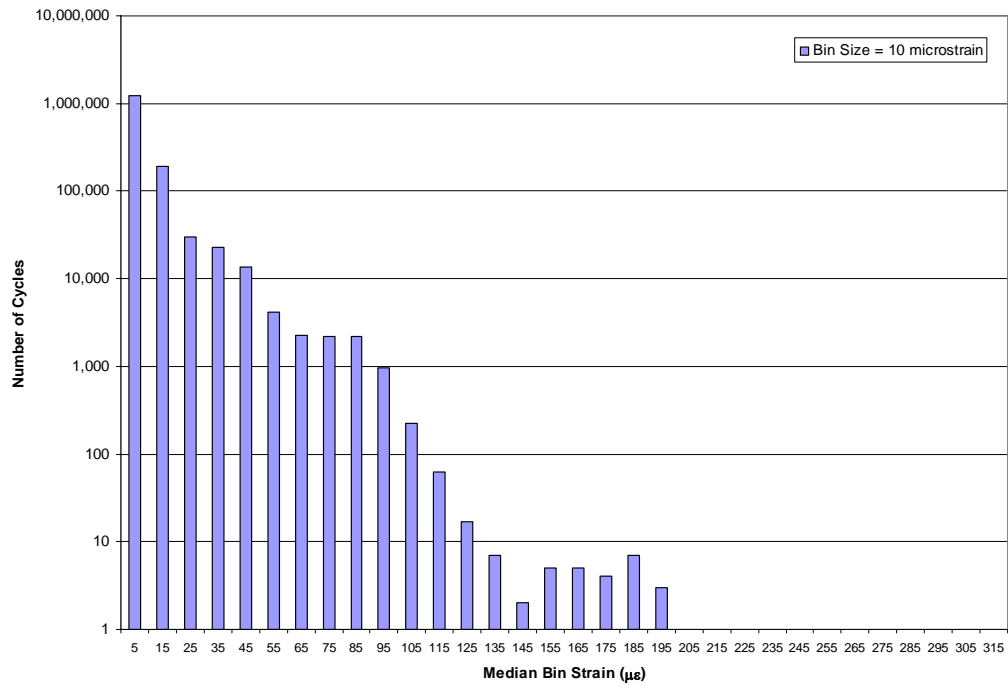
Figure 6-12: Rainflow Data Measured at Location H
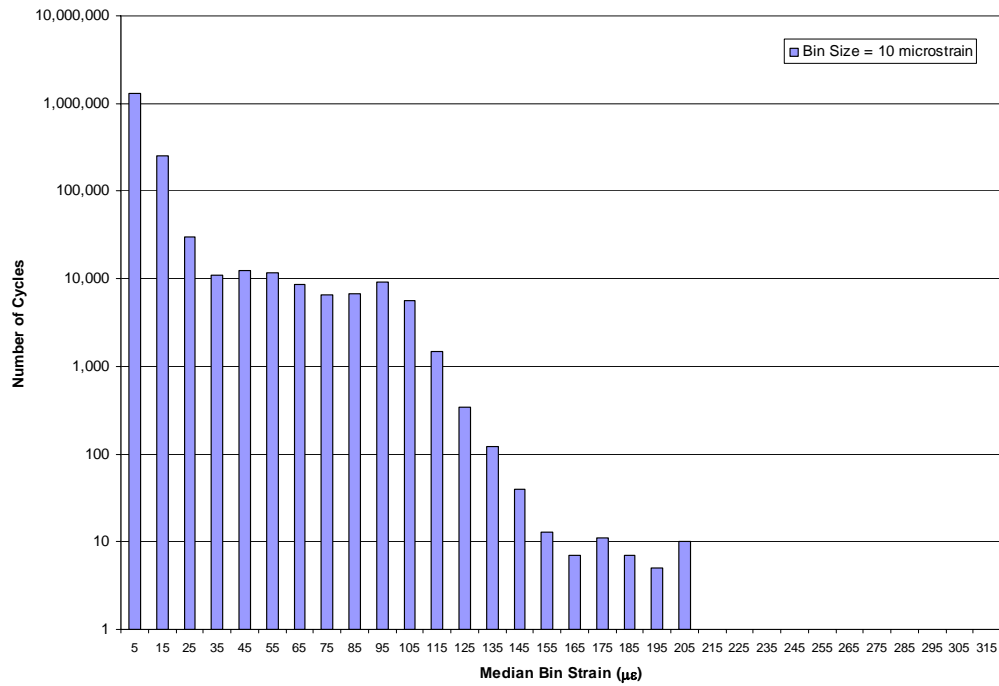
Figure 6-13: Rainflow Data Measured at Location D

A third unit was also placed on the cantilever section. Location E was placed very near the end of the north cantilever on the west girder. This unit was expected to record minimal negative moments due to its proximity to the hinge. The rainflow data from this unit are shown in Figure 6-14.
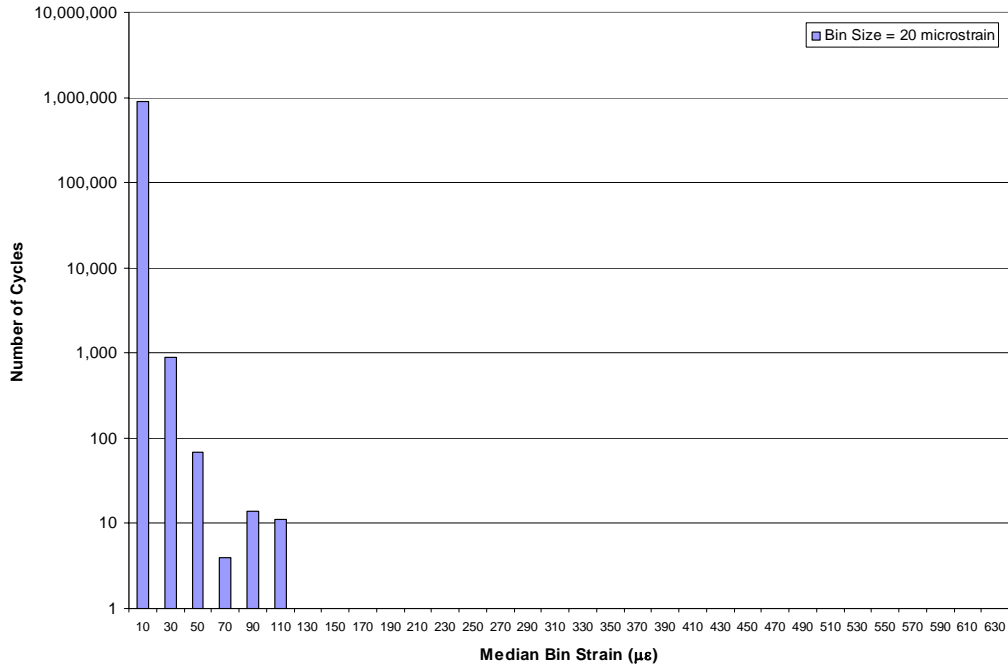
Figure 6-14: Rainflow Data Measured at Location E

6.4.2   Rainflow Data Measured in Anchor Span

The north anchor span of the Medina River Bridge was instrumented with five MicroSAFE units. These units were powered with a set of entirely new batteries. It was discovered in the field that these batteries require a different wiring configuration between the strain gage and the MicroSAFE unit. The proper wiring was determined by a trial-and-error procedure while running 60-second raw data collection periods. When the proper wiring was determined, each unit was programmed to collect 60 to 120 sec of raw data. Upon a successful acquisition of the raw data, each unit was programmed for 28-days of rainflow data.

104

Unfortunately, some of the batteries which performed properly during the raw data acquisition period did not during the rainflow period. Data were collected at locations B, C, and J. The unit at location A recorded data during only for the first 21 days of the test. The units at locations F and G malfunctioned and no data were obtained. Upon completion of this rainflow acquisition period, the units in question were tested. All units worked properly under raw data and rainflow data acquisition. However, approximately one half of the batteries malfunctioned in these control tests [5].

The available data are reported in the section. Locations A and B are situated side-by-side on the west girder, just north of the area of maximum moment. The histograms for these units are found in Figure 6-15 and Figure 6-16.
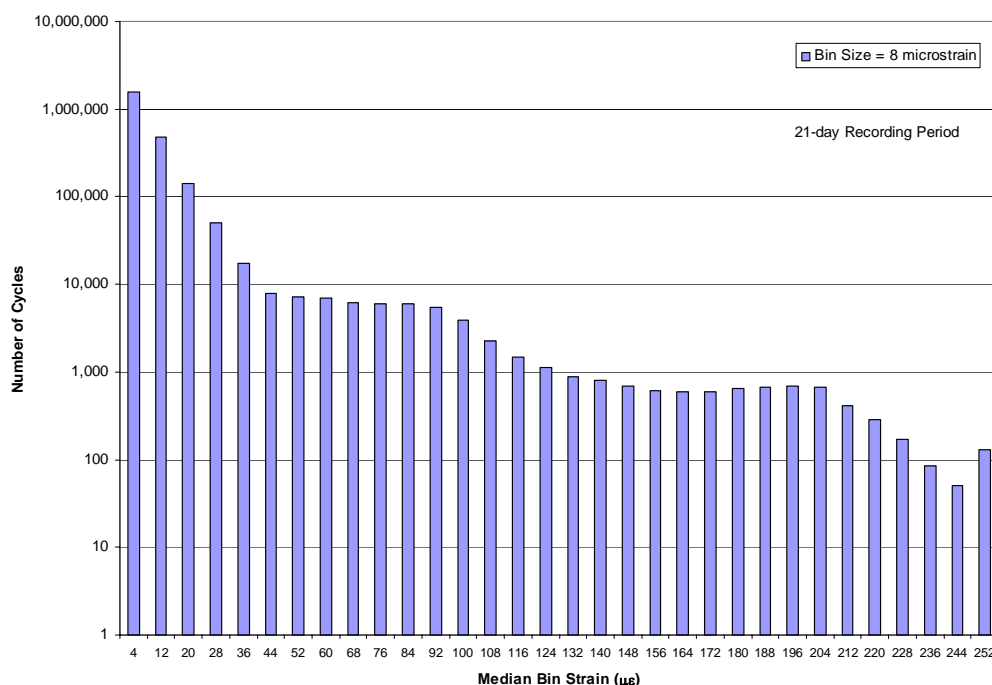
Figure 6-15: Rainflow Data Recorded at Location A

105
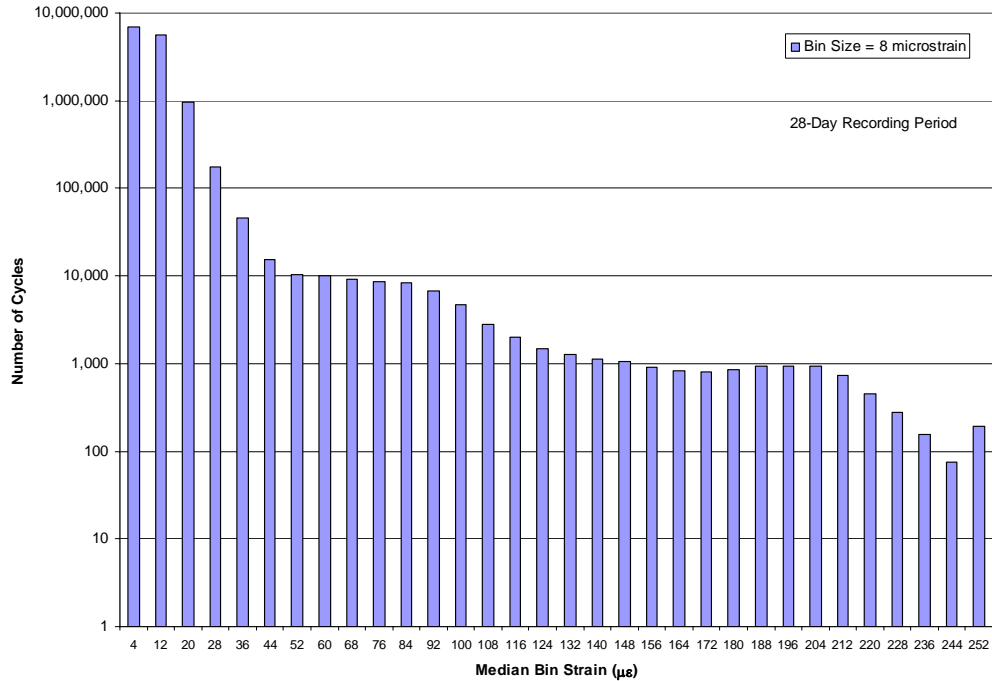
Figure 6-16: Rainflow Data Recorded at Location B

Many more cycles were recorded at location B than location A. Some of the differences can be explained by the shorter recording period at location A (21 days). However, this does not account for the large discrepancies in the lower bins and additional tested is required to resolve this issue.

One other location (C) was also placed on the west girder in the anchor span. It was placed just south of Locations A and B, at the location of maximum positive moment. Figure 6-17 illustrates the histogram from this unit.
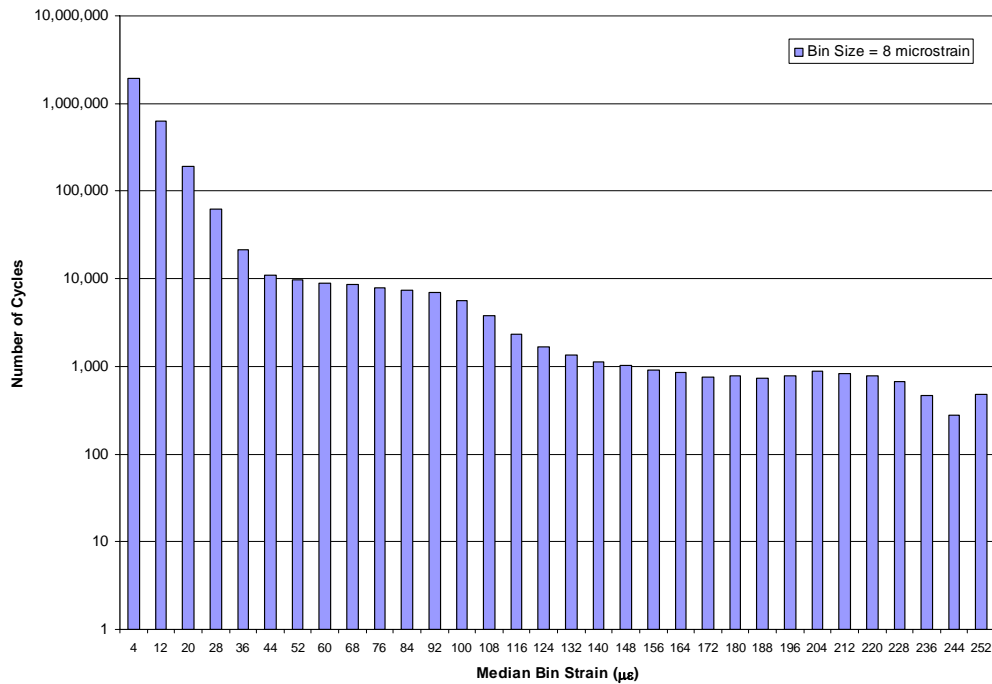
Figure 6-17: Rainflow Data Recorded at Location C

It was expected that location C would experience larger strain ranges than location B. This is not obvious from the figures, but can be seen in the daily rainflow histograms. The difference in the calculated strain range is less than 10% (Figure 6-11). It is unlikely that such a small difference could be detected in a histogram with 100 to 1,000 cycles in all large bins.

It can also be seen that the rainflow histograms were truncated at 256 $\mu\varepsilon$. The 256 $\mu\varepsilon$ cutoff was expected to be conservative based upon the maximum strain range of 145 $\mu\varepsilon$ from Figure 6-11. This was not the case and it is recommended that larger bin sizes be used when instrumenting bridges with such a significant amount of truck traffic.

As was done in Chapter 4, a quick comparison of the rainflow counts at the six instrumented locations is provided to develop a qualitative feel for which area of the bridge is subjected to the highest stress ranges. The highest bin median which has over 10,000, 1000, and 100 rainflow counts are listed in Table 6-4. Because the unit at location A only recorded data for 21 days, the recorded rainflow counts were multiplied by (28/21) for the comparison.

Table 6-4: Simplified Location Comparison for All Units

Rainflow Counts	Median Bin Strains ($\mu\varepsilon$)					
	Location					
	H	D	E	A ☆	B	C
10,000	45	55	10	44	52	44
1,000	85	115	10	140	148	145
100	105	135	30	252 ✦	252 ✦	252 ✦

✦ Cycles in largest bin

☆ Measured counts multiplied by 28/21 for comparison

The critical nature of the anchor span can be seen from Table 6-4. Locations A, B, and C all see larger quantities of high strains than do any locations in the cantilever span. It was expected that A and B would record similar strains, and although they are not exact, the differences will not effect the upcoming fatigue life calculations drastically. The simplified comparison also indicates that the strains at location C are essentially the same as those at locations A and B. Locations H and D were positioned at the same location on the east and west girders in the cantilever span, respectively. From Table 6-4 it can be seen that Location D, which is under the left lane, experiences larger strains than the right lane does. As expected, Location E experiences the smallest strains.

6.5 A COMPARISON OF WEIGH-IN-MOTION AND RAINFLOW DATA

The goal of this section is to develop a correlation between the measured rainflow data and the recorded weigh-in-motion data. This process is approximate at best, but because the traffic crossing the bridge is not known. However, the measured rainflow counts should be related to the daily truck traffic.

A series of problems and issues were discovered and solved during this portion of the project. Each issue and its solution will be discussed individually within this section.

The first issue discussed was the bridge materials themselves. The bridge was originally built in 1936, when a concrete compressive strength of 2500 psi was a safe assumption. The bridge was redesigned in the 1960s when a strength of 3000 psi was used. The entire concrete slab was replaced with 3000 psi concrete. Any calculations done on the current state of the bridge must use this strength concrete.

The concrete strength played an important roll when determining the moment of inertia of the transformed section of the girder. Even more important than the concrete strength was the effective width of the slab which could be counted on in composite action with the girder. For a fully composite slab, AASHTO specifications recommended a slab width of 96.375 inches, or about 8 feet. Unfortunately, the amount of composite action which actually developed is not possible to determine on a 70 year-old bridge which was given a new slab 40 years ago. It was decided to increase the effective width of the slab to 16 feet in order to create better correlations with the rainflow data. Using an effective width of 4-ft or less resulted in T01 truck-induced strains calculated of as high as 385 $\mu\varepsilon$. An effective flange width of 16-ft reduced this maximum strain range to a more reasonable 345 $\mu\varepsilon$. Using a concrete compressive strength of 3000 psi and

an effective flange width of 16 feet, section properties for each instrumented location can be calculated. These are shown in Table 6-5.

Table 6-5: Girder Section Properties at Each Location
Corresponding to an Effective Flange Width of 16 ft

Location	Depth (in)	Distance from Bottom Flange to Centroid of Girder (in)	Moment of inertia (in^4)
A	69.4	34.7	44,680
B	69.4	34.7	44,680
C	71.7	35.8	48,380
D	86.9	38.9	85,690
E	69.5	34.8	44,930
H	86.9	38.9	85,690
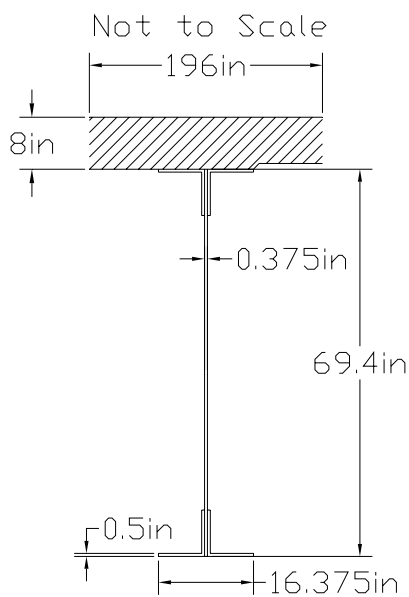
Figure 6-18: Cross Section at Locations A and B

Another issue is that the WIM sensor is located 7 miles south of the Medina River Bridge. Between the sensor and the bridge, there is a major San Antonio Loop route which may reduce the traffic the bridge experiences. In a discussion with a TxDOT representative, the amount of northbound truck traffic which exits after the sensor and prior to the bridge is less than 25%. When correlating data, any large WIM quantities may be reduced by 0 to 25% [10].

The process for developing a correlation between the WIM and rainflow data was begun by comparing the rainflow data for locations D and H. These locations each collected 28-days of data during the first collection period and are located in the same transverse plane on the west and east girders, respectively. By comparing the upper bins of the rainflow data, it can be determined approximately what percentage of truck traffic used each lane. The iterative process begins by determining the strain-range cutoff point for truck versus passenger vehicles. This is done by summing the total number of rainflow cycles for locations D and H above the selected cutoff value. This value should approximately match the number of WIM trucks. Once the cutoff is hypothesized, the number of T02 trucks which fall below this threshold is approximated.

For example, the average T02 truck creates a maximum strain range at location D of 25 $\mu\varepsilon$. If a cutoff value of 35 $\mu\varepsilon$ is chosen, it can be assumed that over 50% of the T02 trucks fall below this value. The smaller T02 trucks caused the smallest moment range of all truck categories because they have only two light axles. The number of T02 trucks below the cutoff is subtracted from the total number of trucks, and a total number of trucks creating strain ranges above the cutoff are left. This can be compared to the number of rainflow cycles above the cutoff that were recorded by the MicroSAFE devices. If the numbers do not match, a new cutoff can be assumed and the process repeated. Table 6-6 shows the final results for the number of WIM trucks above the selected cutoff of 45 $\mu\varepsilon$

111

and the number of rainflow cycles above the cutoff. Ninety percent of the T02 trucks fall below the 45 µε cutoff.

Table 6-6: WIM and Rainflow Cycles at Location D above a 45 $\mu\varepsilon$ Cutoff

	Day													
	1	2	3	4	5	6	7	8	9	10	11	12	13	14
WIM Trucks Above the Cutoff	3,396	3,321	3,176	2,181	1,545	3,226	3,495	3,441	3,384	3,130	1,980	1,470	1,789	3,385
Rainflow Cycles Above the Cutoff	3,942	3,574	2,954	1,629	2,536	4,245	3,962	3,760	3,570	2,771	1,566	1,553	2,677	4,341
Error (%)	14%	7%	7%	25%	39%	24%	12%	8%	5%	11%	21%	5%	33%	22%
	Day													
	15	16	17	18	19	20	21	22	23	24	25	26	27	28
WIM Trucks Above the Cutoff	3,501	3,251	3,207	2,300	1,708	3,256	3,443	3,335	3,239	3,024	2,215	1,480	3,273	3,587
Rainflow Cycles Above the Cutoff	3,775	3,714	3,056	1,689	2,636	4,292	3,987	3,774	3,340	2,805	1,542	2,604	4,212	3,980
Error (%)	7%	12%	5%	27%	35%	24%	14%	12%	3%	7%	30%	43%	22%	10%

The correlations from Table 6-6 are acceptable for the purposes of this project. Although the error ranges from 3% to 43%, the WIM and rainflow data always follow a similar trend; if the WIM trucks decreases from one day to the next, so do the rainflow counts. This is more obvious in Figure 6-19.
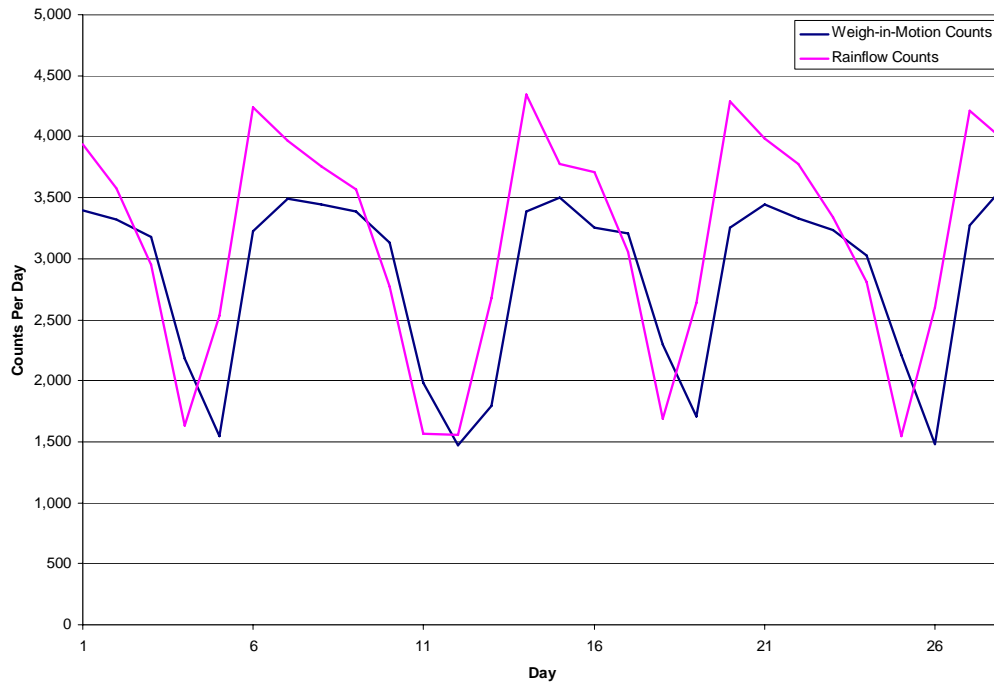
Figure 6-19: WIM and Rainflow Data per Day at Location D, H

Using a comparison of rainflow and moment ranges from WIM data, cutoff values for locations A, B, and C can also be approximated. Locations A and B will use a cutoff of 60 με and location C will use a cutoff of 68 με. Figure 6-20 and Figure 6-21 show the resulting WIM and rainflow comparison at each location.
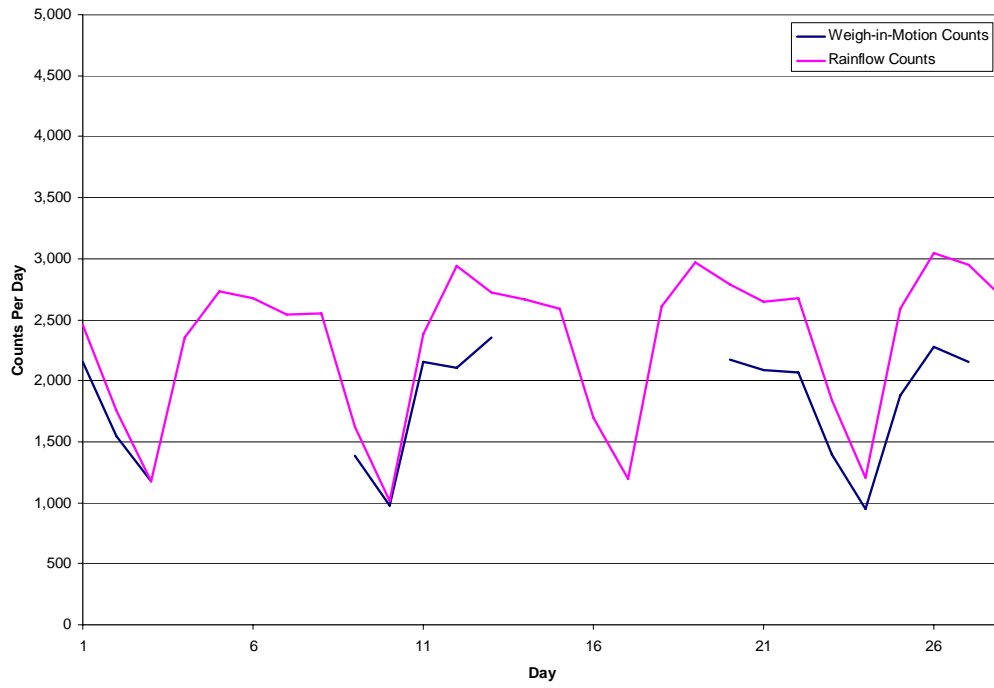
Figure 6-20: WIM and Rainflow Data per Day at Location A, B
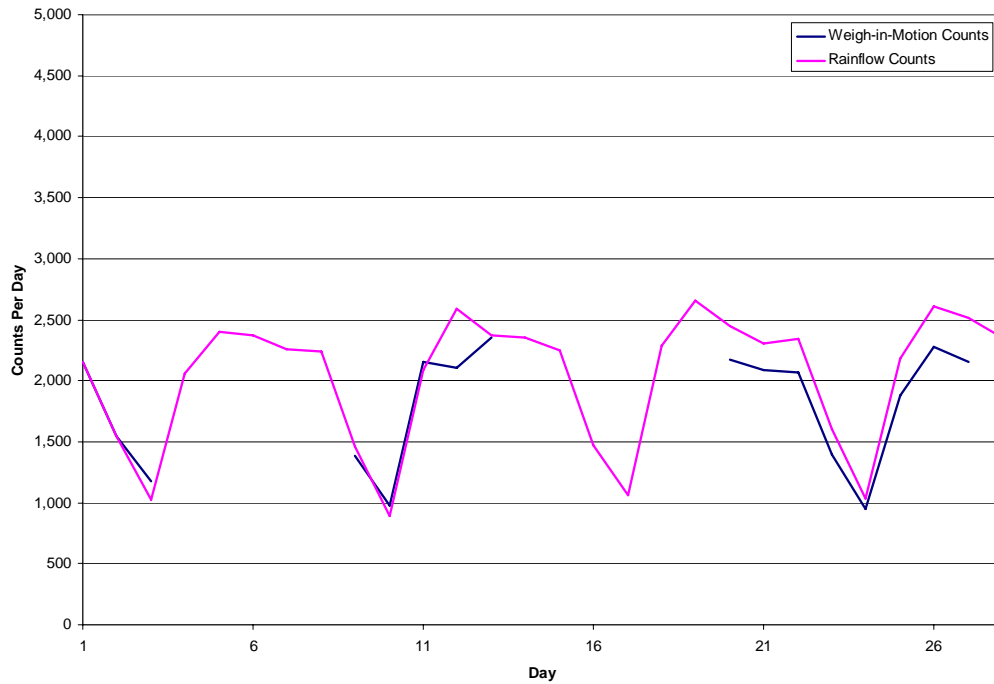
Figure 6-21: WIM and Rainflow Data per Day at Location C

The fewer number of counts in Figure 6-20 and Figure 6-21 than Figure 6-19 are a result of locations A, B, and C only recorded the traffic in one lane while locations D and H captured all traffic in both lanes. Locations A, B, and C were all instrumented in the second collection period when only 16 of 28 days of WIM were received from the sensor. This explains the gaps in the WIM counts in the previous two figures.

6.6   FATIGUE LIFE ANALYSIS

The calculation of the fatigue life at each location will be carried out using the same steps used in Chapter 4. The first step is to determine the detail category for each location. On the Medina River Bridge, each unit was placed on the

bottom flange of the riveted, fracture-critical member. The riveted nature of the cross section corresponds to a detail category D. The fatigue threshold given by AASHTO for this detail category is 7.0 ksi (Table 2-3). The maximum stress ranges for each of the locations in summarized in Table 6-7. The maximum stress range was calculated by multiplying the largest rainflow bin that had at least 1 cycle by Young's modulus. The number of cycles above this threshold are not important, only the fact that this threshold has been reached gives the structure a finite fatigue life.

Table 6-7: Maximum Stress Range and Fatigue Threshold for each Unit

Location	Maximum Stress Range (ksi)	Fatigue Threshold (ksi)	Fatigue Life
A	7.31	7.0	Finite
B	7.31	7.0	Finite
C	7.56	7.0	Finite
D	7.65	7.0	Finite
H	5.85	7.0	Infinite
E	3.30	7.0	Infinite

The comparisons of maximum stress range and fatigue life in Table 6-7 provide expected results. All instrument locations within the anchor span are considered to have a finite fatigue life. In the cantilever span, the midspan location on the west girder also has a finite fatigue life, while the corresponding location on the each girder has an infinite life. The pin also has an infinite fatigue life. The differences between the east and west girder in the cantilever span are attributed to the traffic patterns, more trucks crossed the bridge in the left (west) lane.

For locations with a finite fatigue life, the detail category constant A must be used. A value of 22.0×10^8 ksi^3 is determined from Table 2-2.

The fatigue life is the calculated using the number of cycles, the effective stress range, and A. Based on the discussion in Chapter 4, all cycles including noise, were used to determine the fatigue life. Table 6-8 includes all necessary fatigue life calculation information.

Table 6-8: Fatigue Life Information for Each Unit

Location	Lowest Stress Range Used (ksi)	Number of Cycles	S_{RE} (ksi)	Fatigue Life (years)
A	0.00	16,573,828	0.486	66.6
B	0.00	24,504,594	0.505	53.6
C	0.00	21,789,117	0.542	48.7
D	0.00	23,166,899	0.338	188.5
H	0.00	23,511,334	0.219	Infinite
E	0.00	24,920,668	0.134	Infinite

The fatigue life information in Table 6-8 correlates well with the information in Table 6-4. It was expected that the locations A, B, and C would have the lowest fatigue life. Location E was expected to have a very high fatigue life, which it does, and location D was expected to be more critical than location H, which was also true. Location A did not record data for the last 25% of the test. This reduces the total number of cycles, but should not drastically affect the fatigue life. As expected, the effective stress range for locations A and B were comparable.

CHAPTER 7

Conclusions and Recommendations

7.1   OVERVIEW

The conclusions will be divided into three sections. Final recommendations for the 12th Street Exit Ramp are discussed in Section 7.2. Recommendations and concerns for the Medina River Bridge are discussed in Section 7.3. Suggestions concerning the applicability of using the MicroSAFE units during inspections of fracture critical bridges are presented in Section 7.4.

7.2   12TH STREET EXIT RAMP RECOMMENDATIONS

When the 12th Street Exit Ramp was initially discussed as a candidate for instrumentation, it was suspected that this structure experienced low daily traffic. Even more importantly, the daily truck traffic on this bridge was expected to be nearly zero.

These expectations were confirmed by the rainflow data recorded during two collection periods. The largest strain ranges experienced by the bridge were less than 30% of the design load of two HS-20 vehicles. These results demonstrate that the loads on the bridge are significantly less than the design loads.

The calculated fatigue life of the longitudinal girders provided similar information. The fatigue life is more than 500 years for this bridge, which is much longer than the bridge is expected to remain in service.

These low loads and modest strain cycles indicate that this structure may not need to be inspected as often as other fracture critical bridges.

These minimal loads and strains also show that this structure may not need to be inspected with the regularity of other fracture critical bridge.

7.3 MEDINA RIVER BRIDGE RECOMMENDATIONS

The Medina River Bridge was instrumented primarily because it is fracture critical, but also because the bridge was behaving oddly. TXDOT inspectors noticed that uplift of the bridge deck had occurred at north and south anchor piers. Between the two collection periods, the bridge deck rocked completely off its bearing on the north anchor pier. The observed behavior was probably caused by the widening of the bridge in the 1960s. When the bridge was widened, the new structure became an entrance ramp and the original structure carries two full lanes of truck traffic. The entrance ramp is seldom used, and the new structure experiences hardly any load. Over the past 40 years, the increased loading of two lanes of truck traffic was enough to lift the deck off the anchor pier bearings. In contrast to the 12th Street Exit Ramp, the Medina River Bridge was expected to experience significant strains.

A high-speed weigh-in-motion sensor is located 7 miles south of the Medina River Bridge. This sensor records up to 4500 trucks a day.

As expected, the fatigue life for the anchor span of the Medina River Bridge was short. The fatigue life was less than 50 years for the longitudinal girders.

It is recommended that the short inspection schedule be maintained for this bridge. The bridge experiences unusual behavior, carries significant daily truck traffic, and has a short fatigue life.

7.4   MICROSAFE UNIT SUGGESTIONS

The benefits of instrumenting a bridge with the MicroSAFE units has been clearly demonstrated. The units can be used to determine areas of maximum stress and the fatigue life of the structure. The use of these units in the future is highly recommended by the research team.

However, two issues require additional comments. The location of the instruments and the user-selected bin sizes can make the difference between a successful instrumentation and a disappointing failure.

When conducting a preliminary analysis to determine the best locations for the instruments, a few common pitfalls must be avoided. (1) A detailed analytical model is required to obtain accurate results. If a simplified model is used, small errors in connection details, section properties, and moving loads can cause large inaccuracies in the model output. (2) When converting calculated moments to strain ranges, the assumptions made about the slab have a significant influence on the results. The compressive strength of the slab, effective width, and degree of composite action should be studies in detail before decisions regarding instrument locations are made. (3) The maximum strain range does not necessarily occur at the point of maximum moment. Changes in girder depth and web and flange thicknesses will affect the maximum strain range as much as the maximum moment does.

The user-selected bin sizes must also be evaluated carefully. The recommended technique is to obtain raw data at a location for a short period and use that information to estimate the maximum strain that the bridge will experience. It is essential to set the bin sizes so the maximum expected strain range is within the upper bins. The maximum strain should be at least 2.5 times the largest strain range observed during the raw data collection period for a bridge

with low amounts of truck traffic. For a bridge with a high daily truck traffic count, a factor of 5 should be used.

The most important factor to consider when setting the bin size is the fatigue threshold (Table 2-3). The largest strain bin must correspond to a stress range greater than the fatigue threshold. If it does not, then it will be impossible to determine if the fatigue life of the bridge is finite or infinite. It is essential to program the bin sizes to achieve this strain level or greater.

References

1. AASHTO. Guide Manual for Condition Evaluation and Load and Resistance Factor Rating (LRFR) of Highway Bridges. American Association of State Highway and Transportation Officials. 2003.

2. ASTM E 1049 – 85. Standard Practices for Cycle Counting in Fatigue Analysis. American Society for Testing and Materials. 1997.

3. Bilich, Chris T. Evaluation of Two Monitoring Systems for Significant Bridges in Texas. Masters of Science in Engineering Thesis, The University of Texas at Austin, August, 2003.

4. Fisher, John W. Fatigue and Fracture in Steel Bridges. John Wiley & Sons, Inc.U.S.A. 1984.

5. Haigood, Alan. *E-mail conversation with Invocon staff.* April, 2005.

6. Hoadley, Peter W., Frank, Karl H., and Yura, Joseph A. Estimation of the Fatigue Life of a Test Bridge From Traffic Data. The University of Texas at Austin, May, 1983.

7. Holman, Randall A. User's Guide: Micro Stress Analysis and Forecasted Endurance (MicroSAFE) Program. Invocon, Inc. November 4, 2003.

8. Instron Website. http://instron.com, 2005.

9. Kaiser Aluminum Website. http://www.kaisertwd.com, 2005.

10. Kowalik, Alan. *Personal conversation with TxDOT staff.* March, 2005.

11. Ohio Department of Transportation Website. www.dot.state.oh.us, 2005.

12. Wood, Sharon L. Evaluation and Monitoring of Texas Major and Unique Bridges. Project Proposal. August, 2001.

VITA

Peter Kenneth Dean was born in Wilmington, Delaware on March 7, 1981 to Christine and Ken Dean. Following graduation from Bohemia Manor High School in June of 1999, Peter matriculated to the University of Delaware. During his time at the University of Delaware, Peter worked for the Corps of Engineers, was a part of summer scholarship programs, and completed an undergraduate thesis entitled, "Experimental Investigation of the Effect of Vertical Load on the Capacity of Wood Shear Walls." Peter graduated from the University of Delaware in May of 2003 with his Bachelor of Civil Engineering, Degree with Distinction. Peter enrolled at the University of Texas at Austin in August of 2003.

Permanent Address: 1138 Old Telegraph Rd

Warwick, MD 21912

petedean@mail.utexas.edu

This thesis was typed by the author.